

INTERFERENCE MITIGATION FOR
GPS BASED ATTITUDE DETERMINATION



MATTHEW DAVID MARKEL

A DISSERTATION PRESENTED TO THE GRADUATE SCHOOL
OF THE UNIVERSITY OF FLORIDA IN PARTIAL FULFILLMENT
OF THE REQUIREMENTS FOR THE DEGREE OF
DOCTOR OF PHILOSOPHY

UNIVERSITY OF FLORIDA

2002

Copyright 2002

by

Matthew David Markel

This work is dedicated to my wife and best friend, Colleen. Her unending support through every facet of this program was truly an inspiration. On an uncountable number of occasions she has been a source of both encouragement and enlightenment.

ACKNOWLEDGMENTS

I express my great appreciation to my parents, David and Linda Markel, for their encouragement and support. For as long as I can remember, they have encouraged me to make the most of the gifts I have been given. My success is a direct consequence of their encouragement.

It goes without saying that I am in the debt of my wife, Colleen, to whom this work is dedicated. She has graciously given of herself to allow me the means to pursue this program. On more days than I can count she, without complaint, has sacrificed so that I could complete this program. She was understanding when I was not present because of school and when I was physically present although elsewhere in thought. I will spend the rest of my life repaying her for what she has without question provided me these last three years.

I have been extremely fortunate to have had Professors Henry Zmuda and Eric Sutton as my co-advisors. Their insight, encouragement, and talent have been a genuine blessing. The attitude and dedication they have shown throughout this work have made this research an exciting and fulfilling endeavor for me. I will truly miss our weekly research meetings.

I am grateful as well for the other members of my research committee, Professors Pasquale Sforza and Tan Wong. In addition to serving on the my research committee, I was fortunate to take a class taught by Professor Wong, where several key concepts used in this dissertation were presented. Professor Sforza, as director of the Graduate Engineering Research Center (GERC), has succeeded in the difficult task of providing a center that provides a university setting beneficial to the unique challenges of a military base environment.

I am also thankful for the generosity of my dissertation reviewers: Dr. Timothy J. (TJ) Klausutis, Mr. James Ciccarelli, and Mr. Jerry Weed. Each provided a wealth of

constructive comments and critiques, and their contributions without doubt have made this a stronger dissertation. I have been fortunate to take classes taught by the talented and dedicated Dr. Klausutis. More than the academic material, however, Dr. Klausutis has been a source of much needed information and inspiration concerning the Ph.D. process and experience. Mr. Ciccarelli, in addition to reviewing the dissertation, has contributed to our research team since June 2001, providing both a sounding board for the technical details and an independent review of my simulation code. Mr. Weed was the first to encourage me to pursue this Ph.D. For years he has been the instigator of stimulating technical discussion between us concerning nearly every aspect of radar and signal processing, forcing us each to a higher level of understanding.

The logistics of taking classes, receiving and presenting assignments and tests, registration, and general communication with the Department and Graduate School is often taken for granted by students on campus. However, for the off-campus students at the GERC, it would be a significant challenge were it not for the professionalism of the GERC staff, especially Ms. Judi Shivers. I am extremely grateful for the help each has provided me during both my master's and doctoral work.

Sverdrup Technology, through its Edwin "Bud" George Fellowship, has financed my academic pursuit. Without their support and flexibility I would not have been successful. This fellowship is a benefit to the company, its employees, and the symbiotic relationship among Sverdrup, Eglin Air Force Base, and the University of Florida. It is my sincere hope that it endures and continues to attract students.

Finally, I would like to thank God for the talents and blessings He has provided. I truly believe that with Him all things are possible.

TABLE OF CONTENTS

	<u>page</u>
ACKNOWLEDGMENTS	iv
LIST OF TABLES	viii
LIST OF FIGURES	ix
ABSTRACT	xvi
 CHAPTERS	
1 INTRODUCTION	1
1.1 Motivation	1
1.2 Contributions of This Dissertation	3
1.3 Dissertation Overview	4
2 BACKGROUND	5
2.1 Introduction	5
2.2 GPS Overview	5
2.3 Conventional Attitude Determination Using GPS	7
2.3.1 Attitude and Coordinate Frames	7
2.3.2 Parameterization of Attitude	8
2.3.3 Conventional Phase Difference Model	10
2.4 Direction Finding	13
3 AN ANTI-JAM ATTITUDE DETERMINATION RECEIVER	18
3.1 Introduction	18
3.2 A GPS Receiver for Anti-Jam Position Location and Attitude	18
4 MAXIMUM LIKELIHOOD ATTITUDE ESTIMATION	22
4.1 Introduction	22
4.2 Notation, Preliminaries, and Signal Model	23
4.3 Maximum Likelihood Direction Estimation	27
4.4 New Concepts	30
4.5 Maximum Likelihood Attitude Estimation	32
4.6 Discussion	37
4.7 Comments on Searches	40
5 PROPERTIES OF THE MAXIMUM LIKELIHOOD ATTITUDE ESTI- MATOR	42

5.1	Introduction	42
5.2	Consistency	43
5.3	Lemmas on the MLAE	44
5.4	Bias	51
5.5	Efficiency	52
5.6	Conclusions	53
6	ATTITUDE FROM DIRECTION FINDING	54
6.1	Introduction	54
6.2	Conceptual Approach	54
6.3	Equal Satellite Weighting	56
6.4	Satellite Weighting via Adapted SINR	58
6.5	Conclusions	59
7	WIDER BASELINES AND DUAL FREQUENCY USE	61
7.1	Introduction	61
7.2	Dual Frequency Maximum Likelihood Attitude Determination	63
7.3	Reduction in False Attitudes	68
7.4	Dual-Frequency MLAE Performance Increase	80
7.5	Summary	82
8	SIMULATIONS AND RESULTS	84
8.1	Introduction	84
8.2	Simulation Methodology	84
8.3	Mean Total Error	87
8.4	Study 1: Single Jammer with "Random" Location	88
8.5	Study 2: Varying Attitude Update Rate	107
8.6	Study 3: Wider Baselines and Dual Frequency	121
8.7	Conclusions	126
9	CONCLUSIONS	128
9.1	Summary	128
9.2	Future Work	130
	APPENDIX	133
A	CRAMÉR-RAO BOUND	133
B	THE INTERFERENCE COVARIANCE MATRIX	141
B.1	Introduction	141
B.2	Derivation of Interference Statistics	144
B.3	Estimation of Interference Statistics	156
C	RESOLUTION OF THE ATTITUDE AMBIGUITY	160
	REFERENCES	164
	BIOGRAPHICAL SKETCH	168

LIST OF TABLES

<u>Table</u>	<u>page</u>
7.1 Number of false solutions, i.e. points below the "possible minimum" threshold that do not converge to the true solution. Resolution in each Euler angle is two degrees. Scenario is the same as that involving the first jammer in the random jammer study of Chapter 8.	79
8.1 Mean total error performance comparison of the four estimators in an un-jammed environment. Update rate is 50 Hz.	106
8.2 Mean total error performance comparison of the four estimators in an un-jammed environment. Update rate is 12.5 Hz.	106

LIST OF FIGURES

<u>Figure</u>	<u>page</u>
2.1 A two sensor interferometric system. The baseline vector \vec{d} can be determined by the known LOS vector \vec{v} and the phase difference between the signals measured at the two sensors x_0 and x_1	11
2.2 Mean Total Error Performance of the conventional attitude estimator vs. signal to jammer ratio (SJR), shown as the solid line. The dotted line represents the performance of the attitude estimator in an unjammed scenario. Performance of the phase difference approach to attitude estimation is degraded even when the SJR is high.	13
3.1 Receiver block diagram. Demodulated data are provided to the attitude estimator (shown in the circles) as well as to the beamformers. The beamformer output is used for position location and updating the code and Doppler tracking loops.	20
4.1 Visualization of the possible (ambiguous) attitudes corresponding to a single source. The possible array attitudes can be found by "twirling" the LOS vector, which is assumed affixed to the array, while keeping it pointed at the satellite source.	33
4.2 Possible roll and pitch Euler angles arising from the ambiguity in the new array response vector (yaw angles not shown). The true roll is 25 degrees, and the true pitch is 15 degrees, as indicated by the diamond. The locus of possible attitudes is determined by the LOS to the source and the true attitude. A different source LOS would have a different ambiguity.	34
4.3 Contribution to the value of the maximum likelihood attitude estimator of equation (4.49) from the first of seven satellites in view. This satellite provides little information about yaw, and the most in the positive pitch - negative yaw to negative pitch - positive yaw dimension.	38
4.4 Contribution to the value of the maximum likelihood attitude estimator from the fifth of seven satellites in view. This satellite provides little information in the positive pitch - negative yaw to negative pitch - positive yaw dimension, incidentally the dimension satellite in which satellite one provided the most information.	39
4.5 Contribution to the value of the maximum likelihood attitude estimator from the seventh of seven satellites in view.	40

4.6	Total value of the metric including contributions from all satellites in view. Notice that the areas of weak information from any particular satellite have been filled in by the contributions of other satellites.	41
7.1	Normalized likelihood value vs. direction of arrival for a 15 element ULA receiving a narrowband signal at a frequency corresponding to a 2λ spacing. True direction is on boresight, i.e. 0 degrees.	69
7.2	Normalized likelihood value vs. direction of arrival for a 15 element ULA receiving a narrowband signal at a frequency corresponding to a $\frac{2}{1.25}\lambda$ spacing. True direction is on boresight, i.e. 0 degrees.	69
7.3	Likelihood value vs. direction of arrival for a 15 element ULA incorporating data collected at two frequencies corresponding to 2λ and $\frac{2}{1.25}\lambda$ spacing. True direction is on boresight, i.e. 0 degrees. The grating lobes are reduced in amplitude from the true direction of arrival, producing a clear indication which direction is correct.	70
7.4	Three dimensional plot of all attitudes whose metric value is below the 10dB threshold, using Satellites 1 and 4, and frequency L1.	72
7.5	Two dimensional view of all attitudes whose metric value is below the 10dB threshold, using Satellites 1 and 4, and frequency L1.	73
7.6	Two dimensional view of those attitudes whose metric value is below the 10dB threshold that are not contiguous to the true attitude, (i.e. false solutions) using Satellites 1 and 4, and frequency L1.	73
7.7	False attitude solutions using Satellites 1 and 4, and frequency L2.	74
7.8	False attitude solutions using Satellites 1 and 4, and frequency the dual frequency MLAE	74
7.9	False attitude solutions using Satellites 1 and 5, and frequency L1.	75
7.10	False attitude solutions using Satellites 1 and 5, and frequency L2.	75
7.11	False attitude solutions using Satellites 1 and 5, and the dual frequency MLAE. 76	
7.12	False attitude solutions using Satellites 1 and 6, and frequency L1.	76
7.13	False attitude solutions using Satellites 1 and 5, and frequency L2.	77
7.14	False attitude solutions using Satellites 1 and 5, and the dual frequency MLAE. 77	
7.15	False attitude solutions using Satellites 2 and 3, and frequency L1.	78
7.16	False attitude solutions using Satellites 2 and 3, and frequency L2.	78
7.17	False attitude solutions using Satellites 2 and 3, and the dual frequency MLAE. 79	
8.1	Sensor locations for the three antenna topologies. Quad (asterisk), Y (diamond), and Hex (x). The Y antenna is actually a subset of the Hex antenna.	86

8.2	Sensor gain pattern used in the attitude simulation.	87
8.3	Sine-space plot of the satellite (asterisk) and the 12 jammer locations (X) for the random jammer study. Only one jammer is simulated at a time; in the first scenario the jammer location is at $K_y = .7$, and the remaining scenarios use the jammer positions shown in order clockwise. The outer circle represents the horizon, and the area inside the inner circle represents the portion of the sky visible to the sensors.	89
8.4	Standard deviation of antenna roll estimates and CRB for the Quad antenna (star), Y antenna (square), and Hex antenna (diamond). The 12 points along the abscissa correspond to the 12 jammer locations identified in Figure 8.3. The update rate is 50 Hz.	90
8.5	Standard deviation of antenna pitch estimates and CRB for the Quad antenna (star), Y antenna (square), and Hex antenna (diamond). The 12 points along the abscissa correspond to the 12 jammer locations identified in Figure 8.3. The update rate is 50 Hz.	90
8.6	Standard deviation of antenna yaw estimates and CRB for the Quad antenna (star), Y antenna (square), and Hex antenna (diamond). The 12 points along the abscissa correspond to the 12 jammer locations identified in Figure 8.3. The update rate is 50 Hz.	91
8.7	Mean total angle error using the Quad antenna. The 12 points along the abscissa correspond to the 12 jammer locations identified in Figure 8.3. Performance is shown for the MLAE (+), DF-W (diamond with solid line), DF-U (asterisk), and conventional attitude estimation algorithms (diamond with dashed line). The update rate is 50 Hz.	92
8.8	Mean total angle error using the Y antenna. The 12 points along the abscissa correspond to the 12 jammer locations identified in Figure 8.3. Performance is shown for the MLAE (+), DF-W (diamond with solid line), DF-U (asterisk), and conventional attitude estimation algorithms (diamond with dashed line). The update rate is 50 Hz.	93
8.9	Mean total angle error using the Hex antenna. The 12 points along the abscissa correspond to the 12 jammer locations identified in Figure 8.3. Performance is shown for the MLAE (+), DF-W (diamond with solid line), DF-U (asterisk), and conventional attitude estimation algorithms (diamond with dashed line). The update rate is 50 Hz.	94
8.10	Mean total angle error using the MLAE algorithm, comparing the single jammer at "random" locations to the unjammed scenario. The solid lines are with the jammer, and the dashed lines unjammed. Performance is shown for the Hex antenna (+), Y antenna (asterisk), and the Quad antenna (diamond). The update rate is 50 Hz.	95

8.11 Mean total angle error using the DF-W algorithm, comparing the single jammer at "random" locations to the unjammed scenario. The solid lines are with the jammer, and the dashed lines unjammed. Performance is shown for the Hex antenna (+), Y antenna (asterisk), and the Quad antenna (diamond). The update rate is 50 Hz.	96
8.12 Mean total angle error using the DF-U algorithm, comparing the single jammer at "random" locations to the unjammed scenario. The solid lines are with the jammer, and the dashed lines unjammed. Performance is shown for the Hex antenna (+), Y antenna (asterisk), and the Quad antenna (diamond). The update rate is 50 Hz.	96
8.13 Mean total angle error using the conventional algorithm, comparing the single jammer at "random" locations to the unjammed scenario. The solid lines are with the jammer, and the dashed lines unjammed. Performance is shown for the Hex antenna (+), Y antenna (asterisk), and the Quad antenna (diamond). The update rate is 50 Hz.	97
8.14 Standard deviation of antenna roll estimates and CRB for the Quad antenna (star), Y antenna (square), and Hex antenna (diamond). The update rate is 12.5 Hz.	98
8.15 Standard deviation of antenna pitch estimates and CRB for the Quad antenna (star), Y antenna (square), and Hex antenna (diamond). The update rate is 12.5 Hz.	99
8.16 Standard deviation of antenna yaw estimates and CRB for the Quad antenna (star), Y antenna (square), and Hex antenna (diamond). The update rate is 12.5 Hz.	99
8.17 Mean total angle error using the Quad antenna. The 12 points along the abscissa correspond to the 12 jammer locations identified in Figure 8.3. Performance is shown for the MLAE (+), DF-W (diamond with solid line), DF-U (asterisk), and conventional attitude estimation algorithms (diamond with dashed line). The update rate is 12.5 Hz.	100
8.18 Mean total angle error using the Y antenna. The 12 points along the abscissa correspond to the 12 jammer locations identified in Figure 8.3. Performance is shown for the MLAE (+), DF-W (diamond with solid line), DF-U (asterisk), and conventional attitude estimation algorithms (diamond with dashed line). The update rate is 12.5 Hz.	101
8.19 Mean total angle error using the Hex antenna. The 12 points along the abscissa correspond to the 12 jammer locations identified in Figure 8.3. Performance is shown for the MLAE (+), DF-W (diamond with solid line), DF-U (asterisk), and conventional attitude estimation algorithms (diamond with dashed line). The update rate is 12.5 Hz.	102

8.20	Mean total angle error using the MLAE algorithm, comparing the single jammer at "random" locations to the unjammed scenario. The solid lines are with the jammer, and the dashed lines unjammed. Performance is shown for the Hex antenna (+), Y antenna (asterisk), and the Quad antenna (diamond). The update rate is 12.5 Hz.	103
8.21	Mean total angle error using the DF-W algorithm, comparing the single jammer at "random" locations to the unjammed scenario. The solid lines are with the jammer, and the dashed lines unjammed. Performance is shown for the Hex antenna (+), Y antenna (asterisk), and the Quad antenna (diamond). The update rate is 12.5 Hz.	103
8.22	Mean total angle error using the DF-U algorithm, comparing the single jammer at "random" locations to the unjammed scenario. The solid lines are with the jammer, and the dashed lines unjammed. Performance is shown for the Hex antenna (+), Y antenna (asterisk), and the Quad antenna (diamond). The update rate is 12.5 Hz.	104
8.23	Mean total angle error using the conventional algorithm, comparing the single jammer at "random" locations to the unjammed scenario. The solid lines are with the jammer, and the dashed lines unjammed. Performance is shown for the Hex antenna (+), Y antenna (asterisk), and the Quad antenna (diamond). The update rate is 12.5 Hz.	104
8.24	Satellite (asterisk) and Jammer Locations (x) for the varying update rate study. The jammer indicated by the arrow is the only jammer used in case 1. In case 2, all three jammers appear.	108
8.25	Standard deviation of antenna roll estimates and CRB for the Quad antenna (star), Y antenna (square), and Hex antenna (diamond) vs. update rate. One jammer in view.	109
8.26	Standard deviation of antenna pitch estimates and CRB for the Quad antenna (star), Y antenna (square), and Hex antenna (diamond) vs. update rate. One jammer in view.	109
8.27	Standard deviation of antenna yaw estimates and CRB for the Quad antenna (star), Y antenna (square), and Hex antenna (diamond) vs. update rate. One jammer in view.	110
8.28	Mean total angle error using the Quad antenna vs. update rate for 1 jammer. Performance is shown for the MLAE (+), DF-W (diamond with solid line), DF-U (asterisk), and conventional attitude estimation algorithms (diamond with dashed line).	111
8.29	Mean total angle error using the Y antenna vs. update rate for 1 jammer. Performance is shown for the MLAE (+), DF-W (diamond with solid line), DF-U (asterisk), and conventional attitude estimation algorithms (diamond with dashed line).	112

8.30	Mean total angle error using the Hex antenna vs. update rate for 1 jammer. Performance is shown for the MLAE (+), DF-W (diamond with solid line), DF-U (asterisk), and conventional attitude estimation algorithms (diamond with dashed line).	112
8.31	Mean total angle error using the MLAE algorithm, comparing the single jammer at "random" locations to the unjammed scenario, vs. update rate. The solid lines are with the jammer, and the dashed lines unjammed. Performance is shown for the Hex antenna (+), Y antenna (asterisk), and the Quad antenna (diamond).	113
8.32	Mean total angle error using the DF-W algorithm, comparing the single jammer scenario to the unjammed scenario, vs. update rate. The solid lines are with the jammer, and the dashed lines unjammed. Performance is shown for the Hex antenna (+), Y antenna (asterisk), and the Quad antenna (diamond).	114
8.33	Mean total angle error using the DF-U algorithm, comparing the single jammer scenario to the unjammed scenario, vs. update rate. The solid lines are with the jammer, and the dashed lines unjammed. Performance is shown for the Hex antenna (+), Y antenna (asterisk), and the Quad antenna (diamond).	114
8.34	Mean total angle error using the conventional algorithm, comparing the single jammer scenario to the unjammed scenario, vs. update rate. The solid lines are with the jammer, and the dashed lines unjammed. Performance is shown for the Hex antenna (+), Y antenna (asterisk), and the Quad antenna (diamond).	115
8.35	Mean total angle error using the Quad antenna vs. update rate for 3 jammers. Performance is shown for the MLAE (+), DF-W (diamond with solid line), DF-U (asterisk), and conventional attitude estimation algorithms (diamond with dashed line).	116
8.36	Mean total angle error using the Y antenna vs. update rate for 3 jammers. Performance is shown for the MLAE (+), DF-W (diamond with solid line), DF-U (asterisk), and conventional attitude estimation algorithms (diamond with dashed line).	117
8.37	Mean total angle error using the Hex antenna vs. update rate for 3 jammers. Performance is shown for the MLAE (+), DF-W (diamond with solid line), DF-U (asterisk), and conventional attitude estimation algorithms (diamond with dashed line).	117
8.38	Mean total angle error using the MLAE algorithm, comparing the three jammer scenario to the unjammed scenario, vs. update rate. The solid lines are with the jammer, and the dashed lines unjammed. Performance is shown for the Hex antenna (+), Y antenna (asterisk), and the Quad antenna (diamond).	118

8.39	Mean total angle error using the DF-W algorithm, comparing the three jammer scenario to the unjammed scenario, vs. update rate. The solid lines are with the jammer, and the dashed lines unjammed. Performance is shown for the Hex antenna (+), Y antenna (asterisk), and the Quad antenna (diamond).	119
8.40	Mean total angle error using the DF-U algorithm, comparing the three jammer scenario to the unjammed scenario, vs. update rate. The solid lines are with the jammer, and the dashed lines unjammed. Performance is shown for the Hex antenna (+), Y antenna (asterisk), and the Quad antenna (diamond).	119
8.41	Mean total angle error using the conventional algorithm, comparing the three jammer scenario to the unjammed scenario, vs. update rate. The solid lines are with the jammer, and the dashed lines unjammed. Performance is shown for the Hex antenna (+), Y antenna (asterisk), and the Quad antenna (diamond).	120
8.42	Sensor Locations used in the wide baseline study. The three antenna topologies are the Quad (asterisk), Y (diamond), and Hex (x).	122
8.43	Mean total angle error using the Quad antenna vs. update rate for 1 jammer. Performance is shown for the single frequency MLAE at L1 (diamond) and L2 (+), and for the dual frequency MLAE (asterisk).	122
8.44	Mean total angle error using the Y antenna vs. update rate for 1 jammer. Performance is shown for the single frequency MLAE at L1 (diamond) and L2 (+), and for the dual frequency MLAE (asterisk).	123
8.45	Mean total angle error using the Hex antenna vs. update rate for 1 jammer. Performance is shown for the single frequency MLAE at L1 (diamond) and L2 (+), and for the dual frequency MLAE (asterisk).	123
8.46	Mean total angle error using the Quad antenna vs. update rate for 3 jammers. Performance is shown for the single frequency MLAE at L1 (diamond) and L2 (+), and for the dual frequency MLAE (asterisk).	124
8.47	Mean total angle error using the Y antenna vs. update rate for 3 jammers. Performance is shown for the single frequency MLAE at L1 (diamond) and L2 (+), and for the dual frequency MLAE (asterisk).	124
8.48	Mean total angle error using the Hex antenna vs. update rate for 3 jammers. Performance is shown for the single frequency MLAE at L1 (diamond) and L2 (+), and for the dual frequency MLAE (asterisk).	125
B.1	The receiver model used in this dissertation. The output of the chip matched filter is oversampled by a factor of N_c , (N_c is 4 in this figure) and these samples are decimated into sequences composed of 1 sample per chip. The decimated sequences are then despread using the sequency $A(i)$ $i = 1, 2, \dots, N$ to form early, punctual, late, and other temporal gates.	143
B.2	One sided jammer PSD	146

Abstract of Dissertation Presented to the Graduate School
of the University of Florida in Partial Fulfillment of the
Requirements for the Degree of Doctor of Philosophy

INTERFERENCE MITIGATION FOR
GPS BASED ATTITUDE DETERMINATION

By

Matthew David Markel

May 2002

Chair: Henry Zmuda

Major Department: Electrical and Computer Engineering

With its low transmit power and considerable orbit distance from receivers, the global positioning system (GPS) waveforms are known to be susceptible to jamming. Efforts to date have investigated various receiver designs and adaptive antenna arrays to improve the anti-jam capabilities of GPS *position location*, but until this work no extension of anti-jam capabilities to *attitude determination* (determination of the orientation of a body in space) existed. This dissertation provides a comprehensive investigation into the new field of robust, jam-resistant attitude determination using the Global Positioning System.

We present a generic adaptive antenna array and receiver design that provide the necessary data for both position location and attitude determination in a jammed environment. Using the data this receiver provides we develop a new maximum likelihood attitude estimator (the MLAE) that provides attitude determination capability even in jammed environments. In order to accomplish this, new ways of viewing the standard array processing and direction finding tenants are presented. This leads to a new interpretation and parameterization of the array response vector (spatial steering vector) and secondary data covariance matrix. The MLAE optimally includes information from

all satellites in view, and its performance is shown herein to asymptotically achieve the Cramér-Rao Bound (CRB), i.e. the MLAE asymptotically achieves the performance limit for unbiased estimators.

As an approximation to this estimator, a second estimator is developed that, at the expense of performance, may provide increased computational capability. Two versions of this second estimator are presented that combine direction finding with attitude estimation.

A method of optimally incorporating data from both GPS frequencies into the estimation is developed. This approach maintains the jammer mitigation capabilities of the previous estimators and allows for a larger array spacing, therefore increasing the accuracy of the attitude estimates.

Simulation based performance results of the various estimators are presented for various antenna topologies and interference scenarios. The simulation results indicate that the new algorithms provide significant improvement over conventional attitude determination methods. In addition, the MLAE is shown to provide better performance than conventional methods of attitude determination even in *unjammed* environments.

CHAPTER 1 INTRODUCTION

1.1 Motivation

It is well known that adaptive antenna arrays (often referred to as “Smart Antennas” for communications systems) provide significant resistance to unintentional interference and intentional jamming for both signal extraction and direction finding. Global Positioning System (GPS) based attitude determination (AD) systems utilize multiple sensors as well to extract attitude through carrier phase differences between the sensors [1]. However, present AD algorithms typically only offer the jamming resistance inherent in the receiver (i.e. gain from the spread spectrum waveform and perhaps coupling with some form of INS), which for even low powered jammers may not be enough to prevent corruption of the attitude estimates. Therefore, it seems appealing to exploit the similarities between the two fields of adaptive array processing and GPS based attitude determination to increase the anti-jam capabilities of GPS attitude systems. Indeed, this work centers around a substantially different method of approaching the attitude determination task than is typically employed.

The scenario that originally motivated this research involved a medium to long range platform that must fly for extended periods in a severe jamming environment. The platform incorporates an adaptive antenna array to provide GPS jamming resistance for position location and navigation. In response to this scenario, a method has been developed that makes use of an anti-jam antenna array to provide GPS based *attitude* information, as well as the typical position location data, even during periods of jamming.

Three distinct factors motivated this research into anti-jam attitude determination.

1. *Threat from GPS jammers.* The susceptibility to jamming and inadvertent interference is high due to the GPS satellites’ low transmit power and considerable orbital altitude. Even a low power jammer several miles from the GPS user can degrade accuracy

or affect acquisition. With GPS jammers being marketed as commercial items [2], one could control access to GPS over an entire region by deploying several of these low cost/low power jammers throughout an area and activating them only when desired to deny the use of GPS.

2. *Related research.* Previous research in direction finding algorithms using antenna arrays for radar and communications systems provides a substantial mathematical basis and a likelihood of tractability for the approaches developed in this dissertation. At the macro level, attitude determination and direction finding are similar. For example, they both incorporate multiple sensors and use carrier phase interferometry to develop their estimates. Since some direction finding algorithms provide significant performance in external interference environments, it is natural to look to this field with the desire to gain similar anti-jam capabilities for attitude determination.

The primary algorithm developed in this dissertation does not use direction finding directly. However, it is not unlike many direction finding algorithms in the sense that it defines steering vectors that map unknown parameters into a model for observation data from the antenna array, and the unknown parameters are estimated by maximizing (or minimizing) a function of the steering vectors and received data. Suboptimal algorithms developed later in the dissertation directly incorporate direction finding, or more specifically assume that the directions are measured by some method.

3. *Hardware trends.* State of the art systems are incorporating adaptive antenna arrays with the GPS receivers to provide additional anti-jamming resistance for position location, providing much of the hardware and design philosophy for attitude location as well (see, for example, Falcone et al. [3]). A possible direct application of this work would be to incorporate the algorithms developed here into a GPS system that already incorporates multi-sensors for anti-jam position location and navigation in order to additionally provide a GPS based attitude estimate.

Responding to these three motivations (i.e. need, related research, and hardware technology trends), it is natural to investigate a system that makes maximum use of the presence of the anti-jam sensor array by providing attitude as well as position location.

1.2 Contributions of This Dissertation

This work draws on several separate fields of research. The following background chapter provides an overview of the Global Positioning System, attitude and associated “conventional” (i.e. not robust to interference) methods of attitude determination and direction finding because *all* of these fields were used to develop new interference resistant attitude estimation methods. These results are novel because external interference mitigation for GPS based attitude estimation is a completely undeveloped field [4], and the results derived here provide significant improvement over conventional attitude determination algorithms in both jammed and unjammed environments.

The constraints and challenges of this task are different from the “typical” antenna array direction finding and communications applications.¹ To address these challenges the direction finding task is recast as an “attitude finding” problem by redefining such standard and familiar terms as the antenna array response vector (often called the spatial steering vector) and data matrix. This provides increased insight into methods to address the problem and facilitates development of a new maximum likelihood attitude estimation method. This estimator is shown to be asymptotically unbiased, consistent, and efficient (i.e. asymptotically achieves the Cramér-Rao Bound). Another contribution is the extension of maximum likelihood direction/attitude estimation to incorporate both GPS carrier frequencies, as discussed in Chapter 7. Using the method developed in this dissertation, incorporation of the additional GPS frequency provides a signal to noise ratio (SNR) *gain*, as opposed to methods in use today in which the SNR is reduced when the additional frequency is used. Finally, the simulation based performance results provide a quantification of the performance of this work.

¹ Of course, caution is used with the generalization of “typical,” since every application has some unique attributes.

1.3 Dissertation Overview

The remainder of this dissertation is organized as follows. Chapter 2 contains an overview of the multiple research fields from which this dissertation draws. Chapter 3 describes a generic receiver that provides the data necessary to estimate both position and attitude, and the differences between this receiver and those typically employed for either anti-jam position location or attitude determination. Chapter 4 derives a novel algorithm for attitude estimation in an external interference environment. This estimator takes the form of a maximum-likelihood estimator. Chapter 5 presents several statistical properties of this estimator. In Chapter 6, two variants of suboptimal algorithms are developed for attitude estimation. These algorithms have attractive implementation and computational features, but their performance is not as good as the estimator of Chapter 4. Chapter 7 derives a method of improving the attitude estimator of Chapter 4 by using both GPS frequencies. Chapter 8 presents quantification of the performance of these methods through simulation results. Finally, Chapter 9 contains a summary of this work and a discussion of areas of research related to this work, but beyond the scope of this dissertation.

CHAPTER 2 BACKGROUND

2.1 Introduction

This chapter presents an overview of the major fields which provide the foundation for the contributions of this dissertation. Interference mitigation for GPS based attitude determination involves the synthesis of several different fields, so a brief introduction and summary of them is provided here.

This chapter is organized as follows. Section 2.2 provides an overview of the Global Positioning System. Section 2.3 discusses methods and signal models used in attitude determination. These two sections provide the framework for the term “conventional” GPS based attitude determination, which is used in this work to describe the methods of attitude estimation used today. Finally, a survey of direction finding is provided in section 2.4, with an emphasis on maximum likelihood methods.

2.2 GPS Overview

From personal, hand-held civilian units to integrated military systems, the Global Positioning System (GPS) is an important link in the worldwide navigation infrastructure. The Global Positioning System is designed to provide a user with the ability to calculate his position in three dimensional space (i.e. latitude, longitude, and altitude) through reception of signals from a constellation of 24 dedicated satellites orbiting the earth.

The Global Positioning System conceptually consists of three segments. The *space segment* involves the satellites in orbit about the earth. These satellites provide a low-power output signal that may be received on or above the earth. The *control segment* tracks and communicates with the satellites in order to update their navigation information. Finally, the *user segment* represents the receiver and associated equipment required to decode and interpret the signals sent by the satellites and convert this into the user's

position and velocity. With an impressive market penetration, the number of "users" occupying the user segment is steadily increasing.

The ability to calculate position arises from measuring the range to several satellites. If one knows the range to a fixed object, the locus of possible user positions is on the surface of a sphere with its center at the object position and its radius equal to the range to the object. Therefore, if the user knows his range to three satellites, the positions of the satellites (calculated using the satellite's ephemeris parameters), and has a precise measurement of time, then he can solve for his position as the intersection of the three spheres. In practice, less precise clocks are used in the user segment, requiring a minimum of four satellites to obtain a position. Obviously, errors and uncertainty in the ability to measure the range to the satellite directly affect the accuracy of the position measurement.

The GPS satellites incorporate Direct Sequence-Spread Spectrum (DS-SS) modulation. This allows all satellites to occupy the same spectrum and, by monitoring the code tracking loop, enables users to accurately calculate range to the satellite. Two levels of accuracy are currently available through the use of two different spreading sequence architectures. The Standard Positioning Service, which is available to all users, incorporates a 1023 length sequence with a chip rate of 1.023 MHz called the Coarse Acquisition Code (i.e. C/A Code). The Precise Positioning Service (PPS) uses the P(Y) code that operates at a chip rate of 10.23 MHz. The P(Y) codes have very long natural periods (over 6 months); however, they are truncated and restarted every week. While the C/A Code waveform is publicly known and easily obtainable, the P(Y) code sequence is only available to authorized users. Since knowledge of the spreading sequence is required for demodulation and data detection, the PPS is essentially available only to military applications.

The C/A waveform (code and data sequence) modulates a carrier frequency of 1.57542 GHz (often referred to as the L1 frequency). Since several satellites are simultaneously transmitting at the same frequency, Code Division Multiple Access (CDMA) is used to allow unambiguous satellite reception. Each satellite uses a different sequence from a set of 10th order Gold codes. Of the 1025 possible Gold codes available in this family, 37

have been identified for use on satellites. The P(Y) code is broadcast on two frequencies, the L1 frequency defined above (in phase quadrature with the C/A code) and the L2 frequency of 1.2276 GHz. At the time of this work, an effort is underway to enhance GPS with additional frequencies for civilian use and a different waveform, denoted as the M code, for military and other restricted use.

The navigation message data bits (which are modulated by the spreading sequences described above) are transmitted at a rate of 50 Hz. The GPS navigation data consist of synchronization information, satellite ephemeris data, and other satellite parameters. These data are designed to be packaged into 30 second (i.e. 1500 bit) time slices.

An important observation is that unlike many other communication systems where the only information is the demodulated data stream, GPS uses the code timing and tracking information to develop an estimate of *range* to the satellites. This range, coupled with the other information obtained from the GPS data stream, allows a formulation of user position.

2.3 Conventional Attitude Determination Using GPS

2.3.1 Attitude and Coordinate Frames

Attitude determination involves two coordinate systems and the transformation that relates them. The *local-level* coordinate system represents an initial, at rest, or other nominal orientation of the platform of interest. This frame is often referenced in terms of a "North-East-Down" (NED) or "East-North-Up" (ENU) convention. The line of sight (LOS) vectors to the satellites are assumed known in this coordinate system. The second coordinate system is the *antenna frame* of reference, and represents the orientation of the GPS antenna at a particular point in time. The antenna frame and the body frame¹ are related by a known transform; if one is known, the other can be easily found. For this reason the antenna frame is sometimes referred to in this work as the body frame and is

¹ The body frame is defined as the frame of reference along principal platform axes, such as along the fuselage and wings. Typically the body frame is of higher interest from a guidance and navigation perspective.

usually referenced using a “Front-Right-Below” (FRB) convention. The *attitude* is then defined as the relation between the local-level and the antenna frames of reference at any point in time.

2.3.2 Parameterization of Attitude

Some common parameterizations of the attitude include Euler angles, quaternions, and direction cosine matrices. Throughout this work, this attitude is referred to generically as q , to remain independent of any particular parameterization.² However, at times a specific parameterization is required either to clearly demonstrate a point or prevent ambiguities. When specific parameterizations of this attitude are employed they follow the notation and description below.

q = the attitude of the antenna

ξ_ϕ = the antenna roll Euler angle

ξ_θ = the antenna pitch Euler angle

ξ_ψ = the antenna yaw Euler angle

$\mathbf{q} = [q_1, q_2, q_3, q_4]^T$, the attitude quaternion

\mathbf{Q} = the 3x3 direction cosine matrix that transforms local level to antenna frame

The Euler angles represent successive rotations about the three coordinate axes. The roll angle, ξ_ϕ , represents rotation about the local level x axis, the pitch angle ξ_θ about the y axis, and the yaw angle ξ_ψ the z axis. The *order* of rotation determines the final orientation. In this work we employ a “3-1-2” rotation, meaning the rotations are performed first in yaw, then roll, and then pitch. A drawback with the Euler angle

² Notice that the unparameterized attitude q in this work is not represented in bold type, even though at least three parameters are required to specify the attitude. This is to emphasize that when this notation is used, the attitude may be specified *in any manner*.

representation is the possibility of encountering singularities; however, in general they provide an intuitive, clear interpretation of the rotations.

Another method of defining attitude is with the direction cosine matrix \mathbf{Q} . Each term in the direction cosine matrix represents the cosine of the angle between an axis of the local level frame and the antenna frame. For example, $Q(2, 2)$ is the cosine of the angle between the y axis of the local level frame and the y axis of the antenna frame [5]. The direction cosine matrix is orthonormal.

$$\mathbf{Q}^T = \mathbf{Q}^{-1} \quad (2.1)$$

$$|\mathbf{Q}| = 1 \quad (2.2)$$

This orthogonal nature of the direction cosine matrix is very useful, since an inverse rotation (say, transforming from the body frame back to the local level frame) can be performed without inverting the matrix.

The final method of specifying attitude is with a quaternion. In order to define the quaternion's ability to represent a rotation, first consider that between any two coordinate systems sharing a common origin, a single axis exists in which measurements along that axis are the same in both coordinate systems. The relation between the two coordinate systems (i.e. the attitude) is then defined by this axis and an angle of rotation about it. If we take the axis as \mathbf{V} and the angle of rotation as ω , then

$$\mathbf{V} = \begin{bmatrix} V_x \\ V_y \\ V_z \end{bmatrix} \quad (2.3)$$

where

$$|\mathbf{V}| = 1 \quad (2.4)$$

and using these the quaternion \mathbf{q} may be written as

$$\mathbf{q} = \begin{bmatrix} \sin(\frac{\alpha}{2}) \begin{bmatrix} V_x \\ V_y \\ V_z \end{bmatrix} \\ \cos(\frac{\alpha}{2}) \end{bmatrix} \quad (2.5)$$

and

$$|\mathbf{q}| = 1 \quad (2.6)$$

The identity quaternion, which performs no rotation, is

$$\mathbf{q}_{\text{Identity}} = \begin{bmatrix} 0 \\ 0 \\ 0 \\ 1 \end{bmatrix} \quad (2.7)$$

For an excellent discussion and history of attitude and its parameterizations, the reader is referred to Schleppe [5].

2.3.3 Conventional Phase Difference Model

In order to describe the operation of a conventional attitude determination system, we first describe the signal model employed and the assumptions it incorporates. Consider the two GPS sensor scenario of Figure 2.1. After downconversion, despreading, and integration the signal received at sensor x_0 consists of a contribution from the satellite and a noise term.

$$x_0 = ge^{j\phi_0} + n_0 \quad (2.8)$$

The response for the second sensor may be written in a similar manner.

$$x_1 = ge^{j(\phi_0 + \delta\phi)} + n_1 \quad (2.9)$$

Notice that the second sensor also receives the same satellite signal only shifted in time (i.e. phase). This phase difference is related to the projection of the baseline vector \vec{d} onto

the LOS and the wavelength:

$$\delta\phi = \frac{2\pi}{\lambda} \vec{v} \bullet \vec{d} \quad (2.10)$$

The noise terms n_0 and n_1 are assumed uncorrelated and moreover are assumed to be small compared to the received gain from the satellite signal g . The attitude determi-

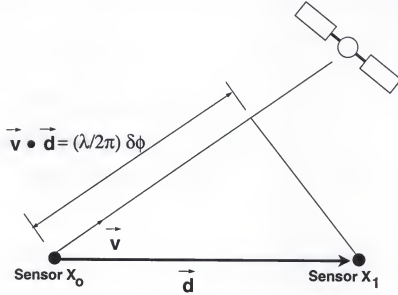


Figure 2.1: A two sensor interferometric system. The baseline vector \vec{d} can be determined by the known LOS vector \vec{v} and the phase difference between the signals measured at the two sensors x_0 and x_1 .

nation problem is to estimate the baseline vector \vec{d} . It is clear to see that by taking the difference $\Delta\phi$ between the phase measured at x_0 and x_1 , then the following relationship between the orientation of the vector \vec{d} , the known LOS vector to the satellite \vec{v} , and the phase difference may be obtained as [6]

$$\Delta\phi = \Phi(x_1) - \Phi(x_0) \quad (2.11)$$

$$\approx \frac{2\pi}{\lambda} (\vec{v} \bullet \vec{d} + k\lambda) \quad (2.12)$$

$$\approx \delta\phi + k(2\pi) \quad (2.13)$$

where $\Phi(\cdot)$ implies taking the phase angle of (\cdot) , i.e.

$$\Phi(\cdot) = -j \ln(\cdot) \quad (2.14)$$

and \approx implies “is approximately equal to.”

The reason that equation (2.13) holds is due to the previous assumption that the amplitude of the interference terms is much smaller than the amplitude of the satellite terms, and therefore the satellite components dominate the phase of the sum of satellite signal and noise. The $k(2\pi)$ term represents the integer portion of the phase difference between the two sensors and is called the “integer ambiguity,” since it cannot be measured. By using at least three sensors (in a non-collinear arrangement) and two satellites [7], the complete attitude of the antenna may be found, once the integer ambiguity values have been found. Several methods (see for example Sutton [8] and its references) exist for resolving the integer ambiguities.

Since the attitude estimation process makes use of knowledge of the LOS vectors to the satellites in the local level frame, a question to consider is the sensitivity to error in the antenna *position* estimate. It turns out that small errors (within typical GPS accuracies) in position estimation will not have a substantial impact on the LOS angles for essentially every ground and air based application. This is due to the large distance to the satellites of approximately 23,000km from the earth’s center. Even for very high altitudes of 100kft, the angular error is negligible.

The extension of equation (2.13) to multiple sensors and satellites provides a straightforward and computationally simple method to estimate the antenna attitude when the assumptions of the signal model are met. However, when an interference source such as a jammer is present, the accuracy quickly degrades. Figure 2.2 indicates the level of degradation a jammer can cause to an attitude determination system. The parameter “mean total error” is the average of the total errors from 500 realizations of the attitude estimation, where the total error is defined as the angular rotation between the estimated attitude (using the attitude estimator defined above) and the true attitude.³ Notice that even with relatively high signal to jammer ratios, the performance is degraded. The

³ Chapter 8 provides a mathematical definition of the mean total error.

fundamental thrust of this dissertation is the development of algorithms that increase the resistance of the attitude estimator to external interference.

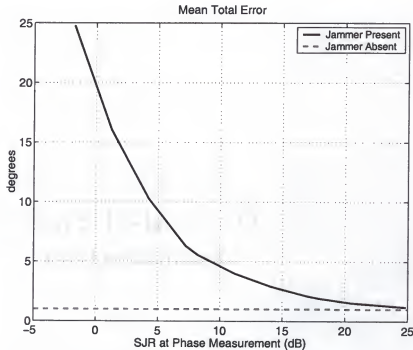


Figure 2.2: Mean Total Error Performance of the conventional attitude estimator vs. signal to jammer ratio (SJR), shown as the solid line. The dotted line represents the performance of the attitude estimator in an unjammed scenario. Performance of the phase difference approach to attitude estimation is degraded even when the SJR is high.

2.4 Direction Finding

The direction finding problem is the determination of the directions of arrival (DOA) of multiple sources impinging on an array of sensors. Since the problem may be viewed as estimating how radiated energy is distributed over space, it is often referred to as “spatial spectral estimation” [9].

Depending upon the application, DOA may be considered as a single parameter (e.g. azimuth angle) or two parameters (azimuth and elevation angle). When the application only requires a single direction parameter, simple antenna topologies like the uniform linear array (ULA) may be employed. Several algorithms make use of this topology to provide computationally efficient estimates of direction. However, since attitude estimation is intrinsically a multidimensional problem requiring full angular information to the

satellite source, little insight can be obtained from these single angle parameter algorithms for the attitude determination application. Therefore, we have limited the discussion of this section to those algorithms that can provide both parameters of direction to the source. This is not to say that the single DOA parameter algorithms are without merit, just that they are not applicable for attitude estimation.

Through the last several decades advances in direction finding theory have been extensive, so much so that even a survey of the major contributions is difficult. One method of gaining insight into these advances is to partition direction finding approaches into the two classes of *maximum likelihood* and *suboptimal*. As is often the case, suboptimal algorithms offer computational savings, but at the cost of reduced performance.

The first algorithms we consider are the maximum likelihood estimators. These optimal estimators may be further partitioned by considering the parameters estimated. The earliest works in this field were improvements to radar and sonar systems that considered the angle and complex amplitude estimation problem for a single source in a jammed environment [10]. These works focused on maximum likelihood estimators approximated by adaptive monopulse ratios (i.e. adapted delta to adapted sum ratio) [11, 12]. Although four unknowns exist in the scenario addressed by these algorithms (two parameters of the complex gain and two of the angle), only a two dimensional search (over the two angle parameters) of the maximum likelihood metric is required, since the complex gain at the solution point can be explicitly expressed in terms of the angle.

More recently, adaptive array technology is beginning to be applied to communication systems to aid in multi-user wireless systems [13]. In this extension of the estimation problem, the unknown parameters estimated are not only the directions and a complex gain, but also an *entire signal waveform* for *multiple* signals impinging simultaneously on the array. For N snapshots of data and L sources, there are $(2N + 2) \times L$ real parameters to estimate (the complex gain is incorporated into the unknown waveform). As with the single source problem, the waveform parameters may be expressed in terms of the unknown angles, resulting in a search of the likelihood function over the $2L$ angular parameters.

Two distinct signal models have been used in the multiple source plus waveform estimation problem, with differing results. The “deterministic” or “conditional” maximum likelihood approach considers the source waveforms to be unknown deterministic signals in an additive Gaussian noise environment. The noise is often assumed temporally uncorrelated, complex circularly symmetric, and spatially white. The mechanization of the maximum likelihood metric for estimating the directions is to fit the subspace spanned by the matrix of array response vectors (also called steering vectors) to the sources to the measurements in a least squares sense [14, 15]. Several direction finding algorithms are cast as variations of the weighted subspace fitting algorithm in Viberg and Ottersten [15].

Some important results have been found concerning the conditional maximum likelihood signal model assumption. First, the direction estimates obtained from this estimator are consistent [16]. Second, because the number of waveform parameters required to estimate increases with each new snapshot of data, the waveform estimates are not consistent, and the estimator is not statistically efficient, i.e. does not achieve the Cramér Rao Bound (CRB), for a finite number of sensors [16]. However, as the number of sensors increases, or the signal to noise ratio increases, this estimator asymptotically approaches the CRB [17].

The “stochastic” or “unconditional” maximum likelihood approach is derived from a model where *both* the signals and the noise are stationary, temporally white, zero-mean complex Gaussian random processes [18]. It has been shown that the unconditional maximum likelihood method is statistically more efficient than the conditional approach [17, 19]. A more computationally efficient implementation that uses a Cholesky decomposition instead of an eigenvalue decomposition is presented in Swindlehurst [18].

The next class to consider is estimation of the directions when the signal waveforms are known *a priori* to the estimation process. This situation occurs in communications systems when a known special preamble is added to a packet of data. In addition, the GPS waveforms fall into this category once code lock is obtained. As expected, significant performance gains may be obtained when the signal waveforms are (to within a complex gain) known as compared to when they must additionally be estimated. In Li [20] and

Li and Compton [21] the CRBs for several cases where the signal waveform is known to within a complex gain (and the gain is either known or partially known) are derived and compared to the CRB when the signal waveform is completely unknown.

Finally, Li et al. show that the estimation process of the directions to the multiple sources may be performed *independently* when each of the source waveforms are uncorrelated with each other [22, 23]. This is the so-called decoupled maximum likelihood, or “DEML” estimator. The DEML is shown to be consistent and asymptotically efficient for uncorrelated waveforms. In addition, the performance of this estimator does not degrade as either the number of signals increases or the angular separation between the sources decreases. The concepts presented in these two works provide the most direct applicability of direction finding to the attitude estimation process derived later in this work, since the GPS $P(Y)$ waveforms are indeed uncorrelated and known, and the number of source (i.e. satellite) waveforms impinging upon the antenna array is typically greater than the number of sensors.

Several suboptimal direction finding algorithms have been introduced in addition to the maximum likelihood methods discussed above, and a few of the more popular algorithms are now briefly discussed. The Multiple Signal Classification (MUSIC) algorithm is based on an eigenvalue decomposition of the sample covariance matrix [24]. The algorithm partitions this eigenvalue decomposition into “signal” and “noise” subspaces and, by observing that steering vectors to the sources present will lie in the signal subspace, estimates directions by minimizing projections of steering vectors onto the noise subspace. Typically, this will involve a two dimensional search across angle. However, for some array topologies a significantly simpler rooting algorithm named PRIME may be employed [25]. An algorithm that relaxes the requirement for a calibrated array (one where the steering vector is known for all possible direction of arrival angles) is the Estimation of Signal Parameters via Rotational Invariance Techniques (ESPRIT) [26]. Although this is typically an azimuth only algorithm and would therefore not meet our discussion criteria, it has been extended to two parameter angle estimation by Swindlehurst and Kailath [27].

Finally, for two excellent survey articles on a variety of direction finding algorithms, the reader is referred to Godara [28] and Krim and Viberg [29]. In addition to a summary of the algorithms, Godara [28] presents several implementation issues common in array processing such as array calibration (knowledge of the exact array response vector), failed sensors, and errors in beamformer weights.

CHAPTER 3 AN ANTI-JAM GPS RECEIVER FOR ATTITUDE DETERMINATION

3.1 Introduction

In this chapter we develop a functional GPS receiver architecture that provides data for both position location and attitude determination in a jammed environment. We apply the following notation when describing the receiver. A *hardware channel* is the portion of the receiver from the antenna through the analog to digital converter, containing the mixers for down conversion, filters, amplifiers, etc. A *satellite channel* performs the Direct Sequence-Spread Spectrum (DS-SS) demodulation, Doppler demodulation, and integration for one satellite. Outputs from the satellite channel are used to keep the satellite waveform in code and Doppler track, as well as to provide data for position location. As an example, a simple single-antenna GPS receiver that can simultaneously track 5 satellites would have (without incorporating any multiplexing) one hardware channel and 5 satellite channels. Using this notation, we review “conventional” attitude determination and anti-jam receivers, and then contrast them with a proposed receiver designed to implement the algorithms of Chapters 4 and 6.

3.2 A GPS Receiver for Anti-Jam Position Location and Attitude

Attitude determination from GPS is based on measuring the satellite time (phase) differences of arrival between multiple sensors. Using the terminology above, an attitude determination system with M antennas that tracks L satellites would have M hardware channels, and (again ignoring multiplexing) L satellite channels per hardware channel. Since phase *differences*, not the absolute phase of the carrier sinusoid, are used to determine attitude, the M hardware channels may be physically separate and independent receivers using different clocks, local oscillators, etc. The output phases from each of

the L satellite channels for all M sensors, with knowledge of the sensor-to-sensor baseline vectors, provide the data necessary for attitude determination in a low interference environment.

Historically, anti-jam antenna arrays have operated as pre-processors to a GPS receiver [3, 30–32]. The function of the anti-jam antenna is to weight and combine the voltages received at the various sensors into one time signal, which is then passed to the single hardware channel. With the interference attenuated by the adaptive array, the tracking loops following the satellite channels are able to keep the satellites in track and provide data for position location. Note that since the anti-jam antenna is often designed as an applique, the post-antenna portion of the GPS receiver operates as if a single sensor had provided the time signal, even though it is actually the linear combination of data from several sensors.

It is clear that a pre-processor type anti-jam antenna, although it uses multiple sensors, does not provide the data required for attitude determination. The data signal presented to the hardware channel is the weighted combination of the data collected by the multiple sensors. Even if the weights are known, determining the satellite phase differences across sensors from the weighted combination of these sensors is an underdetermined problem. However, the receiver can collect the data required for *both* position location and attitude determination by increasing the number of hardware channels and incorporating the weight application into the receiver.

Figure 3.1 shows the top level architecture for one possible GPS system that provides adaptive array-processing levels of anti-jam performance for both position location and attitude determination. This system begins with an array of M sensors. The output of each sensor is downconverted from the GPS carrier frequency to an intermediate frequency (IF), using In-phase (I) and Quadrature (Q) downconversion. The same mixing signals (from the same local oscillator) are used in each of the M hardware channels. The signals in each channel pass through an anti-aliasing matched filter and are sampled in I and Q.

For ease of notation and discussion, we define a *Vector Demodulation* block as a collection of M satellite channels, one per hardware channel, with each block demodulating

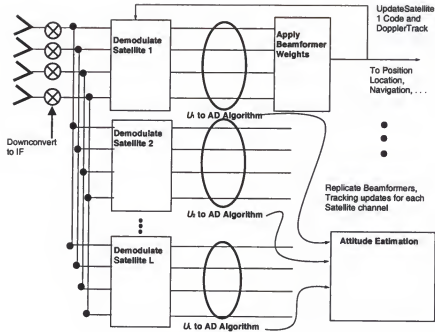


Figure 3.1: Receiver block diagram. Demodulated data are provided to the attitude estimator (shown in the circles) as well as to the beamformers. The beamformer output is used for position location and updating the code and Doppler tracking loops.

the same satellite spreading sequence. It is useful to visualize this process as a block operation on all M signals simultaneously, since the same satellite demodulation sequence is applied to all M signals from the hardware channels. The outputs of this vector demodulator are $M \times 1$ data vectors for the various code delays required to track the satellite signal in time, e.g. an early, punctual, and late delay. More than three code delays may be implemented to increase satellite acquisition time or to provide a quicker reacquisition time if the satellite signal is temporarily lost. For the multi-sensor receiver to process L satellites, it needs L vector demodulators. The outputs of the L vector demodulators, u_i , are used separately for two functions, updating the tracking loops to provide position location information, and as input to the attitude determination algorithm.

Although the demodulator output vectors have received the spread spectrum processing gain, in a jammed environment the signal to interference plus noise ratio (SINR) for each vector element may still be too small for satellite tracking until beamformer weights are applied. By projecting the $M \times 1$ data vectors onto the adaptive beamformer weights, the SINR is increased to an acceptable level to calculate the discriminants used for code

and Doppler tracking. Ignoring the effects of finite precision arithmetic, the beamformer weights may be applied *before* the satellite channel demodulation (as with the anti-jam array pre-processor) or *after* satellite channel demodulation (as is shown here) with equivalent results. In addition, the method proposed here allows for different weights for each satellite, improving tracking performance over a single set of weights for all satellites.

The second use of the data vectors is for attitude determination. As discussed above, attitude determination requires the data from multiple sensors to determine the time (phase) differences. Therefore it must operate on data obtained prior to beamforming, even though this may contain significant interference power, since as mentioned earlier the beamforming operation destroys the individual sensor phases. The algorithms developed in the next section estimate attitude even with the interference present.

In summary, this section developed the top-level architecture for a multi-sensor GPS receiver that combines the anti-jam benefit of adaptive beamforming with development of data required for anti-jam attitude determination algorithms of the next section. This system is like conventional attitude determination systems in that it uses data from multiple sensors and hardware channels. However, it differs in that adaptive weights are applied after the satellite channel demodulation, and that the data passed to attitude determination algorithms are the complex data vectors for each satellite and sensor, not just the phase information. This system is similar to an adaptive array pre-processor architecture, but differs in that multiple hardware channels (instead of a single channel) are employed, and the array weights are applied after demodulation.

CHAPTER 4 MAXIMUM LIKELIHOOD ATTITUDE ESTIMATION

4.1 Introduction

In this chapter we derive a new method of for GPS based attitude estimation. This method uses the receiver construct developed in Chapter 3. Motivated by Figure 2.2, the desire is to develop an attitude estimator that is jammer resistant. This development begins by evaluating the mathematics of jammer resistant direction finding algorithms, and using this background re-derives the approaches in terms of the attitude estimation field.

This chapter is organized as follows. Section 4.2 provides a discussion of the signal models and notation used throughout this chapter. In section 4.3 the multi-source direction finding problem is reviewed, to introduce the multi-source maximum likelihood method. Specifically in this section the task at hand is to develop direction estimates to each satellite in view. Section 4.4 presents some new and modified concepts that are required for the new attitude estimator, which is developed in section 4.5. Finally, section 4.6 provides a discussion of this estimator and some graphical illustrations of its performance.

4.2 Notation, Preliminaries, and Signal Model

We begin this section by reviewing the matrix and vector notation used throughout this work.

\mathbf{A}^T = the transpose of the matrix \mathbf{A}

\mathbf{A}^H = the conjugate transpose of \mathbf{A}

$\mathbf{A} \otimes \mathbf{B}$ = the Kronecker (Tensor) product of \mathbf{A} and \mathbf{B}

\mathbf{I}_j = the $j \times j$ identity matrix

$\mathbf{0}_j$ = the $j \times j$ matrix of zeros

$\mathbf{A} > 0$ = \mathbf{A} is positive definite

$\mathbf{Z} \in \mathcal{C}^{a \times b}$ = \mathbf{Z} is a complex matrix of size $a \times b$

$$\text{diag}[\gamma_1, \dots, \gamma_L] = \begin{bmatrix} \gamma_1 & 0 & 0 \\ 0 & \ddots & 0 \\ 0 & 0 & \gamma_L \end{bmatrix}$$

$\mathbf{q}_1 \star \mathbf{q}_2$ = quaternion multiplication

$\text{TR}(\mathbf{A})$ = trace of \mathbf{A}

In addition, the following variables are consistently used in the following roles.

L = the number of satellites being tracked

M = the number of sensors in the array

N = the number of snapshots of data available

(4.1)

Consider the following popular baseband model for the signals received by the M element array of antennas. The total data, $\mathbf{x}(t)$, received by the M elements are composed of the contributions from each of the L satellites, $\mathbf{p}_l(t)$, and the interference $\mathbf{n}(t)$:

$$\mathbf{x}(t_n) = \sum_{l=1}^L \mathbf{p}_l(t_n) + \mathbf{n}(t_n), \quad n = 1, \dots, N \quad (4.2)$$

where $\mathbf{x}(t)$, $\mathbf{p}_l(t)$, and $\mathbf{n}(t) \in \mathcal{C}^{M \times 1}$. We now build up $\mathbf{p}_l(t)$ by its components. Let γ_l represent an unknown complex gain and θ_l the direction corresponding to the l th satellite source. The direction θ_l , which is always referenced in the antenna frame, is completely specified by two parameters. To illustrate this, consider an antenna located at the origin of the antenna coordinate system. The vector from the antenna to any source can be described in spherical coordinates by a distance and two angular parameters, say r , φ_1 , and φ_2 . Then the two angles φ_1 and φ_2 comprise θ , and the LOS unit vector $\boldsymbol{\nu} = [\nu_x \ \nu_y \ \nu_z]^T$ in antenna coordinates is found from:

$$\boldsymbol{\nu} = \begin{bmatrix} \cos(\varphi_1) \cos(\varphi_2) \\ \cos(\varphi_1) \sin(\varphi_2) \\ \sin(\varphi_1) \end{bmatrix} \quad (4.3)$$

The array response vector (spatial steering vector), $\mathbf{a}(\theta_l)$, is defined as the response of the array to a signal impinging from direction θ_l , including both the gain and phase response of the array. Using this definition the array response vector can be written in terms of the components of $\boldsymbol{\nu}$ and a series of vectors $\mathbf{b}_i, i = 1, \dots, M$ from the array reference point to the sensor locations.

$$\mathbf{a}(\theta) = \begin{bmatrix} e^{j\frac{2\pi}{\lambda} \mathbf{b}_1^T \boldsymbol{\nu}} \\ e^{j\frac{2\pi}{\lambda} \mathbf{b}_2^T \boldsymbol{\nu}} \\ \vdots \\ e^{j\frac{2\pi}{\lambda} \mathbf{b}_M^T \boldsymbol{\nu}} \end{bmatrix} \quad (4.4)$$

The signal from the l th satellite, $s_l(t)$, contains the sampled spreading waveform $d_l(t)$, and the sampled Doppler $e^{j\omega_{d_l} t}$ referenced at the array reference point, defined as the origin of the antenna frame.

$$s_l(t_n) = d_l(t_n) e^{j\omega_{d_l} t_n} \quad n = 1, \dots, N \quad (4.5)$$

Lastly, $\beta_l(t)$ is the low rate (50 Hz for GPS) data sequence that modulates the fast rate spreading waveform.

Using these definitions, the vector representation of the signal received from source l at the M sensors is

$$\mathbf{p}_l(t_n) = \gamma_l \beta_l(t_n) \mathbf{a}(\theta_l) s_l(t_n), \quad n = 1, \dots, N \quad (4.6)$$

For this analysis, we assume that $\beta_l(t)$ is constant over the period of interest, and include this constant in the unknown gain γ_l . If the data bit is not constant but its values are known, they can be included in the waveform sequence $s_l(t_n)$. Equation (4.2) may now be written in a more compact form as

$$\begin{aligned} \mathbf{x}(t_n) &= \sum_{l=1}^L \gamma_l \mathbf{a}(\theta_l) s_l(t_n) + \mathbf{n}(t_n) \\ &= \mathbf{A}(\boldsymbol{\Theta}) \boldsymbol{\Gamma} \mathbf{s}(t_n) + \mathbf{n}(t_n) \quad n = 1, \dots, N \end{aligned} \quad (4.7)$$

where

$$\begin{aligned} \boldsymbol{\Theta} &= [\theta_1, \theta_2, \dots, \theta_L] \\ \mathbf{A}(\boldsymbol{\Theta}) &= [\mathbf{a}(\theta_1), \mathbf{a}(\theta_2), \dots, \mathbf{a}(\theta_L)] \\ \boldsymbol{\Gamma} &= \text{diag}[\gamma_1, \gamma_2, \dots, \gamma_L] \\ \mathbf{s}(t_n) &= [s_1(t_n), s_2(t_n), \dots, s_L(t_n)]^T \end{aligned} \quad (4.8)$$

and the time varying components of the satellite signals at time t_n are contained in $\mathbf{s}(t_n)$.

The signal portion of the received data from each source may be interpreted as the Kronecker product of the $M \times 1$ *spatial steering vector* $\mathbf{a}(\theta_l)$ and the $1 \times N$ *temporal steering vector* \mathbf{y}_l for each source (we use \mathbf{y}_l for the temporal steering vector to minimize confusion with the column vector $\mathbf{s}(t)$, which contains information from all sources at time t).

$$\mathbf{y}_l = [s_l(t_1), s_l(t_2), \dots, s_l(t_N)] \quad (4.9)$$

This product is the so-called *space-time steering vector* $\mathbf{v}(\theta_l, \mathbf{y}_l)$ [33],

$$\mathbf{v}(\theta_l, \mathbf{y}_l) = [y_l(t_1) \mathbf{a}^T(\theta_l), y_l(t_2) \mathbf{a}^T(\theta_l), \dots, y_l(t_N) \mathbf{a}^T(\theta_l)]^T \quad (4.10)$$

which may be written concisely as

$$\mathbf{v}(\theta_l, \mathbf{y}_l) = \mathbf{a}(\theta_l) \otimes \mathbf{y}_l \quad (4.11)$$

Using this notation allows us to write the $MN \times 1$ received data vector in terms of the space-time steering vectors, complex gains, and additive interference.

$$\mathbf{x} = \sum_{l=1}^L \gamma_l \mathbf{v}(\theta_l, \mathbf{y}_l) + \mathbf{n} \quad (4.12)$$

where \mathbf{x} and $\mathbf{n} \in \mathcal{C}^{MN \times 1}$ as below.

$$\mathbf{x} = [\mathbf{x}^T(t_1), \mathbf{x}^T(t_2), \dots, \mathbf{x}^T(t_N)]^T \quad (4.13)$$

$$\mathbf{n} = [\mathbf{n}^T(t_1), \mathbf{n}^T(t_2), \dots, \mathbf{n}^T(t_N)]^T \quad (4.14)$$

The model for the interference is left relatively unstructured, allowing for thermal noise, multiple jammers, and other interfering signals. We assume that the interference noise waveform vector, $\mathbf{n}(t)$, $\mathbf{n} \in \mathcal{C}^{M \times 1}$, is zero mean, wide sense stationary, and circularly symmetric complex Gaussian with covariance matrix \mathbf{R}_s , where the subscript “s” implies the spatial, i.e. sensor to sensor covariance. The interference is uncorrelated from all satellite signals. Moreover, we assume the interference is temporally uncorrelated. Since thermal noise will exist in the sensors’ data, it is safe to assume that $\mathbf{R}_s(0)$ is positive definite. These conditions on the interference may be concisely stated as

$$\mathbb{E}[\mathbf{n}(t)] = 0 \quad (4.15)$$

$$\mathbb{E}[\mathbf{n}(t_i) \mathbf{n}^T(t_j)] = \mathbf{0}_M \quad (4.16)$$

$$\begin{aligned} \mathbb{E}[\mathbf{n}(t_i) \mathbf{n}^H(t_j)] &\triangleq \mathbf{R}_s(t_i - t_j) \\ &= \mathbf{R}_s(0) \delta_{t_i - t_j} \end{aligned} \quad (4.17)$$

$$\mathbf{R}_s(0) > 0 \quad (4.18)$$

These assumptions are common for analysis involving jamming or other interfering signals [21, 22] and are less restrictive than those of many works on direction finding for communication systems [16, 34] which require \mathbf{R}_s to be a (scaled) identity matrix, i.e.

$\mathbf{R}_s = \sigma^2 \mathbf{I}$. A final assumption is that the interference covariance is known. In practice, it is not known, but can be estimated. A method of estimating the statistics of the interference is presented in Appendix B.

4.3 Maximum Likelihood Direction Estimation

In general, the task is to estimate $6L$ parameters from the N samples of the data vector $\mathbf{x}(t)$, these being two parameters of the direction θ_l , the real and imaginary components of the complex gain γ_l , and the appropriate delay and Doppler of the temporal steering vector for each source. However, the problem may be simplified by assuming that accurate delay and Doppler estimates are provided from the receiver code and phase tracking loops, providing $\hat{\mathbf{y}}_l$ as the estimate of the temporal steering vector to source l . This leaves $4L$ real parameters to estimate from the MN data samples.

This estimation begins by examining the likelihood function. In general, the space-time likelihood function conditioned on the unknown parameters Θ and Γ is

$$f(\mathbf{x}|\Theta, \Gamma) = \frac{1}{\pi^{(MN)}|\mathbf{R}_{st}|} \exp \left[-[\mathbf{x} - \Upsilon(\Theta, \Gamma)]^H \mathbf{R}_{st}^{-1} [\mathbf{x} - \Upsilon(\Theta, \Gamma)] \right] \quad (4.19)$$

where

$$\Upsilon(\Theta, \Gamma) = \sum_{l=1}^L \gamma_l \mathbf{v}(\theta_l, \mathbf{y}_l) \quad (4.20)$$

The parameters $\hat{\Theta}$ and $\hat{\Gamma}$ that maximize (4.19) are defined to be the maximum likelihood (ML) estimates of Θ and Γ [35]. The space-time interference covariance matrix \mathbf{R}_{st} contains the interference covariances between all sensors $m = 1, \dots, M$ at all times $t = 1, \dots, N$, such that the ij th M by M block is $E[\mathbf{n}(t_i)\mathbf{n}^H(t_j)]$ [36].

By employing the assumption made in (4.17) that the interference is temporally white, the space-time covariance matrix takes on a block diagonal structure, which serves to decompose the argument of the exponential into the sum of the individual time components.

$$\mathbf{R}_{st} = \begin{bmatrix} \mathbf{R}_s & 0 & \cdots & 0 \\ 0 & \mathbf{R}_s & 0 & 0 \\ 0 & \cdots & \ddots & 0 \\ 0 & \cdots & 0 & \mathbf{R}_s \end{bmatrix} \quad (4.21)$$

Taking the negative of the natural logarithm of (4.19), and dropping the constant terms produces the familiar log likelihood ratio (LLR).

$$\text{LLR} = \sum_{n=1}^N [\mathbf{x}(t_n) - \mathbf{A}(\boldsymbol{\Theta})\boldsymbol{\Gamma}\mathbf{y}(t_n)]^H \mathbf{R}_s^{-1} [\mathbf{x}(t_n) - \mathbf{A}(\boldsymbol{\Theta})\boldsymbol{\Gamma}\mathbf{y}(t_n)] \quad (4.22)$$

Since maximizing (4.19) is equivalent to minimizing (4.22), the estimates $\hat{\boldsymbol{\Theta}}$ and $\hat{\boldsymbol{\Gamma}}$ are found as

$$\hat{\boldsymbol{\Theta}}, \hat{\boldsymbol{\Gamma}} = \arg \min_{\boldsymbol{\Theta}, \boldsymbol{\Gamma}} \sum_{n=1}^N [\mathbf{x}(t_n) - \mathbf{A}(\boldsymbol{\Theta})\boldsymbol{\Gamma}\mathbf{y}(t_n)]^H \mathbf{R}_s^{-1} [\mathbf{x}(t_n) - \mathbf{A}(\boldsymbol{\Theta})\boldsymbol{\Gamma}\mathbf{y}(t_n)] \quad (4.23)$$

A significant factor in the estimation of the directions to the satellites (and later, the attitude) is the knowledge of the satellite waveform. Since the waveforms are known, the received data may be de-spread and integrated, increasing the signal to interference ratio. This is accomplished when the estimated temporal steering vector is used to de-spread the signal. De-modulation of the Doppler and spreading sequence is achieved by projecting the data from each sensor onto the estimated temporal steering (row) vector $\hat{\mathbf{y}}_i$ for each source. This process occurs in the “vector demodulators” of Figure 3.1.

As shown in figure 3.1, let \mathbf{u}_i represent this normalized projection onto the $M \times N$ data matrix \mathbf{X} , which is formed by reorganizing the $MN \times 1$ received data vector \mathbf{x} such that the columns correspond to the time snapshots as shown below.

$$\mathbf{u}_i = \frac{\mathbf{X}\hat{\mathbf{y}}_i^H}{\varepsilon_i} \quad (4.24)$$

where

$$\mathbf{X} = [\mathbf{x}(t_1), \mathbf{x}(t_2), \dots, \mathbf{x}(t_N)] \quad (4.25)$$

$$\begin{aligned} \varepsilon_l &= \hat{\mathbf{y}}_l \hat{\mathbf{y}}_l^H \\ &= \sum_{n=1}^N \hat{y}_l(t_n) \hat{y}_l^*(t_n) \end{aligned} \quad (4.26)$$

Each of these projections are normalized by the energy ε_l in the l th source. This is a common normalization and is chosen so that the power in the integrated signal snapshots remains constant, while the signal to interference plus noise ratio (SINR) increases linearly with the number of samples integrated. That is, if $\text{SINR}_l(N)$ is the SINR in the l th satellite component of the data vector \mathbf{u}_l for an integration of N samples, then

$$\frac{\text{SINR}_l(N+1)}{\text{SINR}_l(N)} = \frac{N+1}{N} \quad (4.27)$$

Unless otherwise stated, the remainder of this work assumes that the receiver maintains track on all satellites used for direction or attitude estimation in both time (code) and frequency (Doppler). This allows the substitution $\hat{\mathbf{y}}_l = \mathbf{y}_l$ for $l = 1, \dots, L$. This assumption is justified because the adaptive beamformer, which follows the satellite channel, mitigates the effects of jammers.

We conclude this section by developing concise expressions for the unknown parameters. To review, the problem is to determine, for each of the L satellites, the 2 components of the direction vector and the 2 components (real and imaginary) of the complex gain. It can be shown [22] that if the signal waveforms are uncorrelated, as is the case with the waveforms employed by the satellites, that this multidimensional estimation problem decomposes to a series of decoupled estimations of individual source parameters. At the stationary point corresponding to the (as yet unknown) estimate of direction $\hat{\theta}_l$, the complex gain is found to be

$$\hat{\gamma}_l = \frac{\mathbf{a}^H(\hat{\theta}_l) \mathbf{R}_s^{-1} \mathbf{u}_l}{\mathbf{a}^H(\hat{\theta}_l) \mathbf{R}_s^{-1} \mathbf{a}(\hat{\theta}_l)} \quad l = 1, \dots, L \quad (4.28)$$

and the estimator for θ_l is

$$\hat{\theta}_l = \arg \max_{\theta_l} \frac{|\mathbf{a}^H(\theta_l) \mathbf{R}_s^{-1} \mathbf{u}_l|^2}{\mathbf{a}^H(\theta_l) \mathbf{R}_s^{-1} \mathbf{a}(\theta_l)} \quad l = 1, \dots, L \quad (4.29)$$

Equation (4.29) provides the means to independently estimate the directions of arrival of each of the satellites in view, and concludes the review of direction finding.

4.4 New Concepts

Direction finding, in loose terms, states that the information provided by each source (satellite), through the differences in time or phase of the source signal as received across the sensors, is a *direction*. However, for the GPS attitude determination task consider the new concept that each satellite directly provides an (ambiguous) estimate of the antenna *attitude* when the known direction to the satellite in the local-level frame is included in the estimation process.

An Alternate Array Response Vector

We begin by re-examining the array response vector \mathbf{a} . Previously this was defined as a function of the two parameter valued θ , which was derived from the line of sight vector $\boldsymbol{\nu}$ (in the antenna frame) to the source, as shown in equation (4.4). Indeed, for the last 30 years or so of array processing the argument of the array response vector has been the angular direction to the source. However, another equally valid method of parameterizing this expression is in terms of the line of sight vector in the *local level frame* and the *antenna attitude*. These two LOS vectors (using the subscripts B and LL to denote body frame and local level frame, respectively) are related by the direction cosine matrix that transforms vectors in local level frame to body frame. The direction cosines that comprise the direction cosine matrix are, of course, defined by the body attitude, q .

$$\boldsymbol{\nu}_B = \mathbf{Q}(q) \boldsymbol{\nu}_{LL} \quad (4.30)$$

The new array response vector parameterized on antenna *attitude* is then written as

$$\mathbf{a}(\boldsymbol{\nu}_{LL}, q) = \begin{bmatrix} e^{j\frac{2\pi}{\lambda}} \mathbf{b}_1^T \mathbf{Q}(q) \boldsymbol{\nu}_{LL} \\ e^{j\frac{2\pi}{\lambda}} \mathbf{b}_2^T \mathbf{Q}(q) \boldsymbol{\nu}_{LL} \\ \vdots \\ e^{j\frac{2\pi}{\lambda}} \mathbf{b}_M^T \mathbf{Q}(q) \boldsymbol{\nu}_{LL} \end{bmatrix} \quad (4.31)$$

For the GPS attitude determination application, this method of parameterization is preferred since the line of sight vectors are known in inertial frame, and the body attitude is the desired quantity. It is important to note that when the antenna is actually at the orientation incorporated in the second method, the two array response vectors are identical:

$$\mathbf{a}(\theta_l) = \mathbf{a}(\boldsymbol{\nu}_l, q) \quad (4.32)$$

This redefinition of the array response vector is a critical step in the development of the estimator of the next section. Notice that the directions to the sources in the antenna frame no longer appear in the array response vector, and supports the earlier claim that this algorithm is not strictly a direction finding algorithm. However, this new parameterization introduces a complication not found when parameterized by direction: attitude ambiguity.

Attitude Ambiguity

The attitude ambiguity resulting from the new definition of the array response vector is the manifestation of the fact that attitude cannot be uniquely resolved when using information from only a single satellite source. A useful visualization of this ambiguity is obtained by imagining the LOS vector from the array reference to the satellite source as a “stick,” and this stick is “glued” to the array of sensors at the array reference point. With this physical model the family of possible attitudes is obtained by “twirling the stick” while keeping it pointed at the satellite source, as shown in Figure 4.1.

Mathematically, this ambiguity can be obtained from the quaternion representation of attitude. Let $\hat{\mathbf{q}}$ represent the true attitude of the antenna. The locus of possible attitudes can be determined by the true attitude, the LOS to the satellite source, and a scalar

variable ω where $-\pi \leq \omega < \pi$. Using these factors, the ambiguity in attitude from the new array response vector definition may be represented as

$$\mathbf{a}(\hat{\mathbf{q}}, \nu) = \mathbf{a} \left(\left(\check{\mathbf{q}}(\omega) \star \hat{\mathbf{q}} \right), \nu \right) \quad (4.33)$$

where, from equations (2.5) and (4.3),

$$\check{\mathbf{q}}(\omega) = \begin{bmatrix} \sin(\frac{\omega}{2})\nu \\ \cos(\frac{\omega}{2}) \end{bmatrix} \quad (4.34)$$

and \star represents quaternion multiplication.

Fortunately, this ambiguity can be completely resolved by using *two* non-co-located sources. This is again consistent with standard GPS attitude determination theory, which states that the minimum number of satellites required for attitude determination is two [7]. Appendix A proves this fact.

Since another common phenomenon in GPS based attitude determination is *integer* ambiguity, it is worthwhile to take a moment to clearly delineate the difference between the integer and attitude ambiguities. The integer ambiguity arises when the sensors are spaced farther apart than the Nyquist sampling limit. When this occurs, the spatial spectrum is undersampled, and possibly several discrete attitudes would produce the same phase differences across the antenna array. This is the same phenomena as the antenna design term *grating lobes*. As shown above and in Figure 4.2, the attitude ambiguity in the *array response vector* is actually a continuum of possible attitudes, not a finite discrete set as in the case of the integer ambiguity.

4.5 Maximum Likelihood Attitude Estimation

With the re-parameterization of the array response vector, we now proceed with the development of the maximum likelihood attitude estimator. The observables for this algorithm are the vector outputs of the satellite channels, i.e. the demodulated and integrated data vectors \mathbf{u}_i . There are two reasons this algorithm only considers the demodulated and integrated data vectors. First, the spreading sequence and Doppler

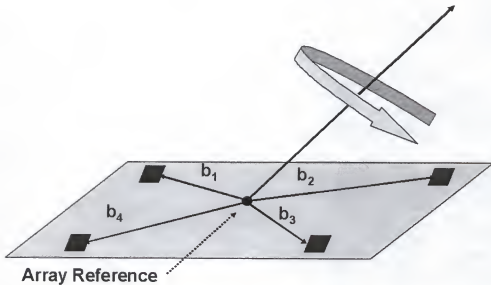


Figure 4.1: Visualization of the possible (ambiguous) attitudes corresponding to a single source. The possible array attitudes can be found by “twirling” the LOS vector, which is assumed affixed to the array, while keeping it pointed at the satellite source.

demodulation is typically implemented in hardware [37]. Second, the GPS signal is too weak to evaluate before significant integration.

Recall from equations (4.12) and (4.24) that \mathbf{u}_l , $l = 1, 2, \dots, L$ contains contributions from all satellites and interference. We denote the signal contribution from the l th satellite as \mathbf{z}_l and the interference (including jammers, thermal noise, and the multiple access interference from other satellites) as \mathbf{w}_l , so that

$$\mathbf{u}_l = \mathbf{z}_l + \mathbf{w}_l \quad (4.35)$$

where

$$\begin{aligned} \mathbf{z}_l &= \frac{1}{\varepsilon_l} \gamma_l \mathbf{a}(\nu_l, \hat{q}) \mathbf{y}_l \hat{\mathbf{y}}_l^H \\ &= \gamma_l \mathbf{a}(\nu_l, \hat{q}) \end{aligned} \quad (4.36)$$

and

$$\mathbf{w}_l = \frac{1}{\varepsilon_l} \left[\mathbf{n}(t_1), \mathbf{n}(t_2), \dots, \mathbf{n}(t_N) \right] + \sum_{p=1, p \neq l}^L \gamma_p \mathbf{a}(\nu_p, \hat{q}) \mathbf{y}_p \hat{\mathbf{y}}_p^H \quad (4.37)$$

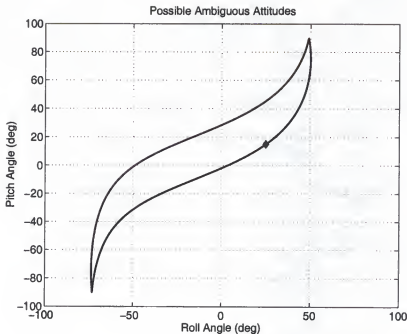


Figure 4.2: Possible roll and pitch Euler angles arising from the ambiguity in the new array response vector (yaw angles not shown). The true roll is 25 degrees, and the true pitch is 15 degrees, as indicated by the diamond. The locus of possible attitudes is determined by the LOS to the source and the true attitude. A different source LOS would have a different ambiguity.

and $\hat{\mathbf{q}}$ represents the actual (true) attitude of the antenna array. As was assumed previously, the signals are assumed in track such that $\hat{\mathbf{y}}_l$ is essentially \mathbf{y}_l . It is clear that \mathbf{u}_l is a consistent estimator of \mathbf{z}_l . Just as with the thermal noise and jammer signals we consider \mathbf{w}_l to be a zero mean, circularly symmetric, complex vector of Gaussian random variables.¹

$$E[\mathbf{w}_l] = 0 \quad (4.38)$$

$$E[\mathbf{w}_l \mathbf{w}_l^T] = 0 \quad (4.39)$$

Using these, we define the *space-satellite data vector*, \mathbf{U} , of the received data as

¹ Using this model for the multiple access interference is similar to approaches used for bit error analysis of multi-user communication systems.

$$\mathbf{U} = \begin{bmatrix} \mathbf{u}_1 \\ \mathbf{u}_2 \\ \vdots \\ \mathbf{u}_L \end{bmatrix} \quad (4.40)$$

\mathbf{Z} and \mathbf{W} , the components of \mathbf{U} , are similarly defined as

$$\mathbf{Z} = \begin{bmatrix} \mathbf{z}_1 \\ \mathbf{z}_2 \\ \vdots \\ \mathbf{z}_L \end{bmatrix} \quad (4.41)$$

$$\mathbf{W} = \begin{bmatrix} \mathbf{w}_1 \\ \mathbf{w}_2 \\ \vdots \\ \mathbf{w}_L \end{bmatrix} \quad (4.42)$$

such that

$$\mathbf{U} = \mathbf{Z} + \mathbf{W} \quad (4.43)$$

Finally, let \mathbf{R}_{ss} denote the $ML \times ML$ space-satellite covariance formed from \mathbf{W} as

$$\mathbf{R}_{ss} = \mathbf{E} [\mathbf{W}\mathbf{W}^H] \quad (4.44)$$

As with the direction finding example earlier, the attitude estimation problem is cast in terms of the log likelihood function. However, now the LLR is a parameterized by the antenna attitude and the complex gains, and as with any likelihood function the true parameter (i.e. the true attitude \hat{q}) is replaced with a variable (q), the parameter to be estimated:

$$\text{LLR} = [\mathbf{U} - \mathbf{Z}(\Gamma, q)]^H \mathbf{R}_{ss}^{-1} [\mathbf{U} - \mathbf{Z}(\Gamma, q)] \quad (4.45)$$

Using the results of Appendix B, the $ML \times ML$ space-satellite interference covariance matrix asymptotically reduces to a block diagonal structure of $M \times M$ blocks:

$$\mathbf{R}_{ss} = \begin{bmatrix} \mathbf{C}_1 & 0 & \cdots & 0 \\ 0 & \mathbf{C}_2 & 0 & 0 \\ 0 & \cdots & \ddots & 0 \\ 0 & \cdots & 0 & \mathbf{C}_L \end{bmatrix} \quad (4.46)$$

Therefore as N becomes large, the LLR asymptotically approaches the following sum of terms:

$$\text{LLR} \simeq \sum_{l=1}^L [\mathbf{u}_l - \gamma_l \mathbf{a}(\boldsymbol{\nu}_l, q)]^H \mathbf{C}_l^{-1} [\mathbf{u}_l - \gamma_l \mathbf{a}(\boldsymbol{\nu}_l, q)] \quad (4.47)$$

Notice that we have reparameterized the LLR in terms of the known satellite LOS directions in the inertial frame, the desired attitude q , and now the unknown complex gains γ_l .

As with the direction finding application, a closed form expression for γ_l at a stationary point may be obtained by setting the partial derivative of (4.47) with respect to γ_l equal to zero and solving for γ_l in terms of q .

$$\hat{\gamma}_l = \frac{\mathbf{a}^H(\boldsymbol{\nu}_l, q) \mathbf{C}_l^{-1} \mathbf{u}_l}{\mathbf{a}^H(\boldsymbol{\nu}_l, q) \mathbf{C}_l^{-1} \mathbf{a}(\boldsymbol{\nu}_l, q)} \quad (4.48)$$

Substituting this into equation (4.47) produces in equation (4.49) the Maximum Likelihood Attitude Estimator (MLAE):

$$\hat{q} = \arg \min_q \sum_{l=1}^L [\mathbf{u}_l - \hat{\gamma}_l \mathbf{a}(\boldsymbol{\nu}_l, q)]^H \mathbf{C}_l^{-1} [\mathbf{u}_l - \hat{\gamma}_l \mathbf{a}(\boldsymbol{\nu}_l, q)] \quad (4.49)$$

One way to view this expression is that it produces a "metric" value at every possible attitude, and the attitude with the lowest metric value is chosen as the estimate.

We now present three alternate forms of the MLAE. The first alternate method of expressing the MLAE is found by expanding the summation above:

$$\begin{aligned} \hat{q} = \min_q \sum_{l=1}^L \mathbf{u}_l^H \mathbf{C}_l^{-1} \mathbf{u}_l - \hat{\gamma}_l^* \mathbf{a}(\boldsymbol{\nu}_l, q)^H \mathbf{C}_l^{-1} \mathbf{u}_l & - \\ \hat{\gamma}_l \mathbf{u}_l^H \mathbf{C}_l^{-1} \mathbf{a}(\boldsymbol{\nu}_l, q) + \hat{\gamma}_l \hat{\gamma}_l^* \mathbf{a}(\boldsymbol{\nu}_l, q)^H \mathbf{C}_l^{-1} \mathbf{a}(\boldsymbol{\nu}_l, q) & \quad (4.50) \end{aligned}$$

and substituting in the expression for the estimate of the complex gain, $\hat{\gamma}$, from (4.48) to produce

$$\hat{q} = \arg \max_q \sum_{l=1}^L \frac{|\mathbf{a}(\nu_l, q)]^H \mathbf{C}_l^{-1} \mathbf{u}_l|^2}{\mathbf{a}^H(\nu_l, q) \mathbf{C}_l^{-1} \mathbf{a}(\nu_l, q)} \quad (4.51)$$

A simpler form of the expression may be written using the shortened form of the array response vector:

$$\mathbf{a}_l = \mathbf{a}(\nu_l, q) \quad (4.52)$$

A "whitened" array response vector may be written in shortened form as well:

$$\tilde{\mathbf{a}}_l = \mathbf{C}_l^{-1/2} \mathbf{a}_l(\nu_l, q) \quad (4.53)$$

where

$$\mathbf{C}_l = \mathbf{C}_l^{1/2} \mathbf{C}_l^{1/2} \quad (4.54)$$

$$\mathbf{C}_l^{1/2} = \left(\mathbf{C}_l^{1/2} \right)^H \quad (4.55)$$

Using these definitions, (4.51) may be rewritten as

$$\hat{q} = \arg \max_q \sum_{l=1}^L \frac{|\mathbf{u}_l^H \mathbf{C}_l^{-1/2} \tilde{\mathbf{a}}_l(q)|^2}{|\tilde{\mathbf{a}}_l(q)|^2} \quad (4.56)$$

$$= \arg \max_q \sum_{l=1}^L \mathbf{u}_l^H \mathbf{C}_l^{-1/2} \mathbf{P}_{\tilde{\mathbf{a}}_l(q)} \mathbf{C}_l^{-1/2} \mathbf{u}_l \quad (4.57)$$

where

$$\mathbf{P}_{\tilde{\mathbf{a}}_l(q)} = \frac{\tilde{\mathbf{a}}_l(q) \tilde{\mathbf{a}}_l^H(q)}{\tilde{\mathbf{a}}_l^H(q) \tilde{\mathbf{a}}_l(q)} \quad (4.58)$$

Finally, a very compact expression for this estimator for q may be written as

$$\hat{q} = \arg \min_q \sum_{l=1}^L \text{TR}[\mathbf{P}_l \mathbf{C}_l^{-1}] \quad (4.59)$$

where

$$\mathbf{P}_l = [\mathbf{u}_l - \hat{\gamma}_l \mathbf{a}(\nu_l, q)] [\mathbf{u}_l - \hat{\gamma}_l \mathbf{a}(\nu_l, q)]^H \quad (4.60)$$

4.6 Discussion

The most salient observation of this estimator is that the likelihood metric is defined as a function of the antenna (body) attitude. Directions to sources in the antenna

frame are not a part of this estimator. Regardless of how parameterized (Euler angles, quaternion, rotation matrix, etc.), the attitude that minimizes (4.49) is the maximum likelihood estimate of the antenna attitude, and since the space-satellite covariance matrix is (for large sample numbers) block diagonal, the estimator decomposes to a sum of terms, each of which contains contributions from a single satellite.

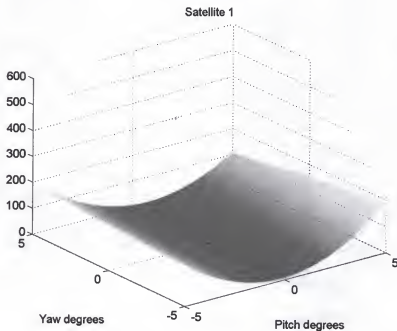


Figure 4.3: Contribution to the value of the maximum likelihood attitude estimator of equation (4.49) from the first of seven satellites in view. This satellite provides little information about yaw, and the most in the positive pitch - negative yaw to negative pitch - positive yaw dimension.

To provide insight into the operation of the estimator, examine these contributions in a neighborhood near the true attitude. When the LOS to an interference source is close to that of the satellite, intuitively the contribution of this satellite to the final solution should be small. Indeed, this is the case with this estimator. In the neighborhood of the true attitude, the contribution to the metric of satellites close to an interference source varies much less than the contribution from those with a large spatial separation from interfering signals. Visually, this causes the metric to appear flatter across attitude, and therefore contribute less to the final attitude estimate. The shape of the likelihood metric contribution from a particular satellite is not uniformly steep or flat across all attitude

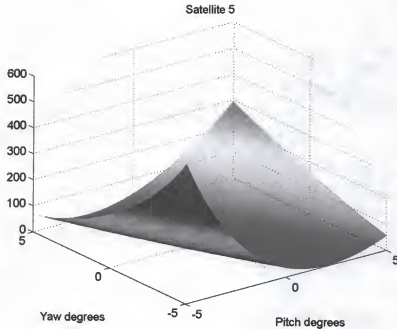


Figure 4.4: Contribution to the value of the maximum likelihood attitude estimator from the fifth of seven satellites in view. This satellite provides little information in the positive pitch - negative yaw to negative pitch - positive yaw dimension, incidentally the dimension satellite in which satellite one provided the most information.

dimensions, but varies with the amount of attitude information that satellite provides in each dimension. For example, in a non-jammed scenario a satellite directly above a level antenna array provides little information about the antenna yaw angle. Similarly, the location of jammers may decrease the amount and type of attitude information a satellite may provide. In effect, the estimator is weighting each satellite's contributions to the attitude estimate by the amount and type of information that they are able to provide.

This phenomena may be observed in Figures 4.3, 4.4, 4.5, and 4.6. Figures 4.3, 4.4, and 4.5, depict the contribution of three individual satellites to the likelihood "metric" as a function of yaw and pitch. Only the two attitude dimensions yaw and pitch are shown for graphical reasons; for the plots the metric is evaluated at the true roll angle. The true attitude in Euler angles is $[0 \ 0 \ 0]$, i.e. the local level frame. Note that the individual satellite contributions contain regions where they provide high quality information (i.e. a steep slope across a dimension) and regions which contribute little information (little slope or flat). When the individual contributions are combined, one satellite's weakness may

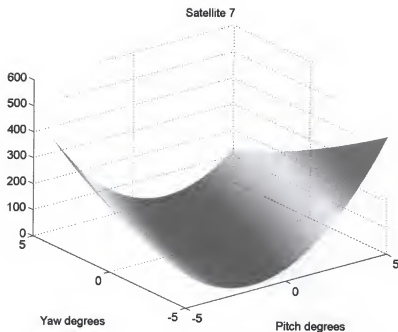


Figure 4.5: Contribution to the value of the maximum likelihood attitude estimator from the seventh of seven satellites in view.

be compensated by another's strength, producing the steep slope in all dimensions easily observable from Figure 4.6.

The nature of the likelihood metric has implementation benefits as well. This separable by satellite structure provides a framework for parallel computations, where for a given attitude under test, the terms of the likelihood for each satellite could be computed simultaneously on multiple processors. In addition, should the receiver lose lock on a particular satellite signal, its contribution to the metric can easily be removed.

4.7 Comments on Searches

There are many ways the two dimensional search of (4.29) or the three dimensional search of (4.49) can be implemented. In general, the likelihood surface does not monotonically converge to a single global minimum, but may have several local minima. However, if a reasonably accurate initial estimate of the antenna attitude is available, it can be used to provide a starting point for a limited search over an uncertainty region that contains only one minimum. One method of searching this surface is to evaluate (4.29) or (4.49) at several points in a coarse grid spanning the uncertainty region. The point with the largest

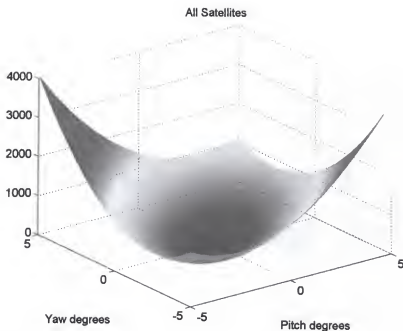


Figure 4.6: Total value of the metric including contributions from all satellites in view. Notice that the areas of weak information from any particular satellite have been filled in by the contributions of other satellites.

likelihood value is then chosen as the center of a finer grid search, where the fine grid size is chosen from the required angular resolution for the particular application.

Another method is to use a variation of the alternating maximization proposed by Ziskind and Wax [14] (for further reference see Press et al. [38]). For a two dimensional direction finding search the process is as follows: First θ_x is fixed at some initial estimate and the LLR is maximized with respect to θ_y across the uncertainty area. Then θ_y is fixed at the value that maximized the likelihood function and the LLR is maximized with respect to θ_x . This iterative method alternates movement throughout the two dimensional likelihood space (parameterized by θ_x and θ_y) along the θ_x and θ_y axes, and will converge to a local minimum. The extension to a three dimensional attitude search is straightforward. Again, if the uncertainty area is reasonably small and contains the true global maximum, then this method will converge to it. If no *a priori* information exists to provide an initial estimate of attitude (and therefore no initial estimate of θ for the search of equation (4.29)), then the problem is significantly more tedious. In this case use of a more exotic method of searching, such as genetic algorithms may be employed [39,40].

CHAPTER 5 PROPERTIES OF THE MAXIMUM LIKELIHOOD ATTITUDE ESTIMATOR

5.1 Introduction

Chapter 4 derived a new method of estimating antenna attitude using the demodulated (despread) data vectors for the satellites in view, the maximum likelihood attitude estimator (MLAE). It showed that by reparamterizing the array response vector in terms of attitude and not antenna-frame direction, the estimator decomposed into a series of components, one per satellite source, parameterized over the antenna attitude.

This attitude estimator is fundamentally different from the direction finding works [22, 23], where each source direction estimation is decoupled from another, even though in both the attitude determination and direction finding cases the source waveforms are known and uncorrelated. However, in this chapter we show that many of the desirable statistical properties of the direction finding estimators apply to the new attitude estimator as well. Specifically, in this chapter we show that the MLAE is asymptotically consistent, unbiased, and efficient.

Recall from Chapter 4 that the MLAE attitude estimate (from equation (4.56), which is repeated here for convenience) is the attitude that maximizes a sum of terms obtained by despreading the sensor data matrix with each satellites spreading waveform:

$$\hat{q} = \max_q \sum_{l=1}^L \mathbf{u}_l^H \mathbf{C}_l^{-1/2} \mathbf{P}_{\tilde{\mathbf{a}}_l(q)} \mathbf{C}_l^{-1/2} \mathbf{u}_l \quad (5.1)$$

where

$$\mathbf{P}_{\tilde{\mathbf{a}}_l(q)} = \frac{\tilde{\mathbf{a}}_l(q) \tilde{\mathbf{a}}_l^H(q)}{\tilde{\mathbf{a}}_l^H(q) \tilde{\mathbf{a}}_l(q)} \quad (5.2)$$

Now consider the right side of equation (5.1) as the function $G(q)$ of the unknown attitude:

$$G(q) = \sum_{l=1}^L \mathbf{u}_l^H \mathbf{C}_l^{-1/2} \mathbf{P}_{\tilde{\mathbf{a}}_l(q)} \mathbf{C}_l^{-1/2} \mathbf{u}_l \quad (5.3)$$

$G(q)$ is simply the value of the estimator “metric,” parameterized on the various hypothesized attitudes of the GPS antenna array, as discussed in Chapter 4.

This chapter is organized as follows. First, using the function $G(q)$ defined above, this chapter proves that the MLAE is a consistent estimator. Consistency is a requirement for the development of the remainder of the chapter. To facilitate proof that the MLAE is unbiased and efficient, a series of lemmas on the asymptotic properties of various aspects of the MLAE are presented. Using these lemmas, this chapter then presents two theorems that show that the MLAE is asymptotically unbiased and statistically efficient. The chapter concludes with a summary and a brief discussion of the validity of asymptotic properties.

5.2 Consistency

A consistent estimator has the desirable property that the estimation error decreases as the number of data samples increases. For the MLAE, this corresponds to the number of samples used for integration, N .

Theorem 1 *The MLAE is a consistent estimator for antenna attitude. That is,*

$$\lim_{N \rightarrow \infty} \hat{q} = \overset{\circ}{q} \quad (5.4)$$

Proof: Consider the contribution of only the *first* satellite to $G(q)$ in equation (5.3), and define this contribution as $G_1(q)$:

$$G_1(q) = \mathbf{u}_1^H \mathbf{C}_1^{-1/2} \mathbf{P}_{\tilde{\mathbf{a}}_1(\overset{\circ}{q})} \mathbf{C}_1^{-1/2} \mathbf{u}_1 \quad (5.5)$$

Now from Chapter 4 \mathbf{u}_1 is a consistent estimator of $\gamma_1 \mathbf{a}(\nu_1, \overset{\circ}{q})$ where $\overset{\circ}{q}$ represents the true attitude. So asymptotically, (5.5) will converge to the maximum of

$$|\gamma_1|^2 \frac{\left| \mathbf{a}^H(\nu_1, q) \mathbf{C}_1^{-1} \mathbf{a}(\nu_1, \overset{\circ}{q}) \right|^2}{\mathbf{a}^H(\nu_1, q) \mathbf{C}_1^{-1} \mathbf{a}(\nu_1, q)} \quad (5.6)$$

or using the whitened array response vector notation, the maximum of

$$|\gamma_1|^2 \frac{\left| \tilde{\mathbf{a}}(\nu_1, q)^H \tilde{\mathbf{a}}(\nu_1, \overset{\circ}{q}) \right|^2}{\tilde{\mathbf{a}}(\nu_1, q)^H \tilde{\mathbf{a}}(\nu_1, q)} \quad (5.7)$$

where $\tilde{\mathbf{a}}(\nu_1, q)$ is defined in (4.53) One could look at equation (5.7) and ascertain, by the Cauchy-Schwarz inequality, that the attitude that maximizes G_1 is \hat{q} . However, this would not be entirely correct. Indeed, \hat{q} would be one attitude to maximize G_1 . But since the array response vector is ambiguous when parameterized in attitude, an *entire family of attitudes* will maximize G_1 . Let $\mathbf{q}_1(\omega_1)$ represent the family of attitudes that asymptotically maximize (5.7). Then using (4.33) and (4.34), $\mathbf{q}_1(\omega_i)$ can be written as

$$\mathbf{q}_1(\omega_1) = \check{\mathbf{q}}_1(\omega_1) \star \hat{\mathbf{q}} \quad (5.8)$$

where \star represents quaternion multiplication.

Now consider the remaining satellites' contributions. In a similar fashion as with satellite one, the family of attitudes $\mathbf{q}_2(\omega_2)$ that asymptotically minimize the second through L th satellite's contribution to (4.49) can be found as

$$\mathbf{q}_i(\omega_i) = \check{\mathbf{q}}_i(\omega_i) \star \hat{\mathbf{q}} \quad i = 2, \dots, L \quad (5.9)$$

For the L satellites, there now exist L families of attitudes that separately minimize each satellites contribution to (4.49). In general, the parameter value that minimizes a sum of functions is not necessarily the value that minimizes any particular function. However, for the attitude determination case, Appendix C states that each of these families of minima intersect in a *single* point, the true attitude $\hat{\mathbf{q}}$. So asymptotically, the estimated attitude is the true attitude, and therefore the MLAE is consistent. ■

5.3 Lemmas on the MLAE

We begin by considering the function $G(q)$ of equation (5.3) near the estimated attitude \hat{q} . A popular method for analyzing $G(q)$, and therefore the estimator performance, is through a Taylor series expansion of the gradient vector $\mathbf{g}'(q)$ near \hat{q} (see, for example [16]). The gradient vector is a 3×1 vector, since there are three independent attitude parameters (for example, the three Euler angles ξ_ϕ , ξ_θ , and ξ_ψ). From (5.1), \hat{q} maximizes $G(q)$, and therefore the gradient $\mathbf{g}'(\hat{q})$ at this stationary point is zero. If the difference

between the estimated and true attitude is small,¹ then the higher order terms in the Taylor series expansion may be ignored, leaving:

$$0 = \mathbf{g}'(\hat{q}) = \mathbf{g}'(\overset{\circ}{q}) + \mathbf{g}''(\overset{\circ}{q})(\hat{q} - \overset{\circ}{q}) + \dots \quad (5.10)$$

such that

$$(\hat{q} - \overset{\circ}{q}) = - \left[\mathbf{g}''(\overset{\circ}{q}) \right]^{-1} \mathbf{g}'(\overset{\circ}{q}) \quad (5.11)$$

where

$$\mathbf{g}'(q) \triangleq \left[\frac{\partial G(q)}{\partial q_1} \quad \frac{\partial G(q)}{\partial q_2} \quad \frac{\partial G(q)}{\partial q_3} \right]^T \quad (5.12)$$

and

$$\mathbf{g}''(q) \triangleq \begin{pmatrix} \frac{\partial^2 G(q)}{\partial q_1 \partial q_1} & \frac{\partial^2 G(q)}{\partial q_1 \partial q_2} & \frac{\partial^2 G(q)}{\partial q_1 \partial q_3} \\ \frac{\partial^2 G(q)}{\partial q_2 \partial q_1} & \frac{\partial^2 G(q)}{\partial q_2 \partial q_2} & \frac{\partial^2 G(q)}{\partial q_2 \partial q_3} \\ \frac{\partial^2 G(q)}{\partial q_3 \partial q_1} & \frac{\partial^2 G(q)}{\partial q_3 \partial q_2} & \frac{\partial^2 G(q)}{\partial q_3 \partial q_3} \end{pmatrix} \quad (5.13)$$

and q_1 , q_2 , and q_3 are the three attitude parameters. We now develop four lemmas describing the terms of equation (5.11).

Lemma 1 *The gradient vector $\mathbf{g}'(q)$ of equation (5.12), evaluated at $q = \overset{\circ}{q}$, asymptotically may be written as*

$$\mathbf{g}'(q) \simeq 2 \operatorname{Re} \left\{ \sum_{l=1}^L \gamma_l^* \bar{\mathbf{D}}^H(l) \mathbf{P}_{\hat{\mathbf{a}}_l(\overset{\circ}{q})}^\perp \bar{\mathbf{w}}_l \right\} \quad (5.14)$$

Proof: This lemma is proven by straightforward evaluation of the terms in (5.12).

We begin by evaluating the partial derivative of $G(\overset{\circ}{q})$ with respect to the i th attitude parameter.

$$\frac{\partial G(\overset{\circ}{q})}{\partial q_i} = 2 \operatorname{Re} \left\{ \sum_{l=1}^L \mathbf{u}_l^H \mathbf{C}_l^{-1/2} \mathbf{P}_{\hat{\mathbf{a}}_l(q)}^\perp \bar{\mathbf{d}}_l(l) \bar{\mathbf{a}}_l^\dagger(q) \mathbf{C}_l^{-1/2} \mathbf{u}_l \right\} \bigg|_{q=\overset{\circ}{q}} \quad (5.15)$$

where

$$\bar{\mathbf{a}}_l^\dagger(q) = (\bar{\mathbf{a}}_l^H(q) \bar{\mathbf{a}}_l(q))^{-1} \bar{\mathbf{a}}_l^H(q) \quad (5.16)$$

¹ The error is small if the integration time (i.e. N) is sufficiently large since the MLAE is a consistent estimator, as previously shown.

and we define

$$\mathbf{d}_i(l) = \frac{\partial \mathbf{a}_i(q)}{\partial q_i} \quad (5.17)$$

and

$$\tilde{\mathbf{d}}_i(l) = \mathbf{C}_i^{-1/2} \mathbf{d}_i(l) \quad (5.18)$$

and have used the fact that the derivative of the projection matrix is [41]

$$\frac{\partial}{\partial q_i} \mathbf{P}_{\tilde{\mathbf{a}}_i(q)} = \mathbf{P}_{\tilde{\mathbf{a}}_i(q)}^\perp \tilde{\mathbf{d}}_i(l) \tilde{\mathbf{a}}_i^\dagger(q) + \left(\mathbf{P}_{\tilde{\mathbf{a}}_i(q)}^\perp \tilde{\mathbf{d}}_i(l) \tilde{\mathbf{a}}_i^\dagger(q) \right)^H \quad (5.19)$$

In (5.12) and the remainder of this chapter we use the shortened array response vector notation of (4.52). Using the method of [22, 23], the second \mathbf{u}_l in (5.15) may be replaced by its asymptotic value $\gamma_l \mathbf{a}_l(\hat{q})$.

$$\frac{\partial G((\hat{q}))}{\partial q_i} \simeq 2 \operatorname{Re} \left\{ \sum_{l=1}^L \mathbf{u}_l^H \mathbf{C}_l^{-1/2} \mathbf{P}_{\tilde{\mathbf{a}}_l(\hat{q})}^\perp \tilde{\mathbf{d}}_i(l) \tilde{\mathbf{a}}_i^\dagger(\hat{q}) \mathbf{C}_l^{-1/2} \gamma_l \mathbf{a}_l(\hat{q}) \right\} \quad (5.20)$$

$$= 2 \operatorname{Re} \left\{ \sum_{l=1}^L \mathbf{u}_l^H \mathbf{C}_l^{-1/2} \mathbf{P}_{\tilde{\mathbf{a}}_l(\hat{q})}^\perp \tilde{\mathbf{d}}_i(l) \tilde{\mathbf{a}}_i^\dagger(\hat{q}) \gamma_l \tilde{\mathbf{a}}_l(\hat{q}) \right\} \quad (5.21)$$

$$= 2 \operatorname{Re} \left\{ \sum_{l=1}^L \mathbf{u}_l^H \mathbf{C}_l^{-1/2} \mathbf{P}_{\tilde{\mathbf{a}}_l(\hat{q})}^\perp \tilde{\mathbf{d}}_i(l) \gamma_l \right\} \quad (5.22)$$

and observing that $\mathbf{P}_{\tilde{\mathbf{a}}_l(\hat{q})}^\perp \mathbf{C}_l^{-1/2} \mathbf{a}_l(\hat{q})$ is zero, equation (5.22) may be equivalently written as

$$\frac{\partial G((\hat{q}))}{\partial q_i} \simeq 2 \operatorname{Re} \left\{ \sum_{l=1}^L \left(\mathbf{u}_l - \gamma_l \mathbf{a}_l(\hat{q}) \right)^H \mathbf{C}_l^{-1/2} \mathbf{P}_{\tilde{\mathbf{a}}_l(\hat{q})}^\perp \tilde{\mathbf{d}}_i(l) \gamma_l \right\} \quad (5.23)$$

$$= 2 \operatorname{Re} \left\{ \sum_{l=1}^L \mathbf{w}_l^H \mathbf{C}_l^{-1/2} \mathbf{P}_{\tilde{\mathbf{a}}_l(\hat{q})}^\perp \tilde{\mathbf{d}}_i(l) \gamma_l \right\} \quad (5.24)$$

where \mathbf{w}_l , defined in (4.37), may be written as

$$\mathbf{w}_l = \mathbf{u}_l - \gamma_l \mathbf{a}_l(\hat{q}) \quad (5.25)$$

and

$$\tilde{\mathbf{w}}_l = \mathbf{C}_l^{-1/2} \mathbf{w}_l \quad (5.26)$$

Therefore, the i th term of the gradient vector may be asymptotically written as

$$\frac{\partial G(\tilde{q})}{\partial q_i} \simeq 2 \operatorname{Re} \left\{ \sum_{l=1}^L \gamma_l^* \tilde{\mathbf{d}}_i^H(l) \mathbf{P}_{\tilde{\mathbf{a}}_i(\tilde{q})}^\perp \tilde{\mathbf{w}}_l \right\} \quad (5.27)$$

Now define the $m \times 3$ matrices

$$\mathbf{D}(l) = [\mathbf{d}_1(l) \ \mathbf{d}_2(l) \ \mathbf{d}_3(l)] \quad (5.28)$$

and

$$\tilde{\mathbf{D}}(l) = [\tilde{\mathbf{d}}_1(l) \ \tilde{\mathbf{d}}_2(l) \ \tilde{\mathbf{d}}_3(l)] \quad (5.29)$$

Using (5.27) and (5.29), the entire gradient vector $\mathbf{g}'(\tilde{q})$ is found as

$$\begin{aligned} \mathbf{g}'(\tilde{q}) &\triangleq \left[\frac{\partial G(q)}{\partial q_1} \quad \frac{\partial G(q)}{\partial q_2} \quad \frac{\partial G(q)}{\partial q_3} \right]^T \\ &= 2 \operatorname{Re} \left\{ \sum_{l=1}^L \gamma_l^* \tilde{\mathbf{D}}^H(l) \mathbf{P}_{\tilde{\mathbf{a}}_i(\tilde{q})}^\perp \tilde{\mathbf{w}}_l \right\} \end{aligned} \quad (5.30)$$

which concludes the proof. \blacksquare

Lemma 2 *The Hessian matrix \mathbf{g}'' of equation (5.13) asymptotically may be written as*

$$\mathbf{g}''(q) = -2 \operatorname{Re} \left\{ \sum_{l=1}^L |\gamma_l|^2 \tilde{\mathbf{D}}^H(l) \mathbf{P}_{\tilde{\mathbf{a}}_i}^\perp \tilde{\mathbf{D}}(l) \right\} \quad (5.31)$$

Proof: This lemma is proven by evaluation of the terms in (5.13). We begin by considering the partial derivative of (5.15) with respect to the k th attitude parameter.

$$\frac{\partial^2 G(q)}{\partial q_i \partial q_k} = 2 \operatorname{Re} \left\{ \sum_{l=1}^L \mathbf{u}_l^H \mathbf{C}_i^{-1/2} \frac{\partial}{\partial q_k} \left[\mathbf{P}_{\tilde{\mathbf{a}}_i}^\perp \tilde{\mathbf{d}}_i(l) \tilde{\mathbf{a}}_l^\dagger \right] \mathbf{C}_i^{-1/2} \mathbf{u}_l \right\} \quad (5.32)$$

where

$$\tilde{\mathbf{a}}_l^\dagger = (\tilde{\mathbf{a}}_l^H \tilde{\mathbf{a}}_i)^H \tilde{\mathbf{a}}_l^H \quad (5.33)$$

Now examine $\frac{\partial}{\partial q_k} [\mathbf{P}_{\tilde{\mathbf{a}}_i}^\perp \tilde{\mathbf{d}}_i(l) \tilde{\mathbf{a}}_l^\dagger]$, the term to be differentiated. From the definition of a $\mathbf{P}_{\tilde{\mathbf{a}}_i}^\perp$, this may be rewritten as

$$\begin{aligned} \frac{\partial}{\partial q_k} [\mathbf{P}_{\tilde{\mathbf{a}}_i}^\perp \tilde{\mathbf{d}}_i(l) \tilde{\mathbf{a}}_l^\dagger] &= \frac{\partial}{\partial q_k} [\mathbf{I} \tilde{\mathbf{d}}_i(l) \tilde{\mathbf{a}}_l^\dagger - \mathbf{P}_{\tilde{\mathbf{a}}_i} \tilde{\mathbf{d}}_i(l) \tilde{\mathbf{a}}_l^\dagger] \\ &= \frac{\partial}{\partial q_k} [\Psi - \mathbf{P}_{\tilde{\mathbf{a}}_i} \Psi] \end{aligned} \quad (5.34)$$

where we define

$$\Psi = \tilde{\mathbf{d}}_i(l) \tilde{\mathbf{a}}_i^\dagger \quad (5.35)$$

Using the chain rule to evaluate the derivatives of the second term in (5.34), we get

$$\frac{\partial \Psi}{\partial q_k} = \left(\tilde{\mathbf{d}}_i(l) \right)'_k \tilde{\mathbf{a}}_i^\dagger + \tilde{\mathbf{d}}_i(l) \left(\tilde{\mathbf{a}}_i^\dagger \right)'_k \quad (5.36)$$

where $()'_k$ implies differentiation with respect to the k th attitude parameter. Using (5.19) and (5.36), the second term of (5.34) is found as

$$\begin{aligned} \frac{\partial}{\partial q_k} \mathbf{P}_{\tilde{\mathbf{a}}_i} \Psi &= \frac{\partial}{\partial q_k} (\mathbf{P}_{\tilde{\mathbf{a}}_i}) \Psi + \mathbf{P}_{\tilde{\mathbf{a}}_i} \frac{\partial}{\partial q_k} (\Psi) \\ &= \mathbf{P}_{\tilde{\mathbf{a}}_i}^\perp \tilde{\mathbf{d}}_k(l) \tilde{\mathbf{a}}_i^\dagger \tilde{\mathbf{d}}_i(l) \tilde{\mathbf{a}}_i^\dagger + \left(\tilde{\mathbf{a}}_i^\dagger \right)^H \tilde{\mathbf{d}}_k^H(l) \mathbf{P}_{\tilde{\mathbf{a}}_i}^\perp \tilde{\mathbf{d}}_i(l) \tilde{\mathbf{a}}_i^\dagger \\ &\quad + \mathbf{P}_{\tilde{\mathbf{a}}_i} \left(\tilde{\mathbf{d}}_i(l) \right)'_k \tilde{\mathbf{a}}_i^\dagger + \mathbf{P}_{\tilde{\mathbf{a}}_i} \tilde{\mathbf{d}}_i(l) \left(\tilde{\mathbf{a}}_i^\dagger \right)'_k \end{aligned} \quad (5.37)$$

The derivative of the psuedo-inverse, $\tilde{\mathbf{a}}_i^\dagger$, is found by direct evaluation to be

$$\begin{aligned} \left(\tilde{\mathbf{a}}_i^\dagger \right)'_k &= \frac{\partial}{\partial q_k} (\tilde{\mathbf{a}}_i^H \tilde{\mathbf{a}}_i)^{-1} \tilde{\mathbf{a}}_i^H \\ &= (\tilde{\mathbf{a}}_i^H \tilde{\mathbf{a}}_i)^{-1} \tilde{\mathbf{d}}_k^H(l) - (\tilde{\mathbf{a}}_i^H \tilde{\mathbf{a}}_i)^{-2} \left(\tilde{\mathbf{d}}_k^H(l) \tilde{\mathbf{a}}_i + \tilde{\mathbf{a}}_i^H \tilde{\mathbf{d}}_k(l) \right) \tilde{\mathbf{a}}_i^H \\ &= (\tilde{\mathbf{a}}_i^H \tilde{\mathbf{a}}_i)^{-1} \left(\tilde{\mathbf{d}}_k^H(l) \mathbf{P}_{\tilde{\mathbf{a}}_i}^\perp - \tilde{\mathbf{a}}_i^H \tilde{\mathbf{d}}_k(l) \tilde{\mathbf{a}}_i^\dagger \right) \end{aligned} \quad (5.38)$$

Substituting (5.38), (5.37), and (5.36) into (5.34) produces the desired partial derivative:

$$\begin{aligned} \frac{\partial}{\partial q_k} \left[\mathbf{P}_{\tilde{\mathbf{a}}_i}^\perp \tilde{\mathbf{d}}_i(l) \tilde{\mathbf{a}}_i^\dagger \right] &= \mathbf{P}_{\tilde{\mathbf{a}}_i}^\perp \left(\tilde{\mathbf{d}}_i(l) \right)'_k \tilde{\mathbf{a}}_i^\dagger - \mathbf{P}_{\tilde{\mathbf{a}}_i}^\perp \tilde{\mathbf{d}}_k(l) \tilde{\mathbf{a}}_i^\dagger \tilde{\mathbf{d}}_i(l) \tilde{\mathbf{a}}_i^\dagger \\ &\quad - \left(\tilde{\mathbf{a}}_i^\dagger \right)^H \tilde{\mathbf{d}}_k^H(l) \mathbf{P}_{\tilde{\mathbf{a}}_i}^\perp \tilde{\mathbf{d}}_i(l) \tilde{\mathbf{a}}_i^\dagger + (\tilde{\mathbf{a}}_i^H \tilde{\mathbf{a}}_i)^{-1} \mathbf{P}_{\tilde{\mathbf{a}}_i}^\perp \tilde{\mathbf{d}}_i(l) \tilde{\mathbf{d}}_k(l)^H \mathbf{P}_{\tilde{\mathbf{a}}_i}^\perp \\ &\quad + (\tilde{\mathbf{a}}_i^H \tilde{\mathbf{a}}_i)^{-1} \mathbf{P}_{\tilde{\mathbf{a}}_i}^\perp \tilde{\mathbf{d}}_i(l) \tilde{\mathbf{a}}_i^H \tilde{\mathbf{d}}_k(l) \tilde{\mathbf{a}}_i^\dagger \end{aligned} \quad (5.39)$$

which may be consolidated and rewritten more simply as

$$\frac{\partial}{\partial q_k} \left[\mathbf{P}_{\tilde{\mathbf{a}}_i}^\perp \tilde{\mathbf{d}}_i(l) \tilde{\mathbf{a}}_i^\dagger \right] = - \left(\tilde{\mathbf{a}}_i^\dagger \right)^H \tilde{\mathbf{d}}_k^H(l) \mathbf{P}_{\tilde{\mathbf{a}}_i}^\perp \tilde{\mathbf{d}}_i(l) \tilde{\mathbf{a}}_i^\dagger + \mathbf{P}_{\tilde{\mathbf{a}}_i}^\perp \Psi_2 \quad (5.40)$$

by defining Ψ_2 to be

$$\begin{aligned} \Psi_2 = \left(\tilde{\mathbf{d}}_i(l) \right)'_k \tilde{\mathbf{a}}_i^\dagger - \tilde{\mathbf{d}}_k(l) \tilde{\mathbf{a}}_i^\dagger \tilde{\mathbf{d}}_i(l) \tilde{\mathbf{a}}_i^\dagger + \\ (\tilde{\mathbf{a}}_i^H \tilde{\mathbf{a}}_i)^{-1} \tilde{\mathbf{d}}_i(l) \tilde{\mathbf{d}}_k(l)^H \mathbf{P}_{\tilde{\mathbf{a}}_i}^\perp + (\tilde{\mathbf{a}}_i^H \tilde{\mathbf{a}}_i)^{-1} \tilde{\mathbf{d}}_i(l) \tilde{\mathbf{a}}_i^H \tilde{\mathbf{d}}_k(l) \tilde{\mathbf{a}}_i^\dagger \end{aligned} \quad (5.41)$$

Substituting (5.40) into (5.32) produces

$$\frac{\partial^2 G(q)}{\partial q_i \partial q_k} = 2 \operatorname{Re} \left\{ \sum_{l=1}^L \mathbf{u}_l^H \mathbf{C}_l^{-1/2} \left[- \left(\tilde{\mathbf{a}}_i^\dagger \right)^H \tilde{\mathbf{d}}_k^H(l) \mathbf{P}_{\tilde{\mathbf{a}}_i}^\perp \tilde{\mathbf{d}}_i(l) \tilde{\mathbf{a}}_i^\dagger + \mathbf{P}_{\tilde{\mathbf{a}}_i}^\perp \Psi_2 \right] \mathbf{C}_l^{-1/2} \mathbf{u}_l \right\} \quad (5.42)$$

Now recall that asymptotically,

$$\mathbf{u}_l \simeq \gamma_l \mathbf{a}_l \quad (5.43)$$

and therefore

$$\mathbf{u}_l^H \mathbf{C}_l^{-1/2} \simeq \gamma_l^* \tilde{\mathbf{a}}_i^H \quad (5.44)$$

resulting in Ψ_2 being pre-multiplied by $\gamma_l^* \tilde{\mathbf{a}}_i^H \mathbf{P}_{\tilde{\mathbf{a}}_i}^\perp$, which is of course zero. Therefore, (5.42) asymptotically approaches

$$\frac{\partial^2 G(q)}{\partial q_i \partial q_k} \simeq 2 \operatorname{Re} \left\{ \sum_{l=1}^L |\gamma_l|^2 \tilde{\mathbf{a}}_i^H \left[- \left(\tilde{\mathbf{a}}_i^\dagger \right)^H \tilde{\mathbf{d}}_k^H(l) \mathbf{P}_{\tilde{\mathbf{a}}_i}^\perp \tilde{\mathbf{d}}_i(l) \tilde{\mathbf{a}}_i^\dagger + \mathbf{P}_{\tilde{\mathbf{a}}_i}^\perp \Psi_2 \right] \tilde{\mathbf{a}}_i \right\} \quad (5.45)$$

$$= -2 \operatorname{Re} \left\{ \sum_{l=1}^L |\gamma_l|^2 \tilde{\mathbf{a}}_i^H \left(\tilde{\mathbf{a}}_i^\dagger \right)^H \tilde{\mathbf{d}}_k^H(l) \mathbf{P}_{\tilde{\mathbf{a}}_i}^\perp \tilde{\mathbf{d}}_i(l) \tilde{\mathbf{a}}_i^\dagger \tilde{\mathbf{a}}_i \right\} \quad (5.46)$$

$$= -2 \operatorname{Re} \left\{ \sum_{l=1}^L |\gamma_l|^2 \tilde{\mathbf{d}}_k^H(l) \mathbf{P}_{\tilde{\mathbf{a}}_i}^\perp \tilde{\mathbf{d}}_i(l) \right\} \quad (5.47)$$

since $\tilde{\mathbf{a}}_i^\dagger \tilde{\mathbf{a}}_i = 1$. To complete the proof, notice that the Hessian matrix of $\mathbf{g}''(q)$ may then be concisely written as

$$\mathbf{g}''(q) = -2 \operatorname{Re} \left\{ \sum_{l=1}^L |\gamma_l|^2 \tilde{\mathbf{D}}^H(l) \mathbf{P}_{\tilde{\mathbf{a}}_i}^\perp \tilde{\mathbf{D}}(l) \right\} \quad (5.48)$$

where $\tilde{\mathbf{D}}(l)$ is defined in (5.29). ■

Lemma 3 The expected value $E[\mathbf{g}'(\hat{q})]$ is asymptotically 0.

Proof:

By using the result of Lemma 1, taking the expected value of (5.14) asymptotically produces

$$\begin{aligned} E[\mathbf{g}'(\hat{q})] &\simeq 2 \operatorname{Re} \left\{ \sum_{l=1}^L \gamma_l^* \tilde{\mathbf{D}}^H(l) \mathbf{P}_{\hat{\mathbf{a}}_l(\hat{q})}^\perp E[\tilde{\mathbf{w}}_l] \right\} \\ &= 0 \end{aligned} \quad (5.49)$$

since, from (4.38), $\tilde{\mathbf{w}}_l$ is zero mean. This may also be seen by substituting the asymptotic value of \mathbf{u}_l , $\gamma_l \mathbf{a}_l$, into (5.15) and observing that $\gamma_l^* \tilde{\mathbf{a}}_l^H \mathbf{P}_{\hat{\mathbf{a}}_l}^\perp$ is zero. ■

Lemma 4 The expected value $E \left[\mathbf{g}'(\hat{q}) \left(\mathbf{g}'(\hat{q}) \right)^T \right]$ may be asymptotically written as

$$E \left[\mathbf{g}'(\hat{q}) \left(\mathbf{g}'(\hat{q}) \right)^T \right] \simeq 2 \operatorname{Re} \left\{ \sum_{l=1}^L |\gamma_l|^2 \tilde{\mathbf{D}}^H(l) \mathbf{P}_{\hat{\mathbf{a}}_l}^\perp \tilde{\mathbf{D}}(l) \right\} \quad (5.50)$$

Proof: Consider the i, j term of the matrix $\mathbf{g}''(q)$. Using (5.27) and taking the expected value, this produces

$$\begin{aligned} E \left[\frac{\partial G(\hat{q})}{\partial q_i} \frac{\partial G(\hat{q})}{\partial q_j} \right] &= \\ E \left[4 \sum_{l=1}^L \sum_{p=1}^L \operatorname{Re} \left\{ \tilde{\mathbf{w}}_l^H \mathbf{P}_{\hat{\mathbf{a}}_l(\hat{q})}^\perp \tilde{\mathbf{d}}_i(l) \gamma_l \right\} \operatorname{Re} \left\{ \tilde{\mathbf{w}}_p^H \mathbf{P}_{\hat{\mathbf{a}}_p(\hat{q})}^\perp \tilde{\mathbf{d}}_j(p) \gamma_p \right\} \right] \Big|_{q=\hat{q}} \end{aligned} \quad (5.51)$$

Using the identity $\operatorname{Re}(A)\operatorname{Re}(B) = \frac{1}{2}\operatorname{Re}(AB + AB^*)$ [23]

$$\begin{aligned} E \left[\frac{\partial G(\hat{q})}{\partial q_i} \frac{\partial G(\hat{q})}{\partial q_j} \right] &= 2 \sum_{l=1}^L \sum_{p=1}^L \operatorname{Re} E \left[\gamma_p^* \gamma_l \tilde{\mathbf{d}}_j^H(p) \mathbf{P}_{\hat{\mathbf{a}}_p(\hat{q})}^\perp \tilde{\mathbf{w}}_p \tilde{\mathbf{w}}_l^H \mathbf{P}_{\hat{\mathbf{a}}_l(\hat{q})}^\perp \tilde{\mathbf{d}}_j(l) \right. \\ &\quad \left. + \gamma_p \gamma_l \tilde{\mathbf{d}}_j^T(p) \mathbf{P}_{\hat{\mathbf{a}}_p(\hat{q})}^\perp \tilde{\mathbf{w}}_p^* \tilde{\mathbf{w}}_l^H \mathbf{P}_{\hat{\mathbf{a}}_l(\hat{q})}^\perp \tilde{\mathbf{d}}_j(l) \right] \end{aligned} \quad (5.52)$$

and employing the conditions on the interference w from (4.39), (5.52) may be written as

$$E \left[\frac{\partial G(q)}{\partial q_i} \frac{\partial G(q)}{\partial q_j} \right] = 2 \sum_{l=1}^L \operatorname{Re} \left\{ |\gamma_l|^2 \tilde{\mathbf{d}}_i^H(p) \mathbf{P}_{\hat{\mathbf{a}}_l}^\perp \tilde{\mathbf{d}}_j(l) \right\} \quad (5.53)$$

Equation (5.53) provides the means to populating the entire 3×3 matrix $E \left[\mathbf{g}'(\hat{q}) \left(\mathbf{g}'(\hat{q}) \right)^T \right]$. By using (5.29), this may be written asymptotically as

$$E \left[\mathbf{g}'(\hat{q}) \left(\mathbf{g}'(\hat{q}) \right)^T \right] \simeq 2 \operatorname{Re} \left\{ \sum_{l=1}^L |\gamma_l|^2 \tilde{\mathbf{D}}^H(l) \mathbf{P}_{\hat{\mathbf{a}}_l}^\perp \tilde{\mathbf{D}}(l) \right\} \quad (5.54)$$

which concludes the proof. \blacksquare

5.4 Bias

The bias of an estimator is the difference between the expected value of the estimate and the true value of the parameter being estimated. Clearly, having an unknown bias in an estimate may have deleterious impacts.

Theorem 2 *The MLAE attitude estimator is asymptotically unbiased, i.e.*

$$E[\hat{q}] - q \simeq 0 \quad (5.55)$$

Proof: The bias may be evaluated by taking the expected value of equation (5.11), since $E[\hat{q}] - q = E[\hat{q} - q]$.

$$E[\hat{q} - q] \simeq -E \left[\left[\mathbf{g}''(\hat{q}) \right]^{-1} \mathbf{g}'(\hat{q}) \right] \quad (5.56)$$

Substituting in the asymptotic values from Lemma (2) provides

$$E[\hat{q} - q] \simeq -E \left[\left[-2 \operatorname{Re} \left\{ \sum_{l=1}^L |\gamma_l|^2 \tilde{\mathbf{D}}^H(l) \mathbf{P}_{\hat{\mathbf{a}}_l}^\perp \tilde{\mathbf{D}}(l) \right\} \right]^{-1} \mathbf{g}'(\hat{q}) \right] \quad (5.57)$$

$$= - \left[-2 \operatorname{Re} \left\{ \sum_{l=1}^L |\gamma_l|^2 \tilde{\mathbf{D}}^H(l) \mathbf{P}_{\hat{\mathbf{a}}_l}^\perp \tilde{\mathbf{D}}(l) \right\} \right]^{-1} E[\mathbf{g}'(\hat{q})] \quad (5.58)$$

Now using the result from Lemma (3) provides the following expression for the asymptotic bias

$$E[\hat{q} - q] \simeq - \left[-2 \operatorname{Re} \left\{ \sum_{l=1}^L |\gamma_l|^2 \tilde{\mathbf{D}}^H(l) \mathbf{P}_{\hat{\mathbf{a}}_l}^\perp \tilde{\mathbf{D}}(l) \right\} \right]^{-1} [0] \quad (5.59)$$

$$= 0 \quad (5.60)$$

which shows that the MLAE, asymptotically, is unbiased. \blacksquare

5.5 Efficiency

A measure of the quality of estimator performance is provided by its mean squared error (MSE). The MSE for the attitude estimate provided by the MLAE (i.e. the covariance matrix of the MLAE estimation error), P_q , is found from

$$P_q = E \left[(\hat{q} - \overset{\circ}{q})(\hat{q} - \overset{\circ}{q})^T \right] \quad (5.61)$$

The Cramér-Rao Bound, P_{CR} is a lower limit on the covariance matrix of the estimation error for unbiased estimators, and an estimator that *achieves* the Cramér-Rao Bound is said to be *statistically efficient* [9]. That is, for the parameter vector θ ,

$$P_{\hat{\theta}} \geq P_{CR}(\theta) \quad (5.62)$$

where the equality holds if $\hat{\theta}$ is an efficient estimate of θ .

Theorem 3 *The MLAE asymptotically achieves the Cramér-Rao Bound on estimation error, and is therefore statistically efficient. That is,*

$$P_q \simeq P_{CR}(q) \quad (5.63)$$

Proof: The estimation error covariance matrix may be evaluated using (5.11):

$$E \left[(\hat{q} - \overset{\circ}{q})(\hat{q} - \overset{\circ}{q})^T \right] = E \left[\left[\mathbf{g}''(\overset{\circ}{q}) \right]^{-1} \mathbf{g}'(\overset{\circ}{q}) \left(\mathbf{g}'(\overset{\circ}{q}) \right)^T \left[\mathbf{g}''(\overset{\circ}{q}) \right]^{-1} \right] \quad (5.64)$$

since $\mathbf{g}''(\overset{\circ}{q})$ is symmetric.

Using lemma (2), we may replace the terms involving $\mathbf{g}''(\overset{\circ}{q})$ by their (deterministic) asymptotic values, represented as $\mathbf{g}_a''(\overset{\circ}{q})$:

$$E \left[(\hat{q} - \overset{\circ}{q})(\hat{q} - \overset{\circ}{q})^T \right] \simeq \left[\mathbf{g}_a''(\overset{\circ}{q}) \right]^{-1} E \left[\mathbf{g}'(\overset{\circ}{q}) \left(\mathbf{g}'(\overset{\circ}{q}) \right)^T \right] \left[\mathbf{g}_a''(\overset{\circ}{q}) \right]^{-1} \quad (5.65)$$

where (from lemma 2)

$$\mathbf{g}_a''(\overset{\circ}{q}) = -2 \operatorname{Re} \left\{ \sum_{l=1}^L |\gamma_l|^2 \tilde{\mathbf{D}}^H(l) \mathbf{P}_{\hat{\mathbf{a}}}^{-1} \tilde{\mathbf{D}}(l) \right\} \quad (5.66)$$

Lemma (4) has previously addressed the quantity involved in the expectation, allowing us to write

$$\mathbb{E} \left[(\hat{q} - \hat{q})(\hat{q} - \hat{q})^T \right] \simeq \left[\mathbf{g}_a''(\hat{q}) \right]^{-1} \left[2 \operatorname{Re} \left\{ \sum_{l=1}^L |\gamma_l|^2 \tilde{\mathbf{D}}^H(l) \mathbf{P}_{\hat{\mathbf{a}}_l}^\perp \tilde{\mathbf{D}}(l) \right\} \right] \left[\mathbf{g}_a''(\hat{q}) \right]^{-1} \quad (5.67)$$

Noting that the first two bracketed terms in (5.67) are inverses (with opposite signs), we get the following expression for the asymptotic covariance of the estimation error:

$$\begin{aligned} P_q &= \mathbb{E} \left[(\hat{q} - \hat{q})(\hat{q} - \hat{q})^T \right] \\ &\simeq \left[2 \operatorname{Re} \left\{ \sum_{l=1}^L |\gamma_l|^2 \tilde{\mathbf{D}}^H(l) \mathbf{P}_{\hat{\mathbf{a}}_l}^\perp \tilde{\mathbf{D}}(l) \right\} \right]^{-1} \end{aligned} \quad (5.68)$$

From (A.61), the Cramér-Rao Bound on the attitude estimation error is

$$P_{CR}(q) = \left[2 \operatorname{Re} \left\{ \sum_{l=1}^L |\gamma_l|^2 \tilde{\mathbf{D}}^H(l) \mathbf{P}_{\hat{\mathbf{a}}_l}^\perp \tilde{\mathbf{D}}(l) \right\} \right]^{-1} \quad (5.69)$$

Observing that P_q and $P_{CR}(q)$ are asymptotically equal completes the proof that the MLAE is asymptotically efficient. ■

5.6 Conclusions

In this chapter we have proven that the Maximum Likelihood Attitude Estimator (MLAE) is statically consistent, and asymptotically unbiased and efficient (i.e. achieves the CRB). These are three useful properties that serve to ensure applicability of the algorithm for realistic applications.

However, it is worthwhile to inquire as to whether an asymptotic (i.e. large sample) property has value for this application. The simple answer for GPS attitude determination is “yes.” The GPS signal strength is extremely low, so significant amounts of despreading and integration are required to achieve a useful SNR. That is, GPS is simply not used in a small sample manner. Therefore the asymptotic properties of the MLAE are useful performance indicators, since the expected region of employment is a large sample application. This is not to say that in all situations the MLAE will *achieve* the CRB, especially in low signal to interference plus noise (SINR) conditions, but that the difference between the MLAE performance and the CRB will decrease as integration time increases.

CHAPTER 6 ATTITUDE FROM DIRECTION FINDING

6.1 Introduction

In Chapter 4 we derived a jammer resistant maximum likelihood estimator for the antenna attitude, the MLAE, and in Chapter 5 this estimator was shown to be asymptotically unbiased, consistent, and efficient. One drawback to the MLAE is the computational burden, since its implementation involves a three dimensional search across attitude. In this chapter we examine methods that, due to their computational efficiency, may prove useful in a resource constrained tactical environment. As is the case with suboptimal methods, the computational savings comes at the cost of decreased estimator performance. In Chapter 2 attitude determination and direction finding are presented as related fields. Using this relation, this chapter develops attitude estimators that operate on the estimated *directions* to the satellites.

This chapter is organized as follows. Section 6.2 introduces the general approach and form these estimators take. In sections 6.3 and 6.4 two formulations of the estimator are presented. Finally, section 6.5 contains a discussion of the attributes and costs of these algorithms.

6.2 Conceptual Approach

The approaches developed in this chapter employ two steps. First, the directions of arrival of each satellite are found. Several methods are presented in section 2.4 that may be used for this purpose. Once the satellite directions in the antenna frame are estimated, the body orientation is then found by minimizing the error between the satellite directions (known in the local level frame) rotated into the antenna frame and the direction estimates. The rotation that minimizes the error is chosen as the antenna attitude.

To set up these direction finding based approaches, we define the following matrices of directions where the subscripts B, and LL denote the body frame and local level frame, respectively: \mathbf{A} is the matrix of *measured* LOS directions to the satellites, \mathbf{B} is the known matrix of LOS vectors in the local level frame, and \mathbf{W} is a weighting matrix.

$$\mathbf{A} = [\hat{\nu}_1 \dots \hat{\nu}_L]_{\mathbf{B}} \quad (6.1)$$

$$\mathbf{B} = [\nu_1 \dots \nu_L]_{\mathbf{LL}} \quad (6.2)$$

$$\mathbf{W} = \text{diag}[w_1, w_2, \dots, w_L] \quad (6.3)$$

where ν_i , $i = 1, 2, \dots, L$ is a 3×1 LOS direction vector.

Then using the measured and known directions to the satellites, the attitude found from the following minimization.

$$\hat{q} = \arg \min_q \|\mathbf{A}\mathbf{W} - \mathbf{Q}(q)\mathbf{B}\mathbf{W}\|_F \quad (6.4)$$

This attitude determination algorithm may be summarized as follows:

- Step 1* For each of the L satellites, estimate the directions θ_i , which correspond to the LOS unit vector $\hat{\nu}_{LB}$. Use an algorithm from Section 2.4 or 4.3.
- Step 2* Use these LOS vectors to estimate attitude from equation (6.4).

Two issues exist in implementing (6.4), once the directions are known. First, the equation is non-linear in the attitude q , and therefore the attitude cannot be found directly through matrix inversion or psuedo-inversion. Second, the choice for the weighting matrix is undefined. We address the first issue through an iterative method based on a linearized version of (6.4). To address the second issue, two options of the weighting matrix are presented. For the remainder of this chapter we parameterize attitude only as a unit-norm quaternion to avoid the convergence issues and singularities that are possible when using Euler angles.

6.3 Equal Satellite Weighting

As in Markel et al. [4], one choice for the weighting matrix is the identity matrix. With this choice every satellite contributes equally to the solution, and (6.4) may be written as

$$\hat{q} = \arg \min_q \|A - Q(q)B\|_F \quad (6.5)$$

Conceptually, the *true* LOS vectors in body frame may be considered to have been rotated by the *true* attitude \hat{q} . Using this concept we define $Z(\hat{q})$ as the matrix of LOS vectors in the local level frame rotated by the true attitude, and $Z(q)$ as the matrix of LOS vectors in the local level frame rotated by the attitude represented by the arbitrary quaternion q .

$$Z(\hat{q}) = Q(\hat{q})B \quad (6.6)$$

$$Z(q) = Q(q)B \quad (6.7)$$

Now A , the matrix of *measured* LOS vectors in body frame, may be considered to be an estimate of $Z(\hat{q})$, say $\hat{Z}(\hat{q})$, since the directions are measured in the body frame and known in the local level frame. In order to extract the attitude from the measured directions in A , i.e. to estimate \hat{q} from the estimate of $Z(\hat{q})$, substitute $\hat{Z}(\hat{q})$ (i.e. A) and $Z(q)$ into (6.5).

$$\hat{q} = \arg \min_q \|\hat{Z}(\hat{q}) - Z(q)\|_F \quad (6.8)$$

In the no-noise case it is easy to see that the quaternion that minimizes (6.8) is $\hat{q} = \hat{q}$, since $\hat{Z}(\hat{q})$ will equal $Z(\hat{q})$.

This quaternion \hat{q} of (6.8) may be found through an iterative process. This procedure follows the general form of Cohen [7] (which was solving for attitude in Euler angles by using phase differences), but has been rewritten for this application. We begin by expressing $Z(\hat{q})$ through its Taylor series expansion.

$$Z(\hat{q}) = Z(\hat{q}) + \sum_{i=1}^4 \frac{\partial Z(\hat{q})}{\partial q_i} (\hat{q} - \hat{q}) + \{\text{higher order terms}\} \quad (6.9)$$

Ignoring the higher order terms, (6.9) may be written as

$$\mathbf{E} = \mathbf{X} \delta \mathbf{q} \quad (6.10)$$

where

$$\mathbf{E} = \text{vec}(\mathbf{Z}(\hat{\mathbf{q}}) - \mathbf{Z}(\hat{\mathbf{q}})) \quad (6.11)$$

$$\mathbf{X} = \begin{bmatrix} \text{vec}(\frac{\partial \mathbf{Z}(\hat{\mathbf{q}})}{\partial q_1}), \text{vec}(\frac{\partial \mathbf{Z}(\hat{\mathbf{q}})}{\partial q_2}), \text{vec}(\frac{\partial \mathbf{Z}(\hat{\mathbf{q}})}{\partial q_3}), \text{vec}(\frac{\partial \mathbf{Z}(\hat{\mathbf{q}})}{\partial q_4}) \end{bmatrix} \quad (6.12)$$

$$\delta \mathbf{q} = \hat{\mathbf{q}} - \hat{\mathbf{q}} \quad (6.13)$$

$$= \begin{bmatrix} \delta q_1 \\ \delta q_2 \\ \delta q_3 \\ \delta q_4 \end{bmatrix} \quad (6.14)$$

and $\text{vec}(\cdot)$ represents stacking all columns of a matrix into a single column vector. The quaternion update vector is found from the psuedo-inverse of \mathbf{X} .

$$\delta \mathbf{q} = (\mathbf{X}^H \mathbf{X})^{-1} \mathbf{X}^H \mathbf{E} \quad (6.15)$$

The iterative algorithm for solving (6.8) may be summarized as follows:

- Step 1* Choose an initial value for the estimated attitude quaternion $\hat{\mathbf{q}}$. This may be the last attitude estimated from the previous data set, or if no *a priori* information exists, the unit quaternion.
- Step 2* Calculate the quaternion update $\delta \mathbf{q}$ from (6.15).
- Step 3* Calculate the new quaternion by adding $\hat{\mathbf{q}}$ to $\delta \mathbf{q}$.
- Step 4* Normalize the new quaternion to unit norm.
- Step 5* Return to step 2 until convergence occurs, i.e. when $\delta \mathbf{q}$ is arbitrarily small.

It is important to include Step 4, since the above method does not intrinsically ensure that the quaternion remain unit norm. This algorithm will be referred to in this work as DFU, since it uses direction finding to obtain the attitude estimate, and does not use an weighting matrix that is the identity matrix (i.e. is unweighted).

6.4 Satellite Weighting via Adapted SINR

The algorithm developed in this section uses the same iterative approach as the DFU algorithm, however now the weighting matrix is not the identity matrix. The choice employed here is to weight each satellite's contribution to the attitude estimate by its *adapted SINR*. The adapted SINR is found from the array response vector to the source, the interference covariance matrix, and the complex gain [42].¹

$$\text{SINR}_{\text{Adapted}} = |\gamma|^2 \mathbf{a}^H(\theta) \mathbf{C}^{-1} \mathbf{a}(\theta) \quad (6.16)$$

where γ is the complex gain, $\mathbf{a}(\theta)$ is the array response vector from the source located at direction θ , and \mathbf{C} is the interference covariance matrix. In practice, these values may be replaced with their estimates.

Throughout this chapter the method of determining the directions to the satellites in the antenna frame has been left unspecified. However, if the maximum likelihood algorithms of (4.28) and (4.29) of Section 4.3 are employed to estimate the directions to the satellites, then calculation of the adaptive SINR is essentially provided by the algorithm already. Notice that the adaptive SINR can be viewed in terms of the whitened array response vector $\tilde{\mathbf{a}}$.

$$\tilde{\mathbf{a}} = \mathbf{C}^{-\frac{1}{2}} \mathbf{a} \quad (6.17)$$

and therefore

$$\text{SINR}_{\text{Adapted}} = |\gamma|^2 |\tilde{\mathbf{a}}|^2 \quad (6.18)$$

The greater the attenuation from the whitening, the lower the adapted SINR. We will refer to this algorithm as DFW, since it uses direction finding and a weighting matrix.

¹ The term adapted SINR is actually not used in Applebaum [42], but is a common term today used to represent the signal to interference plus noise ratio after application of the optimal beamformer weights derived in Applebaum [42].

6.5 Conclusions

Three facets of this method of attitude estimation warrant further discussion. The first is the relationship among the satellites. In a multi-user wireless communications system where the individual sources are essentially unconstrained in their possible location, determining the directions to each source separately is acceptable, and in most cases desirable as it reduces the dimensionality of the search. However, the GPS source (satellite) locations are *constrained* in location by their known flight paths. The constellation, in the local-level frame, is known by the user receiver, as is the receiver position, providing *additional* information that could be used in the direction estimation process. Indeed, the direction to one satellite is not completely independent from the directions to all others. Therefore, to estimate the directions independently, as in (4.29), is a computationally appealing but suboptimal method of attitude estimation. In Chapter 8, simulation results quantify the degradation of performance of these suboptimal algorithms from the optimal MLAE.

The second area of discussion centers around the contribution of each satellite. In section 4.6 a graphical example was used to show that the contribution of each satellite is not the same across attitude-space. Inherent in the metric of equation (4.59) is the (optimal) mechanization of how each satellite contributes *across attitude space* to the attitude estimate, even in the presence of interference and jammers. With the LOS mapping approach, this optimality is lost. Using equal weighting, each satellite not only contributes equally across attitude-space, they all contribute equally relative to each other. With the adapted SINR weighting satellites near the jammer sources will not be allowed to contribute as much to the attitude estimate as those with larger angular separations. However, the contribution from any satellite is still equal across attitude-space, since only a scalar weighting is applied to the satellite. One can clearly see how this is a suboptimal approach by trying to represent the information of Figures 4.3, 4.4, and 4.5 with a single scalar per figure.

The third discussion topic is the relative performance of these two new attitude estimators. In general, weighting the satellite contributions by the adapted SINR in

the attitude minimization process outperforms equal satellite weighting. As shown in Chapter 8, this is often the case for the scenarios simulated. However, in some of the cases examined the weighted estimator has a slightly larger mean total error than the unweighted. This seems to occur when the adapted SINR's are below approximately 6-10 dB, which occurs at the fastest update rates (i.e. smallest integration times), with the fewest sensors, and smallest baseline lengths. It seems that in this case, the weighting puts too great a confidence in the noisy measurements of a few satellite directions.

Although not investigated in this work, one possible improvement to this process would be to use a switchable weighting scheme based on the estimated adapted SINR. As discussed in Chapter 9, this scheme would use the weights only when the adapted SINR's crossed an empirically derived threshold.

CHAPTER 7 WIDER BASELINES AND DUAL FREQUENCY USE

7.1 Introduction

It is well known that as the separation between sensors increases the variance of the direction estimation error decreases.¹ However, this increase in sensor spacing comes at a cost. If the sensors are spaced farther than the Nyquist criterion, grating lobes appear, resulting in an ambiguity of direction.

A similar phenomena arises for the attitude determination application. With the conventional AD approach of using phase differences, only the fractional portion of the total phase may be measured. However, the *total* phase difference between any two sensors receiving a satellite signal is composed of the *fractional* part (i.e. the measured portion), and the *integer* portion. Since the integer portion is not measured, yet must be accounted for to properly determine the antenna attitude, it is referred to as the *integer ambiguity* by the attitude determination community.

Depending on the sensor spacing and the number of satellites used to determine attitude, the integer ambiguity may be resolved uniquely. However, this typically requires an intensive search of all the possible ambiguities. One method to eliminate many of the ambiguities is through a process called “widelaning.” The widelane phase measurement is formed from the difference of the phase measurements from the *two* GPS frequencies, i.e. the L1 and L2 frequencies:

$$\Phi_{\text{widelane}} = \Phi_{L1} - \Phi_{L2} \quad (7.1)$$

¹ This fact is easily demonstrated by the CRB of the direction estimate ν_x for a two sensor array: $\sigma_{\nu_x}^2 \geq 1/[SNR \pi^2 d^2]$, where d is the distance between the sensors.

This gives an effective wavelength of [37]

$$\lambda_{\text{widelane}} = \frac{\lambda_{L1}\lambda_{L2}}{\lambda_{L1} - \lambda_{L2}} \quad (7.2)$$

which for the two GPS frequencies of 1.228 and 1.575 GHz corresponds to .86 meters, or approximately four times the wavelength corresponding to the highest GPS frequency. This significantly reduces the size of the integer ambiguity search. The price paid for the increased effective wavelength is a doubling of the receiver noise, since the receiver noise in each frequency channel is uncorrelated.

The Maximum Likelihood Attitude Estimator (MLAE) of Chapter 4 is, in many cases, unaffected by the integer ambiguity phenomenon. Since the MLAE searches attitude with a fixed array configuration, it can often perform unambiguously even when the sensors are farther apart than the Nyquist criterion. Provided that the uncertainty in attitude over which to search is not too large, the MLAE will converge to a single local minima within the uncertainty when several satellites are being tracked, even if the sensor spacing is greater than the Nyquist criterion. This occurs because inclusion of the additional satellites (over the minimum two required) causes the MLAE metric at the bogus attitudes to indicate that these attitudes are less likely than the true attitude. If the MLAE is cast as a minimization as in equation (4.49), the metric value at the bogus attitudes will not typically be as small as the value at the true attitude.

However, a situation similar to the integer ambiguity problem does exist for the MLAE when the number of satellites being tracked is small, the sensor spacing is greater than the Nyquist criterion, and the attitude uncertainty (i.e. the region to search) is large. In this case the MLAE metric at several regions of attitude space may be close to the value at the true attitude, resulting in local minima of (4.49) that could result in false solutions to a minimization search. Therefore, it would be desirable to develop a dual frequency version of the MLAE developed in chapter 4 that reduces the number of false attitude solutions like the conventional attitude determination process of widelaning. Unfortunately, a simple "phase difference" approach like widelaning is not applicable to

the MLAE. Since the MLAE does not operate on phases alone but on the complex values of the data vectors, a more elaborate estimation process is required.

In this chapter we will develop a method of incorporating the second GPS frequency into the MLAE. We will show that this dual frequency extension provides two positive attributes: a decrease in estimation error and a reduction in possible false attitudes. The following section derives the dual frequency MLAE. Similar to the initial MLAE derivation, this begins with a new look at the array response vector. Following the derivation we present a section that examines the reduction in false attitudes by using the second GPS frequency. Finally, we show that this dual frequency attitude estimator asymptotically achieves the Cramér-Rao Bound, and produces higher quality estimates than the single frequency version.

7.2 Dual Frequency Maximum Likelihood Attitude Determination

Before this section develops the dual frequency attitude estimator, first review the single frequency attitude estimator of Chapter 4. This estimator used the L demodulated data vectors (each $M \times 1$), the L interference covariance matrices, and an array response vector parameterized on the antenna attitude (and using the known directions to the satellites in the local level frame) to define the log likelihood surface. The minima or maxima (depending on whether equation (4.49) or (4.51) are used) of this function is chosen to be the attitude estimate.

Although the development of this estimator is performed using baseband signals, the carrier frequency of the GPS signals appears in the array response vector of equation (4.31) through the division by the wavelength λ . Assuming that the conditions on the interference from Chapter 4 are met for both GPS frequencies, the derivation of this estimator will apply equally well to either frequency, since the statistical properties of the DS-SS satellite waveforms are the same for both the L1 and L2 GPS frequency. Without introducing any additional unknowns into the estimator, the array response vector may be written as a function of the unknown attitude q , the known satellite direction in the local

level frame ν_{LL} , and now the known *wavelength* λ :

$$\mathbf{a}(\nu_{LL}, \lambda, q) = \begin{bmatrix} e^{j \frac{2\pi}{\lambda} \mathbf{b}_1^T \mathbf{Q}(q) \nu_{LL}} \\ e^{j \frac{2\pi}{\lambda} \mathbf{b}_2^T \mathbf{Q}(q) \nu_{LL}} \\ \vdots \\ e^{j \frac{2\pi}{\lambda} \mathbf{b}_M^T \mathbf{Q}(q) \nu_{LL}} \end{bmatrix} \quad (7.3)$$

Now consider a situation that makes use of this modified array response vector. A receiver capable of demodulating both frequencies of the GPS P(Y) code can generate $2L$ data vectors, L per frequency for each integration period. To distinguish the data vectors gathered from the different frequencies, the notation representing the data vector obtained from demodulating with the spreading sequence from satellite l is expanded from \mathbf{u}_l to $\mathbf{u}_{(l,f)}$, where f denotes which of the two possible carrier frequencies. Using this expanded notation, we define the *augmented space-satellite data vector*, \mathbf{U}_a , of the received data similar to equation (4.40):

$$\mathbf{U}_a = \begin{bmatrix} \mathbf{u}_{(1,1)} \\ \mathbf{u}_{(2,1)} \\ \vdots \\ \mathbf{u}_{(L,1)} \\ \mathbf{u}_{(1,2)} \\ \mathbf{u}_{(2,2)} \\ \vdots \\ \mathbf{u}_{(L,2)} \end{bmatrix} \quad (7.4)$$

Letting \mathbf{U}_i represent the space-satellite data vector for frequency i , $i = 1, 2$, equation (7.4) may be written in block form as

$$\mathbf{U}_a = \begin{bmatrix} \mathbf{U}_1 \\ \mathbf{U}_2 \end{bmatrix} \quad (7.5)$$

Now consider the statistics of the interference. Similar to equation (7.5), the augmented interference vector (containing thermal noise, jammers, and the multiple access

interference from other GPS satellites, as in Chapter 4) may be written in block form as

$$\mathbf{W}_a = \begin{bmatrix} \mathbf{W}_1 \\ \mathbf{W}_2 \end{bmatrix} \quad (7.6)$$

where \mathbf{W}_i represents the $ML \times 1$ interference vector for frequency i , $i = 1, 2$. Assuming that the jammer waveforms are uncorrelated frequency to frequency, \mathbf{R}_{ss-a} , the covariance of \mathbf{W}_a , is block diagonal just as \mathbf{R}_{ss} , the covariance of \mathbf{W} for a single frequency in equation (4.46) is block diagonal. This implies that the entire interference at one frequency/satellite channel is uncorrelated from the interference in all other frequencies/satellite channels. Letting $\mathbf{C}_{l,f}$ represent the covariance of the interference in the l th satellite channel, $l = 1, 2, \dots, L$ and the f th frequency, $i = 1, 2$, the augmented interference covariance matrix may be written as

$$\mathbf{R}_{ss-a} = \begin{bmatrix} \mathbf{R}_{ss-1} & 0 \\ 0 & \mathbf{R}_{ss-2} \end{bmatrix} \quad (7.7)$$

$$= \begin{bmatrix} \begin{bmatrix} \mathbf{C}_{1,1} & 0 & \cdots & 0 \\ 0 & \mathbf{C}_{2,1} & 0 & 0 \\ 0 & \cdots & \ddots & 0 \\ 0 & \cdots & 0 & \mathbf{C}_{L,1} \end{bmatrix} & 0 \\ 0 & \begin{bmatrix} \mathbf{C}_{1,2} & 0 & \cdots & 0 \\ 0 & \mathbf{C}_{2,2} & 0 & 0 \\ 0 & \cdots & \ddots & 0 \\ 0 & \cdots & 0 & \mathbf{C}_{L,2} \end{bmatrix} \end{bmatrix} \quad (7.8)$$

Using the above definitions, the asymptotic log likelihood ratio of (4.47) may be written in dual-frequency form as

$$\begin{aligned} \text{LLR} \simeq & \sum_{l=1}^L [\mathbf{u}_{(l,1)} - \gamma_{(l,1)} \mathbf{a}(\nu_l, \lambda_1, q)]^H \mathbf{C}_{(l,1)}^{-1} [\mathbf{u}_{(l,1)} - \gamma_{(l,1)} \mathbf{a}(\nu_l, \lambda_1, q)] + \\ & \sum_{l=1}^L [\mathbf{u}_{(l,2)} - \gamma_{(l,2)} \mathbf{a}(\nu_l, \lambda_2, q)]^H \mathbf{C}_{(l,2)}^{-1} [\mathbf{u}_{(l,2)} - \gamma_{(l,2)} \mathbf{a}(\nu_l, \lambda_2, q)] \end{aligned} \quad (7.9)$$

As with the single frequency attitude estimator, a closed form expression for $\gamma_{(i,f)}$ at a stationary point may be obtained by setting the partial derivative of (7.9) with respect to $\gamma_{(i,f)}$ equal to zero and solving for $\gamma_{(i,f)}$ in terms of q .

$$\hat{\gamma}_{(i,f)} = \frac{\mathbf{a}^H(\nu_i, \lambda_f, q) \mathbf{C}_{(i,f)}^{-1} \mathbf{u}_{(i,f)}}{\mathbf{a}^H(\nu_i, \lambda_f, q) \mathbf{C}_{(i,f)}^{-1} \mathbf{a}(\nu_i, \lambda_f, q)} \quad (7.10)$$

Substituting in the complex gain expression of (7.10) provides the following minimization for the attitude q :

$$\hat{q} = \arg \min_q \sum_{i=1}^L [\mathbf{u}_{(i,1)} - \hat{\gamma}_{(i,1)} \mathbf{a}(\nu_i, \lambda_1, q)]^H \mathbf{C}_{(i,1)}^{-1} [\mathbf{u}_{(i,1)} - \hat{\gamma}_{(i,1)} \mathbf{a}(\nu_i, \lambda_1, q)] + \sum_{i=1}^L [\mathbf{u}_{(i,2)} - \hat{\gamma}_{(i,2)} \mathbf{a}(\nu_i, \lambda_2, q)]^H \mathbf{C}_{(i,2)}^{-1} [\mathbf{u}_{(i,2)} - \hat{\gamma}_{(i,2)} \mathbf{a}(\nu_i, \lambda_2, q)] \quad (7.11)$$

By expanding and removing terms that do not vary with attitude, and substituting in the expression for $\gamma_{(i,f)}$ from equation (7.10), equation (7.11) may be written as a maximization:

$$\hat{q} = \arg \max_q \sum_{i=1}^L \left\{ \left[\frac{|\mathbf{a}(\nu_i, \lambda_1, q)|^H \mathbf{C}_{(i,1)}^{-1} \mathbf{u}_{(i,1)}|^2}{\mathbf{a}^H(\nu_i, \lambda_1, q) \mathbf{C}_{(i,1)}^{-1} \mathbf{a}(\nu_i, \lambda_1, q)} \right] + \left[\frac{|\mathbf{a}(\nu_i, \lambda_2, q)|^H \mathbf{C}_{(i,2)}^{-1} \mathbf{u}_{(i,2)}|^2}{\mathbf{a}^H(\nu_i, \lambda_2, q) \mathbf{C}_{(i,2)}^{-1} \mathbf{a}(\nu_i, \lambda_2, q)} \right] \right\} \quad (7.12)$$

As with the single frequency MLAE, a simpler form of the expression may be written using the shortened form of the array response vector:

$$\mathbf{a}_{(i,f)}(q) = \mathbf{a}(\nu_i, \lambda_f, q) \quad (7.13)$$

And as in (4.53) we may define the "whitened" dual-frequency attitude array response vector:

$$\tilde{\mathbf{a}}_{(i,f)} = \mathbf{C}_{(i,f)}^{-1/2} \mathbf{a}(\nu_i, \lambda_f, q) \quad (7.14)$$

where

$$\mathbf{C}_{(i,f)} = \mathbf{C}_{(i,f)}^{1/2} \mathbf{C}_{(i,f)}^{1/2} \quad (7.15)$$

$$\mathbf{C}_{(i,f)}^{1/2} = \left(\mathbf{C}_{(i,f)}^{1/2} \right)^H \quad (7.16)$$

Using these definitions, (7.12) may be rewritten as

$$\hat{q} = \arg \max_q \sum_{l=1}^L \sum_{f=1}^2 \frac{|\mathbf{u}_{(l,f)}^H \mathbf{C}_{(l,f)}^{-1/2} \tilde{\mathbf{a}}_{(l,f)}(q)|^2}{|\tilde{\mathbf{a}}_{(l,f)}(q)|^2} \quad (7.17)$$

$$= \max_q \sum_{l=1}^L \sum_{f=1}^2 \mathbf{u}_{(l,f)}^H \mathbf{C}_{(l,f)}^{-1/2} \mathbf{P}_{\tilde{\mathbf{a}}_{(l,f)}(q)} \mathbf{C}_{(l,f)}^{-1/2} \mathbf{u}_{(l,f)} \quad (7.18)$$

where

$$\mathbf{P}_{\tilde{\mathbf{a}}_{(l,f)}(q)} = \frac{\tilde{\mathbf{a}}_{(l,f)}(q) \tilde{\mathbf{a}}_{(l,f)}^H(q)}{\tilde{\mathbf{a}}_{(l,f)}^H(q) \tilde{\mathbf{a}}_{(l,f)}(q)} \quad (7.19)$$

The attitude estimators of equations (7.11), (7.12), and (7.31) will be referred to in this work as the dual-frequency MLAE.

Several observations may be made about the dual-frequency MLAE. First, as with the single frequency version, an expression for the complex gain may be found using data from a single satellite and single frequency. However, the attitude estimate includes information from *all* satellites and *both* frequencies. Although coupled, this could be implemented in a parallel structure, having perhaps one computer calculating the metric for a set of attitudes using the data from the first frequency while another processes the data from the second frequency. The metric values could then be combined for the set of attitudes investigated, and the attitude with the minimum combined metric value would be chosen as the estimate.

Although the metric was derived using the same satellites on both bands, this is not a requirement. In fact, none of the satellites need to appear at both frequencies for the algorithm to operate. Similarly, this approach performs if the jammer scenario is different on the two frequencies. For example, if one band was jammed and the other unjammed, this algorithm would perform better than a single frequency MLAE operating at either the jammed or even the unjammed frequency.

7.3 Reduction in False Attitudes

Consider the situation where only a few satellites are visible, a large uncertainty in attitude exists, and to achieve higher resolution attitude estimates the sensors are spaced farther apart than a half wavelength. In practice, this scenario may occur either on startup or if INS aiding is either not available or not operating. In this case, there may be several areas of attitude space that lead to local minima of equation (7.11) (or maxima of equations (7.12) and (7.31)). To find the attitude estimate, the extrema of each area would have to be found and sorted, with the attitude estimate chosen as the attitude corresponding to the global extrema. It is clear that a reduction in the number of areas that may contain an extrema (perhaps crossing a threshold and therefore requiring that the extrema be found and its metric value obtained for comparison to others) would be desirable.

To visualize how incorporation of the second frequency reduces the number of false attitude positions, consider the simpler direction finding application. Figure 7.1 shows the (normalized) likelihood ratio for a received signal impinging on the array from broadside for a 15 element uniform linear array (ULA) with a 2λ spacing between elements. In this example no jammers exist, i.e. the likelihood value is proportional to the quiescent array pattern. Notice that several directions produce likelihood values equal to the maximum at the correct direction. For a radar these grating lobes cause two deleterious effects: they produce an ambiguity in the direction estimation process, and they allow undesired signals from these ambiguous directions to pass through the antenna with the same gain as the desired signal. Now consider the likelihood value for the same array receiving signals at a carrier frequency equal to 1.25 times greater. From Figure 7.2 it can be seen that the locations of the grating lobes have changed. The extension of this example to the dual-frequency MLAE is obtained by *summing* the likelihood values obtained from these two frequencies, as shown in Figure 7.3. In this case the grating lobes are attenuated, since only the *true* direction appears at the same angular location as frequency changes.

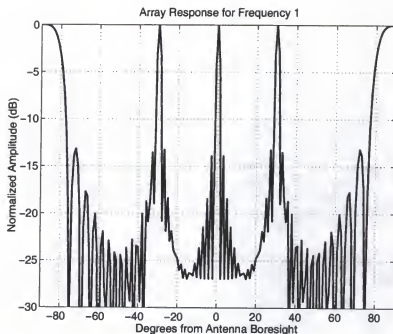


Figure 7.1: Normalized likelihood value vs. direction of arrival for a 15 element ULA receiving a narrowband signal at a frequency corresponding to a 2λ spacing. True direction is on boresight, i.e. 0 degrees.

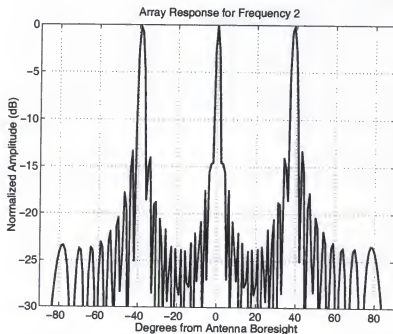


Figure 7.2: Normalized likelihood value vs. direction of arrival for a 15 element ULA receiving a narrowband signal at a frequency corresponding to a $\frac{2}{1.25}\lambda$ spacing. True direction is on boresight, i.e. 0 degrees.

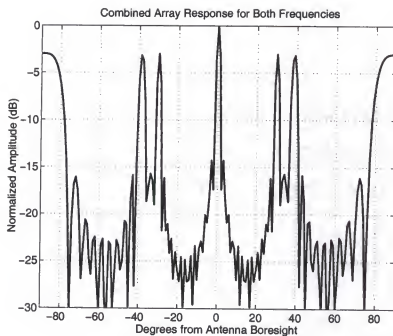


Figure 7.3: Likelihood value vs. direction of arrival for a 15 element ULA incorporating data collected at two frequencies corresponding to 2λ and $\frac{2}{1.25}\lambda$ spacing. True direction is on boresight, i.e. 0 degrees. The grating lobes are reduced in amplitude from the true direction of arrival, producing a clear indication which direction is correct.

Now consider how this applies to the attitude determination case. In the following example, the true attitude (in Euler angles) is $[0,0,0]$, and the attitude uncertainty is assumed to be ± 88 degrees in each coordinate. Three likelihood surfaces are generated at a two degree resolution: the MLAE (equation (4.49)) using frequency L1, the MLAE (equation (4.49)) using frequency L2, and the dual frequency MLAE (7.11). Each of these estimators chooses the attitude that *minimizes* the likelihood expression, and each likelihood surface is calculated using two satellites. A threshold of 10dB below the mean value of each surface was chosen, and all points in attitude space below this threshold were considered possible candidates for the attitude estimate. In order to show the reduction in *false* values of attitude, any point that had a contiguous connection to the true attitude was removed in the following plots. Any point with such a connection would lead, by a simple minimization scheme, to the true attitude. Therefore, for comparison purposes we wish to examine only those points that would lead to *false* values of attitude, i.e. a local minimum that is not at the true attitude. The intent of this is to evaluate the potential decrease in false attitudes when using the dual-frequency MLAE over using a single frequency MLAE.

Figure 7.4 shows a three dimensional representation (over the three Euler coordinates of attitude) of the attitudes where the likelihood value was below the threshold using the L1 frequency. To provide an easier visualization of these points, Figure 7.5 shows a two dimensional version of the same plot, obtained by projecting all points onto the $\xi_\phi = 0$ plane. As discussed above, the attitude values that connect to the true attitude are removed, leaving only points that would lead to a false attitude. To illustrate this, figure 7.5 shows all attitudes with metric values below the threshold, and figure 7.6 shows only those that do not connect to the true attitude. The relatively few points leading to the true attitude have been "thinned out." The jammer scenario used is the same as that involving the first jammer in the random jammer study of Chapter 8. The four sensors used are spaced in a "quad" formation with spacing of approximately .6 meters.

Figure 7.7 presents the false attitudes for the MLAE using the L2 frequency in the same manner. In Figure 7.8, which contains the likelihood points below the threshold

for the dual-frequency MLAE, it is apparent that a significant reduction in the number of points leading to false attitude solutions exists. Similar to the grating lobe reduction in the direction finding application above, the dual-frequency MLAE “smoothes” the likelihood value away from the true value of attitude, reducing the number of points with likelihood values that may be considered candidates for the global minimum.

To illustrate the reduction in false attitudes, three additional data sets are presented. Figures 7.9, 7.10, and 7.11 present the single frequency MLAE for L1 and L2, and the dual-frequency MLAE using satellites 1 and 5. Similarly, figures 7.12, 7.13, and 7.14 present data using satellites 1 and 6, and figures 7.15, 7.16, and 7.17 present data using satellites 2 and 3. Table 7.1 contains the number of false attitude possibilities for the three estimators for several more satellite combinations.

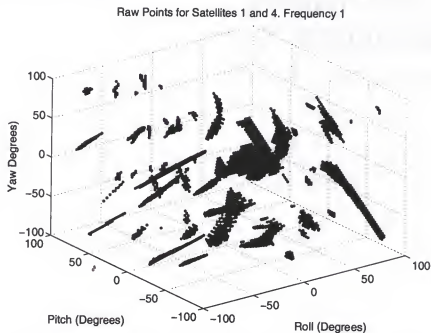


Figure 7.4: Three dimensional plot of all attitudes whose metric value is below the 10dB threshold, using Satellites 1 and 4, and frequency L1.

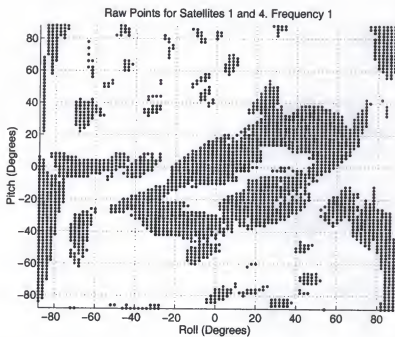


Figure 7.5: Two dimensional view of all attitudes whose metric value is below the 10dB threshold, using Satellites 1 and 4, and frequency L1.

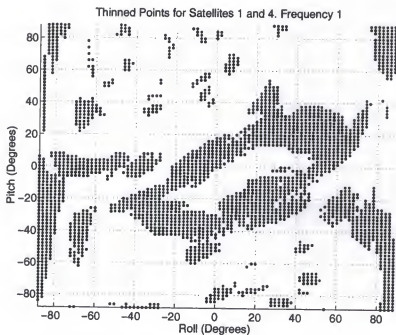


Figure 7.6: Two dimensional view of those attitudes whose metric value is below the 10dB threshold that are not contiguous to the true attitude, (i.e. false solutions) using Satellites 1 and 4, and frequency L1.

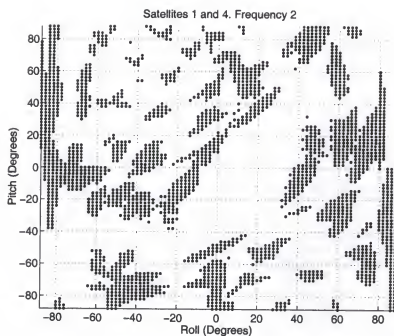


Figure 7.7: False attitude solutions using Satellites 1 and 4, and frequency L2.

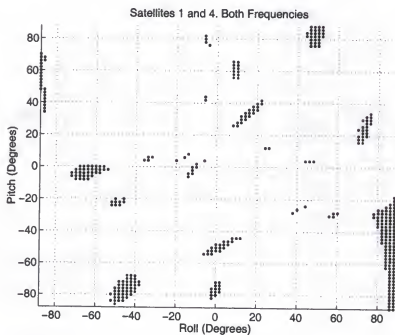


Figure 7.8: False attitude solutions using Satellites 1 and 4, and frequency the dual frequency MLAE

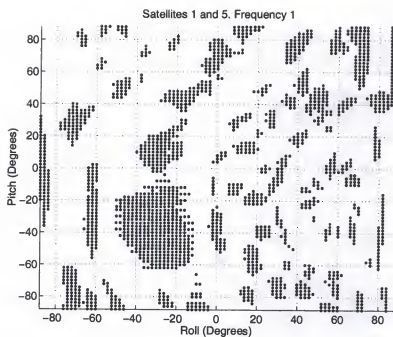


Figure 7.9: False attitude solutions using Satellites 1 and 5, and frequency L1.

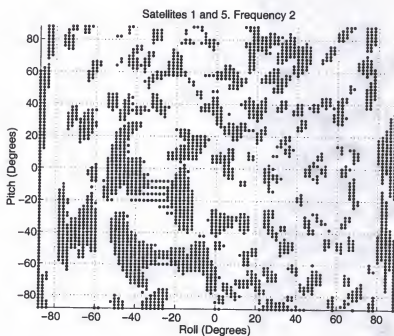


Figure 7.10: False attitude solutions using Satellites 1 and 5, and frequency L2.

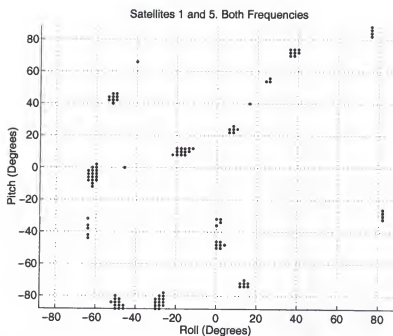


Figure 7.11: False attitude solutions using Satellites 1 and 5, and the dual frequency MLAE.

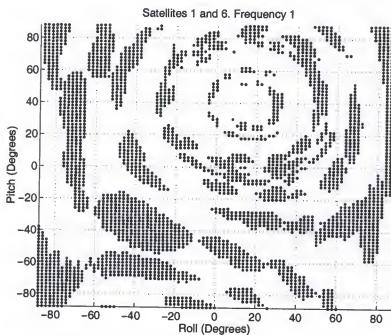


Figure 7.12: False attitude solutions using Satellites 1 and 6, and frequency L1.

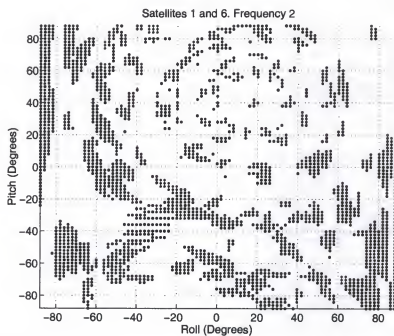


Figure 7.13: False attitude solutions using Satellites 1 and 5, and frequency L2.

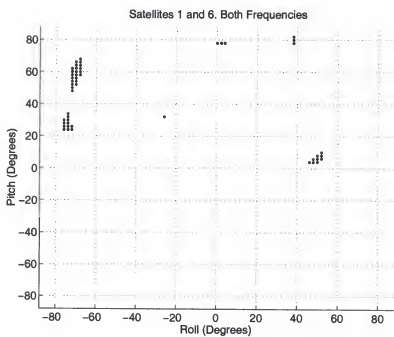


Figure 7.14: False attitude solutions using Satellites 1 and 5, and the dual frequency MLAE.

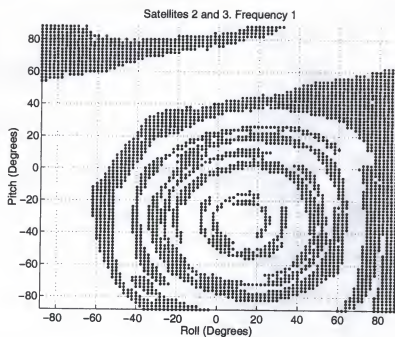


Figure 7.15: False attitude solutions using Satellites 2 and 3, and frequency L1.

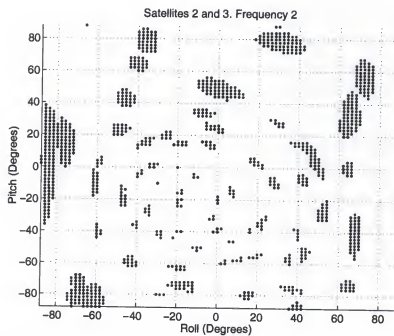


Figure 7.16: False attitude solutions using Satellites 2 and 3, and frequency L2.

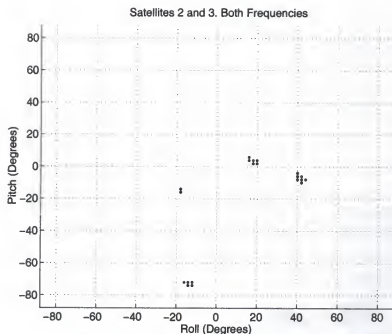


Figure 7.17: False attitude solutions using Satellites 2 and 3, and the dual frequency MLAE.

Table 7.1: Number of false solutions, i.e. points below the “possible minimum” threshold that do not converge to the true solution. Resolution in each Euler angle is two degrees. Scenario is the same as that involving the first jammer in the random jammer study of Chapter 8.

Satellite Combination	MLAE L1	MLAE L2	Dual Freq. MLAE
1-4	3681	5052	683
1-5	3389	4690	153
1-6	5028	3313	55
2-3	6169	1409	28
2-4	733	4670	523
2-5	3875	1743	89
2-6	4358	1826	25
3-4	12095	3667	159
3-5	1772	1654	9
3-6	463	1788	0

7.4 Dual-Frequency MLAE Performance Increase

In this section we analytically examine the performance of the dual-frequency MLAE. Specifically, we will show that the dual-frequency estimator may be written in the form similar to that used for the single frequency estimator. Then, using the results of Chapter 5, we show that the dual-frequency MLAE has the same desirable properties as the single frequency MLAE.

We begin by examining the dual-frequency MLAE from equation (7.11), repeated here for convenience.

$$\hat{q} = \arg \min_q \sum_{l=1}^L [\mathbf{u}_{(l,1)} - \hat{\gamma}_{(l,1)} \mathbf{a}(\nu_l, \lambda_1, q)]^H \mathbf{C}_{(l,1)}^{-1} [\mathbf{u}_{(l,1)} - \hat{\gamma}_{(l,1)} \mathbf{a}(\nu_l, \lambda_1, q)] + \sum_{l=1}^L [\mathbf{u}_{(l,2)} - \hat{\gamma}_{(l,2)} \mathbf{a}(\nu_l, \lambda_2, q)]^H \mathbf{C}_{(l,2)}^{-1} [\mathbf{u}_{(l,2)} - \hat{\gamma}_{(l,2)} \mathbf{a}(\nu_l, \lambda_2, q)] \quad (7.20)$$

This equation may be rewritten in simpler notation as

$$\hat{q} = \arg \min_q \sum_{\zeta=1}^{2L} [\check{\mathbf{u}}_{\zeta} - \check{\gamma}_{\zeta} \check{\mathbf{a}}_{\zeta}(q)]^H \check{\mathbf{C}}_{\zeta}^{-1} [\check{\mathbf{u}}_{\zeta} - \check{\gamma}_{\zeta} \check{\mathbf{a}}_{\zeta}(q)] \quad (7.21)$$

where we have defined

$$\check{\mathbf{a}}_{\zeta}(q) = \begin{cases} \mathbf{a}(\nu_{\zeta}, \lambda_1, q) & 1 \leq \zeta \leq L \\ \mathbf{a}(\nu_{\zeta-L}, \lambda_2, q) & L+1 \leq \zeta \leq 2L \end{cases} \quad (7.22)$$

$$\check{\mathbf{u}}_{\zeta} = \begin{cases} \mathbf{u}_{(\zeta,1)} & 1 \leq \zeta \leq L \\ \mathbf{u}_{(\zeta-L,2)} & L+1 \leq \zeta \leq 2L \end{cases} \quad (7.23)$$

$$\check{\gamma}_{\zeta} = \begin{cases} \hat{\gamma}_{(\zeta,1)} & 1 \leq \zeta \leq L \\ \hat{\gamma}_{(\zeta-L,2)} & L+1 \leq \zeta \leq 2L \end{cases} \quad (7.24)$$

$$\check{\mathbf{C}}_{\zeta} = \begin{cases} \mathbf{C}_{(\zeta,1)} & 1 \leq \zeta \leq L \\ \mathbf{C}_{(\zeta-L,1)} & L+1 \leq \zeta \leq 2L \end{cases} \quad (7.25)$$

With this substitution, the frequency is no longer an argument of the array response vector, the data vector, or the covariance matrices. The terms relating to the second

frequency are simply indexed as the last L ζ 's. With this notation, we can rewrite the maximization equation (7.12) as

$$\hat{q} = \arg \max_q \sum_{l=1}^{2L} \left[\frac{|\check{\mathbf{a}}_\zeta(q)^H \check{\mathbf{C}}_\zeta^{-1} \check{\mathbf{u}}_\zeta|^2}{\check{\mathbf{a}}_\zeta(q)^H \check{\mathbf{C}}_\zeta^{-1} \check{\mathbf{a}}_\zeta(q)} \right] \quad (7.26)$$

As in Chapter 4, we can simplify further by defining the whitened" dual-frequency attitude array response vector:

$$\hat{\mathbf{a}}_\zeta(q) = \check{\mathbf{C}}_\zeta^{-1/2} \check{\mathbf{a}}_\zeta(q) \quad (7.27)$$

where

$$\check{\mathbf{C}}_\zeta = \check{\mathbf{C}}_\zeta^{-1/2} \check{\mathbf{C}}_\zeta^{-1/2} \quad (7.28)$$

$$\check{\mathbf{C}}_\zeta^{-1/2} = (\check{\mathbf{C}}_\zeta^{-1/2})^H \quad (7.29)$$

Using these definitions, (7.12) may be rewritten as

$$\hat{q} = \arg \max_q \sum_{\zeta=1}^{2L} \frac{|\check{\mathbf{u}}_\zeta^H \check{\mathbf{C}}_\zeta^{-1/2} \hat{\mathbf{a}}_\zeta(q)|^2}{|\hat{\mathbf{a}}_\zeta(q)|^2} \quad (7.30)$$

$$= \max_q \sum_{\zeta=1}^{2L} \check{\mathbf{u}}_\zeta^H \check{\mathbf{C}}_\zeta^{-1/2} \mathbf{P}_{\hat{\mathbf{a}}_\zeta(q)} \check{\mathbf{C}}_\zeta^{-1/2} \check{\mathbf{u}}_\zeta \quad (7.31)$$

where

$$\mathbf{P}_{\hat{\mathbf{a}}_\zeta(q)} = \frac{\hat{\mathbf{a}}_\zeta(q) \hat{\mathbf{a}}_\zeta^H(q)}{\hat{\mathbf{a}}_\zeta^H(q) \hat{\mathbf{a}}_\zeta(q)} \quad (7.32)$$

Notice that equation (7.31) is in exactly the same form as the single frequency version of equation (4.56). With this form we can use the same asymptotic formulas for efficiency as in Chapter 5 and Appendix A. The only difference is that caution must be used in calculating the derivative matrices, to ensure that the appropriate effective array spacing is used depending on whether ζ is less than or greater than L .

Using the results of Chapter 5 and Appendix A, the Cramér-Rao Bound on the attitude estimation error using two frequencies is

$$P_{CR}(q) = \left[2 \operatorname{Re} \left\{ \sum_{\zeta=1}^{2L} |\gamma_\zeta|^2 \dot{\mathbf{D}}^H(\zeta) \mathbf{P}_{\hat{\mathbf{a}}_\zeta(q)}^{-1} \dot{\mathbf{D}}(\zeta) \right\} \right]^{-1} \quad (7.33)$$

where, as with the single frequency,

$$\ddot{\mathbf{d}}_i(\zeta) = \frac{\partial \ddot{\mathbf{a}}_\zeta(q)}{\partial q_i} \quad (7.34)$$

$$\dot{\mathbf{d}}_i(\zeta) = \ddot{\mathbf{C}}_\zeta^{-1/2} \ddot{\mathbf{d}}_i(\zeta) \quad (7.35)$$

and

$$\dot{\mathbf{D}}(\zeta) = [\dot{\mathbf{d}}_1(\zeta) \ \dot{\mathbf{d}}_2(\zeta) \ \dot{\mathbf{d}}_3(\zeta)] \quad (7.36)$$

To justify the observation made earlier that the dual-frequency MLAE performed as well or better than the single frequency MLAE using data from either frequency, consider that the Fisher information matrix for the dual-frequency, FIM_{DF} is the *sum* of FIM for each frequency. That is,

$$\begin{aligned} \text{FIM}_{\text{DF}} &= 2 \operatorname{Re} \left\{ \sum_{\zeta=1}^{2L} |\gamma_\zeta|^2 \dot{\mathbf{D}}^H(\zeta) \mathbf{P}_{\dot{\mathbf{d}}_\zeta(q)}^\perp \dot{\mathbf{D}}(\zeta) \right\} \\ &= 2 \operatorname{Re} \left\{ \sum_{\zeta=1}^L |\gamma_\zeta|^2 \dot{\mathbf{D}}^H(\zeta) \mathbf{P}_{\dot{\mathbf{d}}_\zeta(q)}^\perp \dot{\mathbf{D}}(\zeta) \right\} \\ &\quad + 2 \operatorname{Re} \left\{ \sum_{\zeta=L+1}^{2L} |\gamma_\zeta|^2 \dot{\mathbf{D}}^H(\zeta) \mathbf{P}_{\dot{\mathbf{d}}_\zeta(q)}^\perp \dot{\mathbf{D}}(\zeta) \right\} \quad (7.37) \\ &= \text{FIM}_{\text{L1}} + \text{FIM}_{\text{L2}} \quad (7.38) \end{aligned}$$

where FIM_{L1} and FIM_{L2} are the Fisher information matrices for the two single frequency estimations. Since FIM_{L1} , and FIM_{L2} are each always positive definite, FIM_{DF} must be positive definite and greater² than FIM_{L1} and FIM_{L2} .

7.5 Summary

In this chapter we have derived the dual-frequency MLAE. This estimator was shown to optimally incorporate information from the two frequencies that carry the GPS P(Y) waveform. This estimator has the same desirable properties of consistency and asymptotic efficiency as were demonstrated for the single frequency MLAE. By examining the Cramér-Rao Bound for the dual-frequency MLAE, it is clear that it will perform as well as

² That is, $\text{FIM}_{\text{DF}} - \text{FIM}_{\text{L1}} > 0$ and $\text{FIM}_{\text{DF}} - \text{FIM}_{\text{L2}} > 0$.

or better than the single frequency MLAE using data from either of the GPS frequencies. In addition, the dual-frequency MLAE significantly reduces the number of false attitudes (attitudes with metric values numerically close to the value at the true attitude) when the sensors are spaced farther apart than the Nyquist criterion. This gives it a “widelane-like” quality, and allows for better quality attitude estimates without introducing ambiguity.

CHAPTER 8 SIMULATIONS AND RESULTS

8.1 Introduction

This chapter presents quantitative results generated from a simulation of the attitude estimators described in the earlier chapters. The components and assumptions of the simulation are discussed below, followed by a description and the results from three performance studies.

In this chapter abbreviations for the various attitude estimators are often used, especially in the figures. Here we refer to the Maximum Likelihood Attitude Estimator algorithm presented in Chapter 4 as the “MLAE.” Similarly, the direction finding based approaches derived in Chapter 6 are referred to as “DFU” when the direction estimates¹ are un-weighted (i.e. weighting matrix is the identity matrix), and “DFW” when weighted by the adaptive SINR. Finally, “CONV” refers to attitude estimation using the conventional phase difference method described in Chapter 2.

8.2 Simulation Methodology

In the context of this work, a *scenario* constitutes a particular array topology, a set of jammer locations, powers, and bandwidths, a set of satellite locations and received powers, the receiver integration time (time between attitude updates), and of course the antenna attitude. The purpose of this simulation is to demonstrate the relative performance of the estimators described in the previous section for various scenarios. Specifically, the simulation is used to evaluate the statistical performance of the estimators at a static condition in a Monte Carlo fashion. It does not explore the possible performance gains

¹ In the results presented in this chapter both DFW and DFU use decoupled maximum likelihood estimation to produce the direction estimates.

from combining the GPS based attitude estimates with those of an Inertial Navigation System (INS) or other sensors, but focuses solely on the attitude derived from GPS.

The simulation makes a modeling distinction between the satellite waveforms matched to the despreading sequence, which is considered deterministic, and the interference which is modelled as a random process. As such, Monte Carlo evaluation of the estimator performance for a given scenario can be performed by employing the estimator on the superposition of the synthesized deterministic data and multiple *realizations* of the interference. Using this distinction, the simulation operation is as follows: first, the "deterministic" satellite data received at each sensor for all satellites in view are calculated using one of the array topologies discussed below. Then the interference covariance matrices are generated, containing the thermal noise, contributions from each jammer, and a model of the multiple access interference² from other satellites. From the covariance matrix a realization of the interference is formed and added to the satellite contributions, creating the demodulated data vectors u_i . An additional realization of the interference is created to simulate the covariance estimation process; each realization calculates its own estimate of interference covariance. Finally, the simulation implements the various attitude estimators using the covariance matrix estimates and the received data vectors calculated for the realization.

The relevant receiver parameters are as follows. The receiver chain simulated has a system noise figure of 4dB, a coherent signal loss of 5 dB, and a noncoherent signal loss of 2 dB. Each receiver hardware channel is assumed identical. The satellite power received at the antenna is -163 dB. The jammer effective radiated power (ERP) is 20 watts, and the jammers are located 20 nautical miles from the antenna. Multipath, either from the jammer or satellites, is not simulated for the studies below. As is assumed throughout this

² Since the P(Y) code multiple access interference is so small compared to the other components of the interference, including thermal noise, in many of the simulation studies it is not included.

work, all satellites used for attitude determination are assumed to be in code and Doppler track.

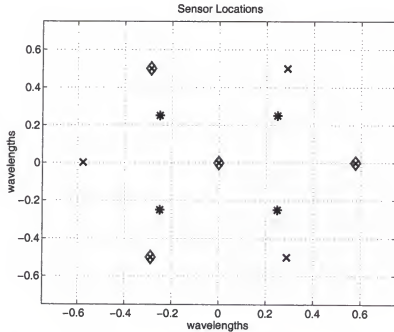


Figure 8.1: Sensor locations for the three antenna topologies. Quad (asterisk), Y (diamond), and Hex (x). The Y antenna is actually a subset of the Hex antenna.

Three planar antenna topologies are used for the studies below. The first antenna uses 4 elements on a rectangularly sampled grid, while the second and third use 4 and 7 elements on a triangularly sampled grid in a “Y” and hexagonal shape, respectively. Figure 8.1 shows the antenna locations, in wavelengths for these antennas. Except for study three, which uses wider baselines, each of these is chosen with the maximum inter-element spacing allowed that prevents grating lobes in visible space [43]. An interesting point is that the term “grating lobes” used by the antenna array/radar community and the phrase “integer ambiguity” used in reference to GPS attitude determination are in fact caused by the same phenomena. Both refer to the situation where the Shannon (or Nyquist) sampling criterion in the spatial domain is not met, resulting in aliasing (see, for example, Oppenheim and Shafer [44]).

Each sensor model incorporates a simple gain pattern. Sources near boresight of the sensor receive the most gain, while the gain drops approximately 10dB near the cutoff

point of 80 degrees from boresight. Satellites beyond the cutoff point are not included in the simulation, since difficulties may exist with maintaining track on them. Figure 8.2 shows this gain pattern.

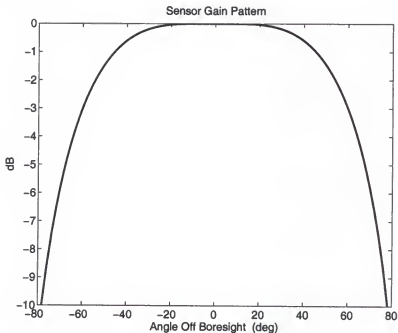


Figure 8.2: Sensor gain pattern used in the attitude simulation.

For the MLAE, DFW, and DFU simulation results, a modified alternating maximization routine was employed to search either the three or two dimensional likelihood space. This approach was used since computational speed was not an issue.

8.3 Mean Total Error

Each realization of the simulation produces an attitude estimate using the estimators discussed in the previous chapters. There are several ways in which the simulation results of this chapter may be presented. The estimated attitude could be expressed in Euler angles, and statistics calculated on the errors in roll, pitch, and yaw independently for every scenario.

A more concise method, and the one employed in this work, is to calculate the *total error* for each realization. The total error is the angular rotation required to rotate the antenna from the *estimated* attitude to the *correct* attitude, and is always greater

than or equal to zero. Calculation of the total error is straightforward using quaternion multiplication. If q_{meas} represents the measured (estimated) attitude quaternion, and \hat{q} the true attitude quaternion, then the quaternion representation the rotation between these two frames of reference, q_{err} is

$$q_{err} = \hat{q} * (q_{meas})^{-1} \quad (8.1)$$

and using the quaternion definition of equation (4.34), where the fourth component of the quaternion corresponds to the angular rotation about the axis defined by the first three components, the total error is simply found to be

$$\text{Total Error} = 2 \arccos [q_{err}(4)] \quad (8.2)$$

For each scenario, the mean total error across all realizations in that scenario is calculated for each of the estimation methods as the average of the total errors from each simulation realization. Since the total error is always non-negative, this method is valid because one error cannot algebraically cancel another.

8.4 Study 1: Single Jammer with "Random" Location

In this study, the estimators are evaluated for the three antenna topologies in a single jammer scenario. The satellite constellation employed in the simulation uses the satellite positions visible at latitude $30^{\circ} 39' 18.70''$ North and longitude $86^{\circ} 39' 9.91''$ West, (located in Ft. Walton Beach, Florida) on 20 April 2001 at the time 21:28 UTC. The antenna orientation was in the local level frame, resulting in 7 satellites being visible to the antenna. In order to evaluate the extent and variability of degradation possible from a jammer at a given displacement from boresight, the jammer location was moved across the simulated sky with a constant angular displacement from boresight of the array of approximately 44 degrees (the projection onto the x-y plane of the antenna was .7). The "randomness" of the jammer location at this boresight angle is simulated by evaluating twelve jammer positions, at $0, 30, 60, \dots, 330$ degrees from North. Figure 8.3 shows a sine-space (i.e. projection of the LOS vectors onto the plane of the antenna) plot of the satellites and all jammer locations used in this study.

For each jammer location two receiver types are evaluated: one in which the receiver is configured to provide attitude estimates at 50 Hz and one that provides estimates at 12.5 Hz. Data for the 50 Hz scenario are presented first, followed by the data for the 12.5 Hz scenario. For each data point, 500 trials are simulated.

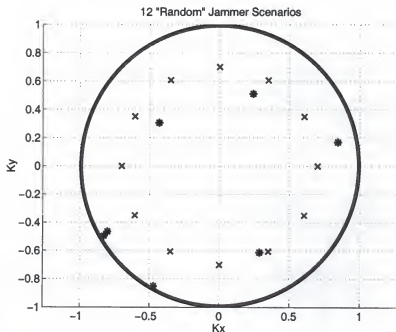


Figure 8.3: Sine-space plot of the satellite (asterisk) and the 12 jammer locations (X) for the random jammer study. Only one jammer is simulated at a time; in the first scenario the jammer location is at $K_y = .7$, and the remaining scenarios use the jammer positions shown in order clockwise. The outer circle represents the horizon, and the area inside the inner circle represents the portion of the sky visible to the sensors.

It is often useful to compare the actual achieved estimator performance to the Cramér-Rao Bound (CRB). For this comparison, we have chosen to parameterize attitude in terms of Euler angles, since it seems more intuitive to discuss variances of Euler angles than variances of quaternion components. Figures 8.4, 8.5, and 8.6 show the standard deviations of MLAE estimates in roll, pitch, and yaw respectively. Each figure contains the MLAE estimates for the Quad, Y, and Hex antennas as well as the CRB for each of these antennas for the 12 simulated “random” jammer locations. Notice that the difference between the MLAE performance and the CRB is in most cases small and in many negligible.

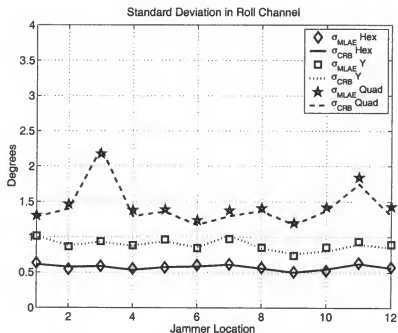


Figure 8.4: Standard deviation of antenna roll estimates and CRB for the Quad antenna (star), Y antenna (square), and Hex antenna (diamond). The 12 points along the abscissa correspond to the 12 jammer locations identified in Figure 8.3. The update rate is 50 Hz.

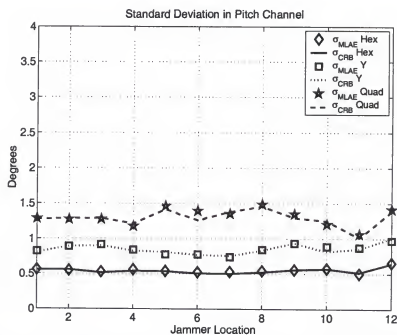


Figure 8.5: Standard deviation of antenna pitch estimates and CRB for the Quad antenna (star), Y antenna (square), and Hex antenna (diamond). The 12 points along the abscissa correspond to the 12 jammer locations identified in Figure 8.3. The update rate is 50 Hz.

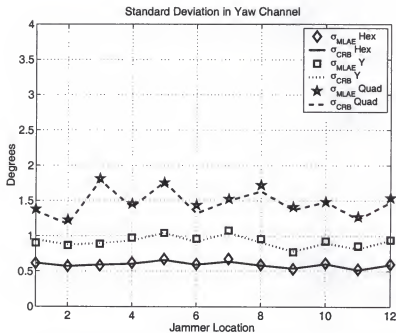


Figure 8.6: Standard deviation of antenna yaw estimates and CRB for the Quad antenna (star), Y antenna (square), and Hex antenna (diamond). The 12 points along the abscissa correspond to the 12 jammer locations identified in Figure 8.3. The update rate is 50 Hz.

Insight into the relative performance of the four attitude estimators discussed above (MLAE, DFW, DFU, and CONV) is provided by comparing the mean total error for each, for each jammer position. Figures 8.7, 8.8, and 8.9 show the mean total error these estimators using the Quad, Y, and Hex antennas respectively.

Several observations may be made about the relative performance of these estimators in the simulation. First, the Conventional approach was always the *poorest* performer, with typical performance levels exceeding 8 degrees of mean total error. Second, the MLAE always provided the *best* performance. In fact, the MLAE in these scenarios seemed the least sensitive to jammer location (among the 12 locations simulated). Finally, the DFW and DFU estimators fell somewhere between the conventional and MLAE. Typically, their performance was much closer to the MLAE than the conventional, with the weighting function operating slightly better than the unweighted.

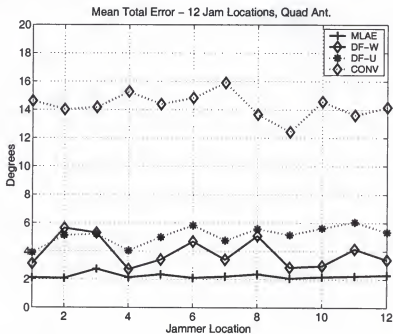


Figure 8.7: Mean total angle error using the Quad antenna. The 12 points along the abscissa correspond to the 12 jammer locations identified in Figure 8.3. Performance is shown for the MLAE (+), DF-W (diamond with solid line), DF-U (asterisk), and conventional attitude estimation algorithms (diamond with dashed line). The update rate is 50 Hz.

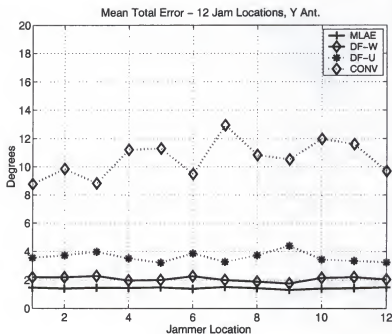


Figure 8.8: Mean total angle error using the Y antenna. The 12 points along the abscissa correspond to the 12 jammer locations identified in Figure 8.3. Performance is shown for the MLAE (+), DF-W (diamond with solid line), DF-U (asterisk), and conventional attitude estimation algorithms (diamond with dashed line). The update rate is 50 Hz.

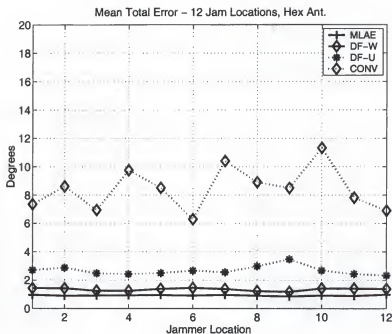


Figure 8.9: Mean total angle error using the Hex antenna. The 12 points along the abscissa correspond to the 12 jammer locations identified in Figure 8.3. Performance is shown for the MLAE (+), DF-W (diamond with solid line), DF-U (asterisk), and conventional attitude estimation algorithms (diamond with dashed line). The update rate is 50 Hz.

Another way to evaluate these estimators is to compare their performance in the jammed environments to an unjammed case. Figures 8.10, 8.11, 8.12, and 8.13 illustrate this comparison for the MLAE, DFW, DFU, and Conventional attitude estimators respectively. Each plot presents data for all three antenna topologies.

An interesting observation is that the performance of the new estimators (MLAE, DFW, and DFU) in the jammed case is not dramatically different than in the non-jammed case. Although there is a degradation, the errors in these single jammer scenarios are only about twice as large as those expected simply from thermal noise, and not orders of magnitude larger as the conventional method experienced.

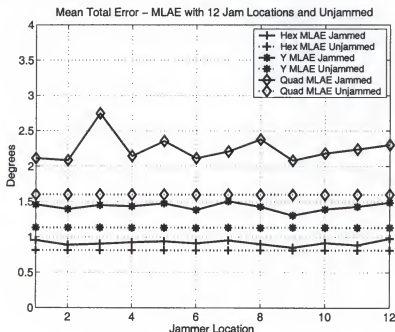


Figure 8.10: Mean total angle error using the MLAE algorithm, comparing the single jammer at “random” locations to the unjammed scenario. The solid lines are with the jammer, and the dashed lines unjammed. Performance is shown for the Hex antenna (+), Y antenna (asterisk), and the Quad antenna (diamond). The update rate is 50 Hz.

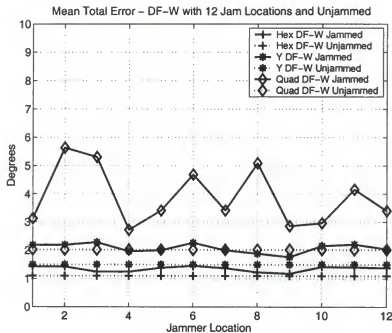


Figure 8.11: Mean total angle error using the DF-W algorithm, comparing the single jammer at “random” locations to the unjammed scenario. The solid lines are with the jammer, and the dashed lines unjammed. Performance is shown for the Hex antenna (+), Y antenna (asterisk), and the Quad antenna (diamond). The update rate is 50 Hz.

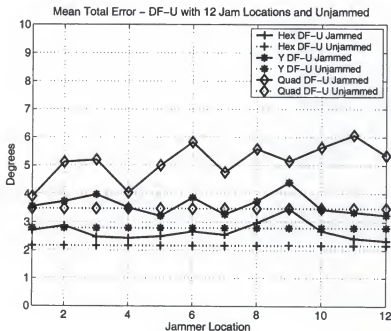


Figure 8.12: Mean total angle error using the DF-U algorithm, comparing the single jammer at “random” locations to the unjammed scenario. The solid lines are with the jammer, and the dashed lines unjammed. Performance is shown for the Hex antenna (+), Y antenna (asterisk), and the Quad antenna (diamond). The update rate is 50 Hz.

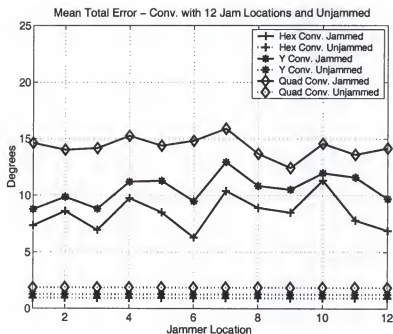


Figure 8.13: Mean total angle error using the conventional algorithm, comparing the single jammer at “random” locations to the unjammed scenario. The solid lines are with the jammer, and the dashed lines unjammed. Performance is shown for the Hex antenna (+), Y antenna (asterisk), and the Quad antenna (diamond). The update rate is 50 Hz.

As the attitude update rate decreases, the amount of time for satellite signal integration and therefore the SNR increases. The previous figures showed performance at an update rate of 50 Hz. For the next set of figures the update was decreased to 12.5 Hz, increasing integration time, SINR, and therefore performance. Keeping the same format as with the 50 Hz data, figures 8.14, 8.15, and 8.16 present the performance comparison to the CRB. Figures 8.17, 8.18, and 8.19 present the mean total error performance for each estimator, and figures 8.20, 8.20, 8.22, 8.23 contain the comparison between jammed and unjammed scenarios.

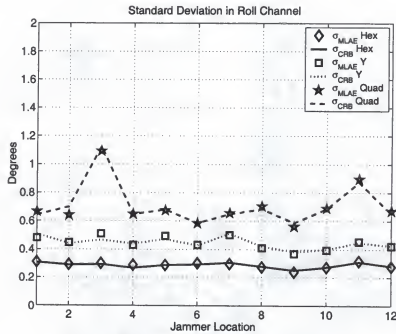


Figure 8.14: Standard deviation of antenna roll estimates and CRB for the Quad antenna (star), Y antenna (square), and Hex antenna (diamond). The update rate is 12.5 Hz.

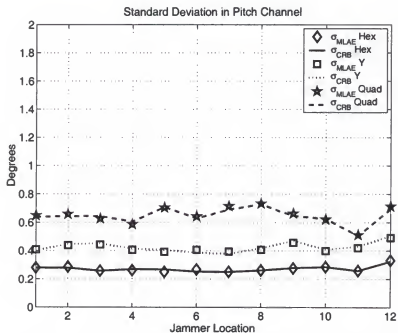


Figure 8.15: Standard deviation of antenna pitch estimates and CRB for the Quad antenna (star), Y antenna (square), and Hex antenna (diamond). The update rate is 12.5 Hz.

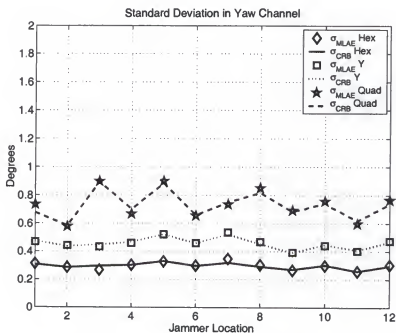


Figure 8.16: Standard deviation of antenna yaw estimates and CRB for the Quad antenna (star), Y antenna (square), and Hex antenna (diamond). The update rate is 12.5 Hz.

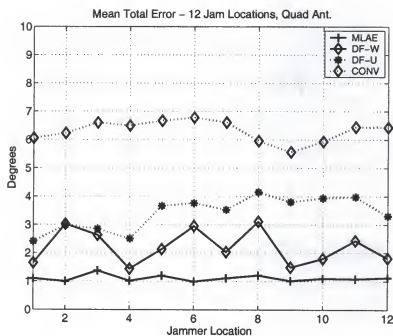


Figure 8.17: Mean total angle error using the Quad antenna. The 12 points along the abscissa correspond to the 12 jammer locations identified in Figure 8.3. Performance is shown for the MLAE (+), DF-W (diamond with solid line), DF-U (asterisk), and conventional attitude estimation algorithms (diamond with dashed line). The update rate is 12.5 Hz.

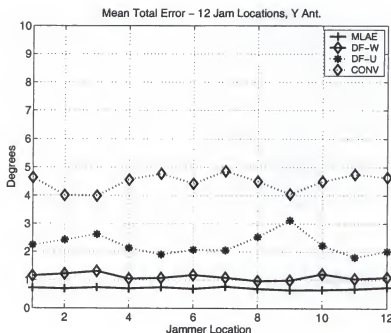


Figure 8.18: Mean total angle error using the Y antenna. The 12 points along the abscissa correspond to the 12 jammer locations identified in Figure 8.3. Performance is shown for the MLAE (+), DF-W (diamond with solid line), DF-U (asterisk), and conventional attitude estimation algorithms (diamond with dashed line). The update rate is 12.5 Hz.

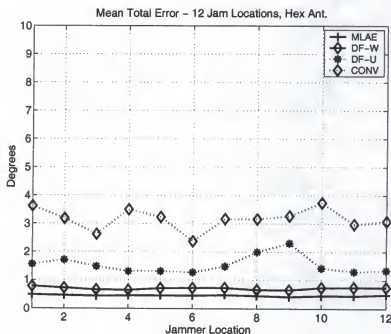


Figure 8.19: Mean total angle error using the Hex antenna. The 12 points along the abscissa correspond to the 12 jammer locations identified in Figure 8.3. Performance is shown for the MLAE (+), DF-W (diamond with solid line), DF-U (asterisk), and conventional attitude estimation algorithms (diamond with dashed line). The update rate is 12.5 Hz.

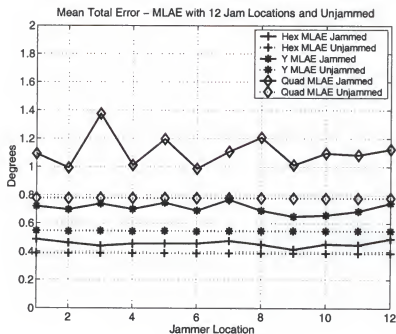


Figure 8.20: Mean total angle error using the MLAE algorithm, comparing the single jammer at “random” locations to the unjammed scenario. The solid lines are with the jammer, and the dashed lines unjammed. Performance is shown for the Hex antenna (+), Y antenna (asterisk), and the Quad antenna (diamond). The update rate is 12.5 Hz.

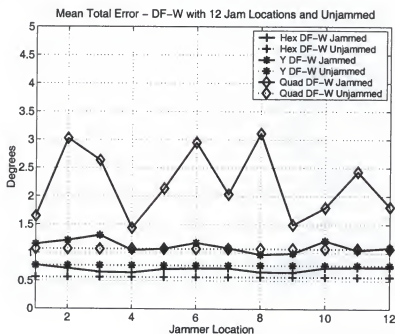


Figure 8.21: Mean total angle error using the DF-W algorithm, comparing the single jammer at “random” locations to the unjammed scenario. The solid lines are with the jammer, and the dashed lines unjammed. Performance is shown for the Hex antenna (+), Y antenna (asterisk), and the Quad antenna (diamond). The update rate is 12.5 Hz.

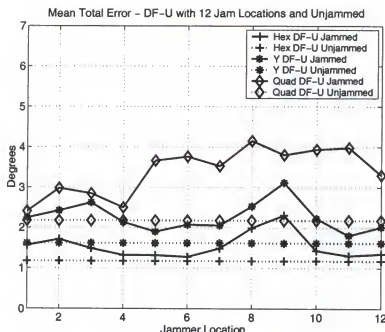


Figure 8.22: Mean total angle error using the DF-U algorithm, comparing the single jammer at “random” locations to the unjammed scenario. The solid lines are with the jammer, and the dashed lines unjammed. Performance is shown for the Hex antenna (+), Y antenna (asterisk), and the Quad antenna (diamond). The update rate is 12.5 Hz.

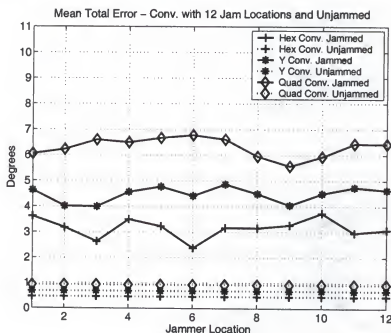


Figure 8.23: Mean total angle error using the conventional algorithm, comparing the single jammer at “random” locations to the unjammed scenario. The solid lines are with the jammer, and the dashed lines unjammed. Performance is shown for the Hex antenna (+), Y antenna (asterisk), and the Quad antenna (diamond). The update rate is 12.5 Hz.

In the above jammed scenarios, the conventional attitude estimator (i.e. using phase differences as the observables) was always the worst performing algorithm. As discussed in Chapter 2, this is because the assumptions in the signal model are violated when the additional interference source is added to the signals from the satellites. However, another method of comparison between these attitude estimators is in the situation where the assumptions used in the conventional model *do* hold, i.e. the unjammed case.

Tables 8.1 and 8.2 provide the mean total error for the unjammed scenario for each of the three estimators developed in this work and the conventional method. Now, unlike the jammed cases, the conventional approach outperforms the two approximations to the MLAE developed in Chapter 6. This is reasonable, since the intermediate step of direction finding involved in the DFW and DFU approaches may introduce error. However, the conventional approach is still inferior to the MLAE. Conceptually, the MLAE outperforms the conventional approach by (optimally) incorporating the *amplitude and phase* of the response from the satellites, where the conventional approach³ uses only the phase. Table 8.1 presents the unjammed performance for the 50 Hz update rate, and Table 8.2 presents the performance for the 12.5 Hz update rate. These two rates correspond to the rates used in the previous plots.

³ Other GPS attitude determination works have investigated using the amplitude information as well as the phase, but for different reasons. In [1], the amplitude is used as a spectral estimator and predictor of the multipath interference.

Table 8.1: Mean total error performance comparison of the four estimators in an un-jammed environment. Update rate is 50 Hz.

Antenna	MLAE	Conventional AD	DF - Weighted	DF - Unweighted
Quad	1.60	1.85	2.02	3.50
Y	1.13	1.26	1.50	2.79
Hex	0.81	0.93	1.10	2.17

Table 8.2: Mean total error performance comparison of the four estimators in an un-jammed environment. Update rate is 12.5 Hz.

Antenna	MLAE	Conventional AD	DF - Weighted	DF - Unweighted
Quad	0.78	0.92	1.07	2.18
Y	0.55	0.68	0.78	1.62
Hex	0.38	0.46	0.57	1.18

8.5 Study 2: Varying Attitude Update Rate

In attitude determination, the attitude should be essentially constant during an integration period to prevent smearing of attitude data. Also, the SNR (and measurement accuracy) increases with integration time. Therefore the update rate is a key design parameter in attitude determination, and involves engineering tradeoffs. More frequent estimates serve to ensure that the attitude is indeed constant during the estimation process, but have a larger variance since less time is available for integration of the GPS signals. Similarly, less frequent updates are more accurate, but only if the antenna attitude is essentially constant during the entire integration process. Additional antennas can be used to improve the accuracy, but at the cost of increased system complexity. The update rate is therefore a compromise between expected platform dynamics, accuracy, and complexity.

In this study, we examine the performance as a function of integration time. Case 1 evaluates this performance for a single jammer, and Case 2 for 3 jammers in the field of view. As in Study 1, the jammers are located at an angle of 44 - 48 degrees from antenna boresight, as shown in figure 8.24. In this scenario, the antenna attitude is non-zero only in yaw, with $\xi_\psi = \frac{\pi}{4}$.

As with the random jammer study, MLAE performance is compared to the CRB. Figures 8.25, 8.26, and 8.27 present the standard deviations of MLAE estimates in roll, pitch, and yaw respectively, as a function of update rate, for all three antenna topologies. Recall from Chapter 5 that the MLAE is *asymptotically efficient*. This is equivalent to stating that as the effective SNR increases, the MLAE approaches the CRB. There are two ways in which the effective SNR may increase: as the integration time increases (update rate decreases), and as the number and / or spacing of sensors increases. The Hex antenna incorporates more sensors than the Quad or Y antenna, and the difference between the MLAE standard deviations and the CRB with this antenna are small throughout the span of update rates investigated. The antenna with the smallest spacing and number of sensors is the Quad. For fast update rates a discernable difference between

the MLAE performance and the CRB exists with this antenna topology, however this difference decreases as the integration time increases.

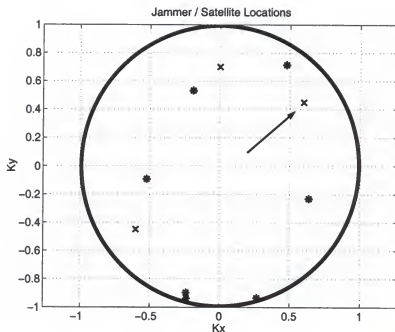


Figure 8.24: Satellite (asterisk) and Jammer Locations (x) for the varying update rate study. The jammer indicated by the arrow is the only jammer used in case 1. In case 2, all three jammers appear.

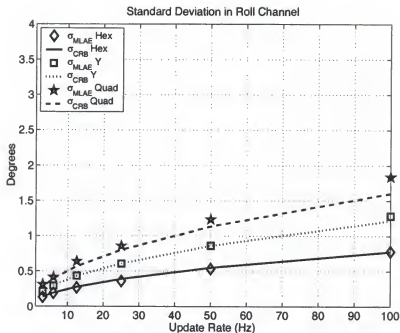


Figure 8.25: Standard deviation of antenna roll estimates and CRB for the Quad antenna (star), Y antenna (square), and Hex antenna (diamond) vs. update rate. One jammer in view.

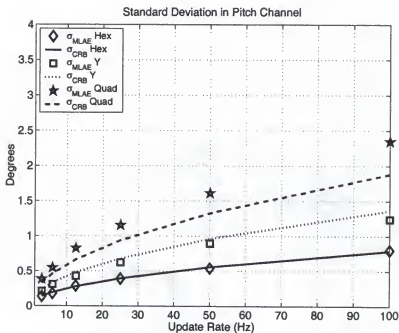


Figure 8.26: Standard deviation of antenna pitch estimates and CRB for the Quad antenna (star), Y antenna (square), and Hex antenna (diamond) vs. update rate. One jammer in view.

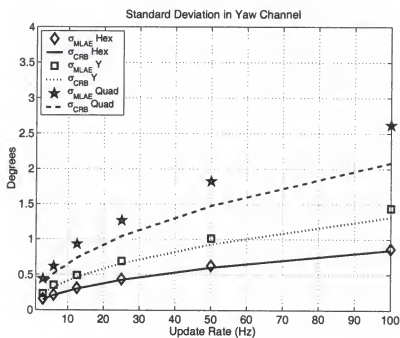


Figure 8.27: Standard deviation of antenna yaw estimates and CRB for the Quad antenna (star), Y antenna (square), and Hex antenna (diamond) vs. update rate. One jammer in view.

It is insightful to compare the relative performance of the four attitude estimators by examining their mean total error as the update rate changes for a fixed jammer scenario. Figures 8.28, 8.29, and 8.30 present this comparison for the Quad, Y, and Hex antennas respectively.

The performance for the Hex antenna topology, which has 7 sensors, is superior to the 4 sensor Y and Quad topologies. The Y, which is set on the triangular lattice, outperforms the rectangular lattice Quad antenna because the sensors are slightly further apart for the Y, resulting in longer baseline lengths. The MLAE estimator always outperforms all other attitude estimators. Performance for any estimator or antenna increases as the update rate decreases, since the resulting longer integration times increase the signal to interference ratio. As the integration increases, the performance of even conventional attitude determination methods improves, however its error is several times greater than the methods developed in this work even at the relative slow attitude update rates of 10 Hz.

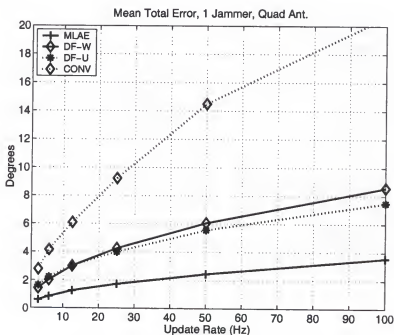


Figure 8.28: Mean total angle error using the Quad antenna vs. update rate for 1 jammer. Performance is shown for the MLAE (+), DF-W (diamond with solid line), DF-U (asterisk), and conventional attitude estimation algorithms (diamond with dashed line).

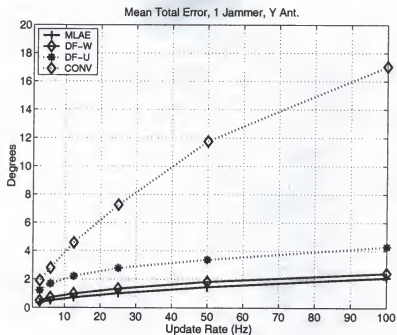


Figure 8.29: Mean total angle error using the Y antenna vs. update rate for 1 jammer. Performance is shown for the MLAE (+), DF-W (diamond with solid line), DF-U (asterisk), and conventional attitude estimation algorithms (diamond with dashed line).

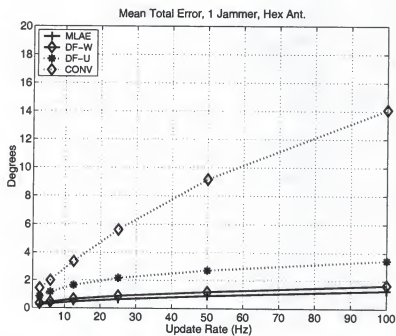


Figure 8.30: Mean total angle error using the Hex antenna vs. update rate for 1 jammer. Performance is shown for the MLAE (+), DF-W (diamond with solid line), DF-U (asterisk), and conventional attitude estimation algorithms (diamond with dashed line).

Figures 8.31, 8.32, 8.33 and 8.34 compare the performance of the MLAE, DFW, DFU and conventional attitude estimators in the single jammer environment to their performance in an unjammed environment. This provides an indication as to the level of robustness, or jammer tolerance of each algorithm. The MLAE has the greatest jammer tolerance. The maximum increase in mean total error between jammed and unjammed is a factor of around 1.5 for the Quad antenna and much less for the other two. The DFW maximum increase is greater than three for the Quad antenna, and less for the others as well. It is interesting that the DFU maximum increase is less than the DFW, but in general its ratio of jammed to unjammed mean total error is larger than that of the DFW, and the unjammed performance of the DFU is worse than the DFW. Finally, the conventional approach has the largest increase in mean total error in a jammed environment over an unjammed scenario. Of course, this was expected and was in fact the motivation behind this research.

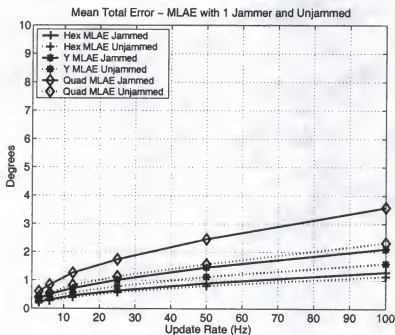


Figure 8.31: Mean total angle error using the MLAE algorithm, comparing the single jammer at "random" locations to the unjammed scenario, vs. update rate. The solid lines are with the jammer, and the dashed lines unjammed. Performance is shown for the Hex antenna (+), Y antenna (asterisk), and the Quad antenna (diamond).

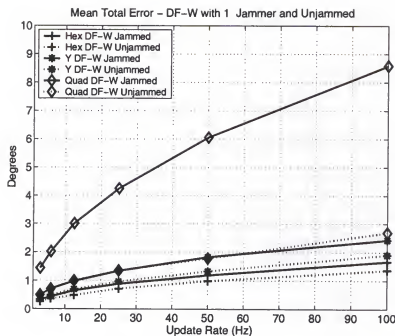


Figure 8.32: Mean total angle error using the DF-W algorithm, comparing the single jammer scenario to the unjammed scenario, vs. update rate. The solid lines are with the jammer, and the dashed lines unjammed. Performance is shown for the Hex antenna (+), Y antenna (*), and the Quad antenna (diamond).

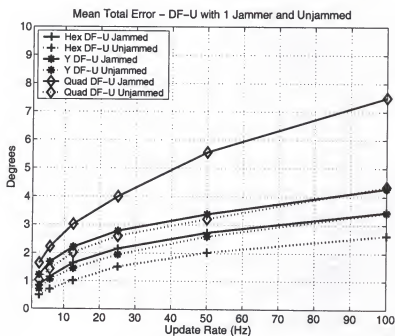


Figure 8.33: Mean total angle error using the DF-U algorithm, comparing the single jammer scenario to the unjammed scenario, vs. update rate. The solid lines are with the jammer, and the dashed lines unjammed. Performance is shown for the Hex antenna (+), Y antenna (*), and the Quad antenna (diamond).

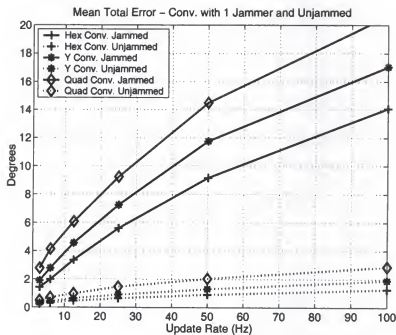


Figure 8.34: Mean total angle error using the conventional algorithm, comparing the single jammer scenario to the unjammed scenario, vs. update rate. The solid lines are with the jammer, and the dashed lines unjammed. Performance is shown for the Hex antenna (+), Y antenna (asterisk), and the Quad antenna (diamond).

Figures 8.35, 8.36, and 8.37 present the mean total error for the four attitude estimators in a three jammer scenario. This scenario with three jammers is stressing for the four sensor antenna topologies, and this is reflected in the performance estimates. Not every scenario involving three jammers will exhibit the performance reported here. In fact, the three jammers are spaced throughout the sky, in essentially a “worst case” type scenario.

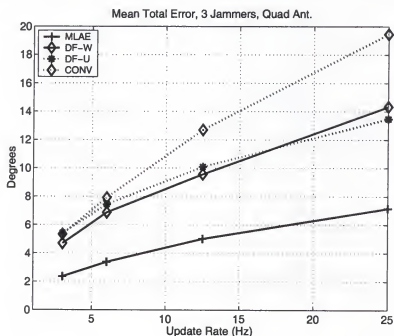


Figure 8.35: Mean total angle error using the Quad antenna vs. update rate for 3 jammers. Performance is shown for the MLAE (+), DF-W (diamond with solid line), DF-U (asterisk), and conventional attitude estimation algorithms (diamond with dashed line).

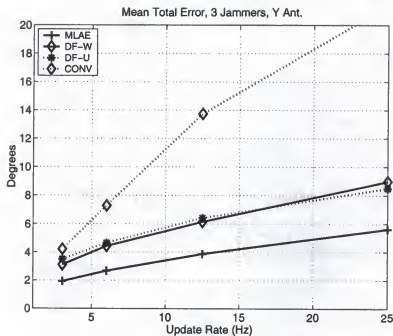


Figure 8.36: Mean total angle error using the Y antenna vs. update rate for 3 jammers. Performance is shown for the MLAE (+), DF-W (diamond with solid line), DF-U (asterisk), and conventional attitude estimation algorithms (diamond with dashed line).

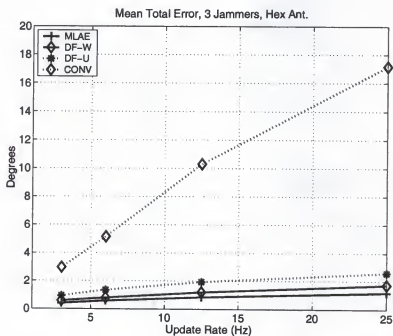


Figure 8.37: Mean total angle error using the Hex antenna vs. update rate for 3 jammers. Performance is shown for the MLAE (+), DF-W (diamond with solid line), DF-U (asterisk), and conventional attitude estimation algorithms (diamond with dashed line).

Figures 8.38, 8.39, 8.40, and 8.41 present the performance of the MLAE, DFW, DFU and conventional attitude estimators in the three jammer environment and their performance in an unjammed environment. In all cases the ratio between the jammed and unjammed cases is larger in this three jammer case than in that of the single jammer. However, the same relative robustness exists among the four estimators, with the MLAE being the most robust and the conventional approach the least.

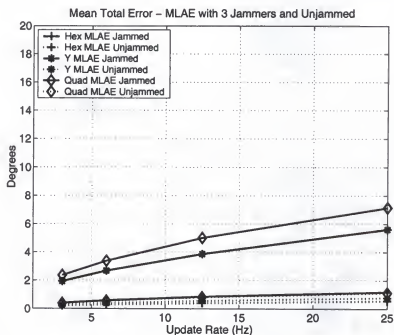


Figure 8.38: Mean total angle error using the MLAE algorithm, comparing the three jammer scenario to the unjammed scenario, vs. update rate. The solid lines are with the jammer, and the dashed lines unjammed. Performance is shown for the Hex antenna (+), Y antenna (asterisk), and the Quad antenna (diamond).

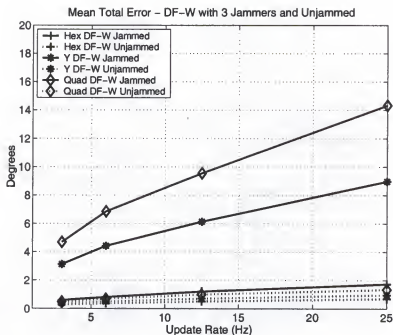


Figure 8.39: Mean total angle error using the DF-W algorithm, comparing the three jammer scenario to the unjammed scenario, vs. update rate. The solid lines are with the jammer, and the dashed lines unjammed. Performance is shown for the Hex antenna (+), Y antenna (asterisk), and the Quad antenna (diamond).

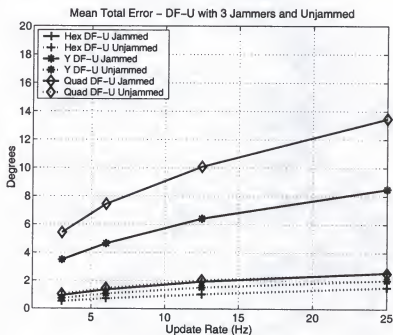


Figure 8.40: Mean total angle error using the DF-U algorithm, comparing the three jammer scenario to the unjammed scenario, vs. update rate. The solid lines are with the jammer, and the dashed lines unjammed. Performance is shown for the Hex antenna (+), Y antenna (asterisk), and the Quad antenna (diamond).

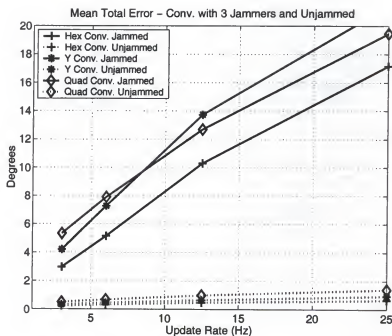


Figure 8.41: Mean total angle error using the conventional algorithm, comparing the three jammer scenario to the unjammed scenario, vs. update rate. The solid lines are with the jammer, and the dashed lines unjammed. Performance is shown for the Hex antenna (+), Y antenna (asterisk), and the Quad antenna (diamond).

8.6 Study 3: Wider Baselines and Dual Frequency

In this study we will show performance results from simulations of the dual-frequency attitude estimator. In addition, this study considers a larger baseline length than the Nyquist spacing used in the previous studies. The sensors are spaced at five times the spacing used before, which corresponds to approximately .6 meters apart for the quad antenna, and slightly larger for the other two antennas. Figure 8.42 shows the sensor locations used in this study. This is why the performance is so dramatically better than in the two previous studies.

This study does not address the decrease in false attitudes discussed in Chapter 7, but only the increase in performance attained by including the second frequency. In addition, like all the previous studies, assumed that the adaptive antenna array is able to keep the satellites in code and Doppler track even in the presence of jammers.

Figures 8.43, 8.44, 8.45 present the mean total error performance of the single frequency MLAE operating at the L1 GPS frequency, the L2 GPS frequency, and the dual-frequency MLAE which uses both frequencies. The scenario is the single jammer scenario used in Study 2 Case 1. Figures 8.46, 8.47, 8.48 present similar plots but using the three jammer scenario of Study 2 Case 2. However in the scenario that provided the data for all of these figures the jammers were present on *both* GPS frequencies at the same power levels per band as used before.

Some observations may be drawn from these simulation results. When the performance is noticeably better at one frequency than the other (due to the complex grating lobe structure and the jammer location), the dual-frequency MLAE performs slightly better than the best performing single frequency. When the two single frequency MLAE's perform about the same, the dual-frequency MLAE performs noticeably better than the two single frequencies. In all cases the dual-frequency MLAE performed as well as or better than the single frequency MLAE operating on either band. These observations are consistent with the performance improvements and CRB derivation discussed in Chapter 7.

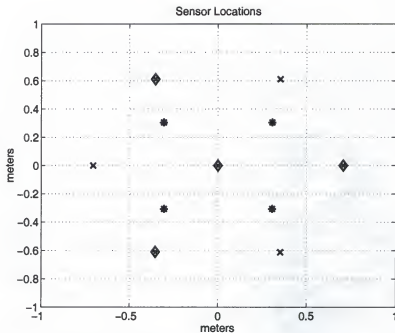


Figure 8.42: Sensor Locations used in the wide baseline study. The three antenna topologies are the Quad (asterisk), Y (diamond), and Hex (x).

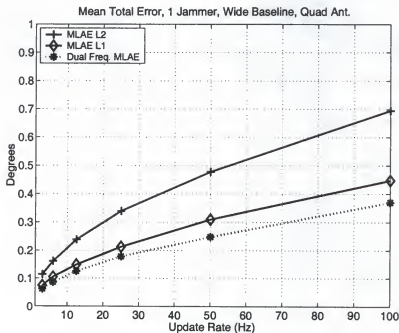


Figure 8.43: Mean total angle error using the Quad antenna vs. update rate for 1 jammer. Performance is shown for the single frequency MLAE at L1 (diamond) and L2 (+), and for the dual frequency MLAE (asterisk).

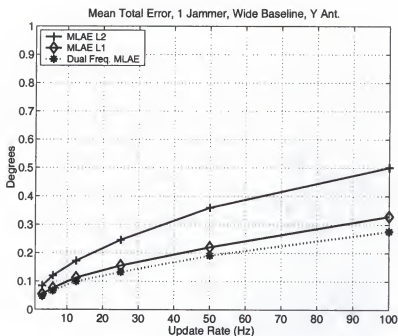


Figure 8.44: Mean total angle error using the Y antenna vs. update rate for 1 jammer. Performance is shown for the single frequency MLAE at L1 (diamond) and L2 (+), and for the dual frequency MLAE (asterisk).

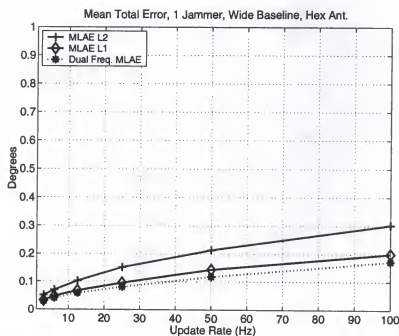


Figure 8.45: Mean total angle error using the Hex antenna vs. update rate for 1 jammer. Performance is shown for the single frequency MLAE at L1 (diamond) and L2 (+), and for the dual frequency MLAE (asterisk).

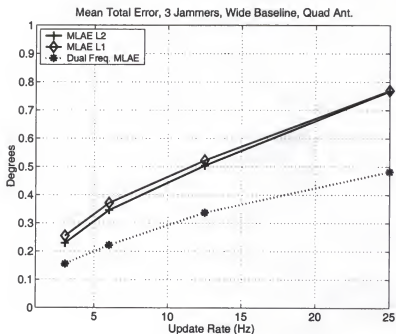


Figure 8.46: Mean total angle error using the Quad antenna vs. update rate for 3 jammers. Performance is shown for the single frequency MLAE at L1 (diamond) and L2 (+), and for the dual frequency MLAE (asterisk).

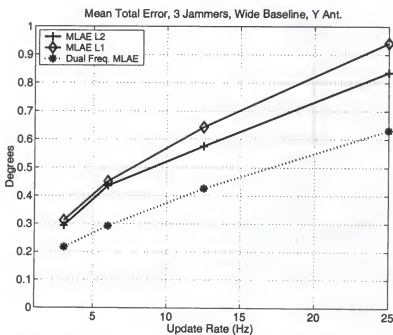


Figure 8.47: Mean total angle error using the Y antenna vs. update rate for 3 jammers. Performance is shown for the single frequency MLAE at L1 (diamond) and L2 (+), and for the dual frequency MLAE (asterisk).

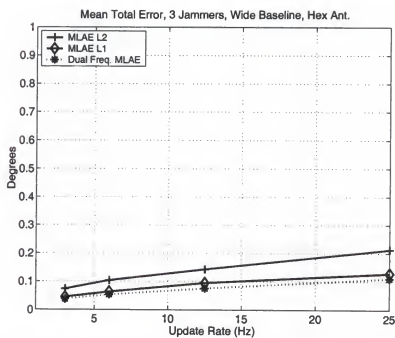


Figure 8.48: Mean total angle error using the Hex antenna vs. update rate for 3 jammers. Performance is shown for the single frequency MLAE at L1 (diamond) and L2 (+), and for the dual frequency MLAE (asterisk).

8.7 Conclusions

In this chapter we have demonstrated via simulation the performance of the three new attitude estimators developed in the previous chapters. Three separate studies were undertaken, and performance of the estimators was compared to each other, the conventional attitude determination method, the Cramér-Rao Bound, and to unjammed cases for three antenna topologies.

Several observations were made from these studies that are summarized here. First, the MLAE always provides the best mean total attitude error performance. This is true regardless of the antenna topology, number of jammers, or update rate. Second, the MLAE was shown to approach (or essentially equal) the CRB. Since the MLAE is asymptotically efficient, the difference between MLAE performance and the CRB depends on the number of sensors, number of jammers, array topology, and update rate. In general, the stronger the satellite signal in comparison to the interference, the smaller the difference between the MLAE and the CRB.

Third, the two approximations to the MLAE, i.e. the DFW and DFU algorithms, often estimate attitude with errors close to but slightly larger than the MLAE, with DFW typically outperforming DFU. This is important, since the computational savings from these suboptimal algorithms may be significant in a tactical application.

Fourth, the conventional attitude estimation approach (using phase differences) has very little performance in a jammed environment. As discussed earlier, this is expected and provided the motivation to investigate jam-resistant algorithms. It is interesting to note, however, that in an *unjammed* environment the conventional approach outperforms all other estimators except the MLAE. This implies that a tactical approach using the DFW or DFU methods might need to investigate switching between the direction finding algorithms and the conventional approach depending on the presence or absence of interference sources.

Finally, the study involving the dual-frequency MLAE showed that it always outperformed the single frequency MLAE at either band. The amount of the performance gain is driven by the relative performance in each band. That is, if one band is providing poorer

performance that the other, the performance gain of the dual-frequency MLAE over the single frequency MLAE at the better performing band will be small.

CHAPTER 9 CONCLUSIONS

9.1 Summary

This dissertation provides a comprehensive investigation into the new field of robust, jam-resistant attitude determination using the Global Positioning System. With its low transmit power and considerable distance from receivers, GPS is known to be susceptible to jamming. Efforts to date have investigated various receiver designs and adaptive antenna arrays to improve the anti-jam capabilities of GPS *position location*, but until this work no extension of anti-jam capabilities to *attitude determination* existed.

Direction finding and GPS based attitude determination are similar concepts related by their use of carrier phase interferometry. Historically, direction finding algorithms cast in terms of a maximum likelihood estimator have shown significant interference resistance, so the approach of this work was to exploit similarities between these estimators and attitude determination. Recent works in multiple source direction finding have demonstrated that if the source waveforms are uncorrelated, the maximum likelihood estimates of all directions are (asymptotically) equal to decoupled estimates of individual directions, i.e. the direction to one source may be found without knowledge or use of the direction to any other. This is an important result for the direction finding application, and provided key insight for this dissertation. However, use of the sources independently does *not* lead to the best possible performance for the attitude determination application. Since the positions of the sources (the GPS satellites) with respect to each other are known, to treat each source independently and to not make use of this information would lead to a sub-optimal solution.

An optimal solution does exist if some of the concepts from the direction finding field are redefined. Specifically, by reparameterizing the argument of the array response vector to be antenna attitude and local level frame direction instead of direction in the antenna

frame, a coupled estimator is derived that makes use of the known relative positions of the satellites. This approach is named the Maximum Likelihood Attitude Estimator (MLAE). By using estimates of the interference statistics, this estimator reduces to a simple search over the uncertainty in (the three parameters of) attitude of the maximum likelihood metric. The estimator decomposes into a sum of terms, where each term is composed of data relating to a single satellite, providing for a parallel implementation architecture.

In this dissertation the MLAE is shown to possess several desirable statistical properties. The MLAE is proven to be a consistent estimator. That is, as the integration time increases the variance of the estimation error decreases. In addition, it is asymptotically statistically efficient. As the integration time increases, the estimation error approaches the lower limit of any unbiased estimator.

In addition to the MLAE, this work considers two approximations to this algorithm. These approaches reduce the computational burden of searching a three dimensional attitude space by finding the directions to the satellites independently, which is typically a series of independent two dimensional searches, one per source. The difference between the two approximations is in the conversion from the direction estimates back to the attitude. In the first algorithm, the contribution from each satellite is weighted equally, while in the second each satellite is weighted by its adaptive signal to interference ratio (SINR). Simulation results indicate that, in general, inclusion of the adaptive SINR weighting improves performance of the estimator with a very small increase in the number of computations.

Currently each satellite broadcasts the GPS P(Y) code on two frequencies. This provides additional information that can be incorporated to improve the quality of the attitude estimate. To exploit this information, the dissertation develops the *dual-frequency* MLAE. The dual-frequency MLAE is also asymptotically statistically efficient, and provides two benefits over the single frequency version. First, the estimation error is reduced by incorporating the second frequency. Second, when only a few satellites are being tracked and used for attitude estimation and the sensor spacing is greater than the Nyquist criterion, incorporating the second frequency "smooths" the likelihood surface,

providing less areas that may lead to incorrect solutions. This important result provides robustness against false solutions when the sensor spacing is increased, which is known to increase estimator accuracy.

A series of performance studies were performed and documented in this dissertation. These studies compared the performance of the various attitude estimators in a variety of jammed environments to one another, to the Cramér-Rao Bound (CRB), and to performance in an unjammed case. In all cases the MLAE provided superior performance to all other attitude estimators simulated. Furthermore, the MLAE and its approximations significantly outperformed the conventional approach in all *jammed* cases investigated.

9.2 Future Work

This research has taken important steps towards understanding and mitigating jamming and other interference for GPS attitude determination. There are, however, additional contributions beyond this research that will increase the performance of these methods, provide better estimates of sensitivity to real world limitations, or both. A few of these contributions are listed below.

As discussed in Chapter 4, the MLAE involves a three dimensional search over attitude. This can be computationally expensive, and may be prohibitive for large uncertainties in attitude. Although several maximization/minimization techniques exist, a comparison or optimization of them has not been performed for this particular application. In addition, it may be possible to develop a reasonably accurate *model* for the likelihood volume, and with a few hundred data points estimate the parameters of this model. If the parameters are estimated with sufficient accuracy, the model will provide a good estimate of the location of the extrema. From this model estimate, either a fine grid search or simply a check of neighboring points could be performed to produce the final attitude estimate.

Several assumptions which tend to idealize performance were made concerning the antenna and receiver characteristics. Mutual coupling between sensors was ignored, and the receiver channels were assumed to be perfectly matched. These “real world”

imperfections will tend to degrade performance. However, this effect can be mitigated to some degree by levying appropriate specifications on the hardware design.

Another real world area of investigation involves error in the array calibration. The simulation results provided in this dissertation assume that the array is calibrated (i.e. the array response vector is known for all spatial locations of interest). However, if the effective locations (phase centers) of the sensors are in error, the array response vector will not be correct. This will degrade performance for both the MLAE and the direction finding based approaches. One investigation would be to study the relative robustness of the MLAE and the direction finding attitude determination approaches to array calibration errors.

In this research, simulation results have focused on the statistics (either standard deviation in Euler angle measurements or mean total error) of the estimators at a static snapshot in time. In addition, an assumption on results has been that the adaptive beamformer portion (the typical GPS anti-jam system for position location) has converged to keep the satellites in track. The next level of investigation of these concepts is to explore the performance of a closed loop system. This could include a tracker design that incorporates both the GPS based attitude information and an inertial navigation system (INS) that uses gyros for attitude estimation. Inherent in this design would be a method to estimate the attitude errors from the new algorithms, possibly via the Cramér Rao Bound. This investigation could also include antenna (body) motion. This may have the effect of smearing data during the observation interval, and would allow the beamformer to adaptively attempt to remove jammers to keep the satellites in track in code and Doppler.

The derivations in this work do not include multipath reflections of either the jammer waveforms or the satellites. To account for these, multiple snapshots of demodulated data may be used to optimally remove interference and estimate the attitude. This would essentially be a Space - Time Adaptive Processing (STAP) extension to attitude determination. Research in this area may focus on quantifying the extent of possible performance gains, and the best integration of STAP and code tracking loops.

Finally, further research is warranted in the dual frequency work Chapter 7. The dual frequency extension of the MLAE developed in that chapter may be just one example in a class of multi-spectral estimation algorithms.

APPENDIX A CRAMÉR-RAO BOUND

The Cramér-Rao Bound (CRB) provides a lower bound on the mean squared error (MSE) of the estimation error. An estimator whose MSE *achieves* the CRB is said to be statistically efficient (see, for example, Stoica and Moses [9]). In this section we will derive the CRB for the attitude estimation problem.

The Cramér-Rao Bound (CRB) matrix \mathbf{P}_{cr} is found from [9] as

$$\mathbf{P}_{cr} = \left(\mathbb{E} \left\{ \left[\frac{\partial \ln f_X(\chi|\rho)}{\partial \rho} \right] \left[\frac{\partial \ln f_X(\chi|\rho)}{\partial \rho} \right]^T \right\} \right)^{-1} \quad (\text{A.1})$$

where ρ is a vector of the real unknown parameters (i.e. the parameters to be estimated), and $f_X(\chi|\rho)$ is the likelihood function. Before performing the matrix inversion, the right side of the equation, before performing the inversion (i.e. \mathbf{P}_{cr}^{-1}), is the “Fisher Information Matrix,” and will be denoted here by FIM. For the attitude determination when the interference covariance is known and each satellite return is scaled by an unknown complex gain, ρ consists of the three unknown parameters of attitude, q_i , $i = 1, 2, 3$ and the $2 \times L$ real components of the L complex gains. It is useful to organize these terms in

the following order:

$$\rho = \begin{bmatrix} q_1 \\ q_2 \\ q_3 \\ \text{Re}(\gamma_1) \\ \text{Re}(\gamma_2) \\ \vdots \\ \text{Re}(\gamma_L) \\ \text{Im}(\gamma_1) \\ \text{Im}(\gamma_2) \\ \vdots \\ \text{Im}(\gamma_L) \end{bmatrix} \quad (\text{A.2})$$

A convenient parameterization of the three attitude parameters for the CRB calculation, and the one used in this work, is to choose the three Euler angles ξ_Φ , ξ_Θ , and ξ_Ψ .

Using (4.49), the log-likelihood ratio (LLR) may be written as

$$\ln f_X(\chi|\rho) = \{\text{constant terms}\} - \sum_{l=1}^L [\mathbf{u}_l - \gamma_l \mathbf{a}_l(q)]^H \mathbf{C}_l^{-1} [\mathbf{u}_l - \gamma_l \mathbf{a}_l(q)] \quad (\text{A.3})$$

In order to evaluate (A.1) (i.e. to generate the various terms of the FIM), the following three derivative formulas are required:

$$\frac{\partial \ln f_X(\chi|\rho)}{\partial \text{Re}(\gamma_l)} = 2 \text{Re} \{ \mathbf{a}_l^H(q) \mathbf{C}_l^{-1} \mathbf{w}_l \} \quad (\text{A.4})$$

$$\frac{\partial \ln f_X(\chi|\rho)}{\partial \text{Im}(\gamma_l)} = 2 \text{Im} \{ \mathbf{a}_l^H(q) \mathbf{C}_l^{-1} \mathbf{w}_l \} \quad (\text{A.5})$$

$$\frac{\partial \ln f_X(\chi|\rho)}{\partial q_i} = 2 \text{Re} \left\{ \sum_{l=1}^L \gamma_l^* \mathbf{d}_i^H(l) \mathbf{C}_l^{-1} \mathbf{w}_l \right\} \quad (\text{A.6})$$

where \mathbf{w}_l is defined in (4.35) and $\mathbf{d}_k(l)$ is defined as the derivative of \mathbf{a}_l with respect to the k th term of attitude q , q_k .

$$\mathbf{d}_k(l) = \frac{\partial \mathbf{a}_l}{\partial q_k} \quad (\text{A.7})$$

Note that each of the L array response vectors corresponding to the L satellites will have different derivative vectors. The convention used here is as follows: the subscript indicates the attitude parameter with respect to which the derivative is being taken, while the value in parentheses indicates the satellite to which the array response vector corresponds. For notational convenience, a whitened form of the derivative vectors is defined as

$$\tilde{\mathbf{d}}_k(l) = \mathbf{C}_l^{-1/2} \mathbf{d}_l \quad (\text{A.8})$$

where

$$\mathbf{C}_l^{-1} = \mathbf{C}_l^{-1/2} \mathbf{C}_l^{-1/2} \quad (\text{A.9})$$

$$\mathbf{C}_l^{-1/2} = \left(\mathbf{C}_l^{-1/2} \right)^H \quad (\text{A.10})$$

The order of the terms in the vector ρ determines the structure of the FIM. It is easy to see that ρ is composed of three types of terms: “attitude” terms, “real gain” terms, and “imaginary gain” terms. The FIM will then be composed of blocks of (the expected value of) the products of the derivatives with respect to each of the types of terms. For example, the upper 3×3 block of the FIM is the “attitude-attitude” block, and the $3 \times L$ block immediately to the right is the “attitude-real gain” block, and so on. The approach employed here for populating the components of the FIM will be to evaluate a representative term in each block, followed by a general expression for the block itself.

The i, j term of the upper 3×3 (“attitude-attitude”) block is found (A.6) and (A.1)

as

$$\begin{aligned} \text{FIM}_{i,j} &= 2 \operatorname{Re} \left\{ \sum_{l=1}^L |\gamma_l|^2 \mathbf{d}_i^H(l) \mathbf{C}_l^{-1} \mathbf{d}_j(l) \right\} \\ &= 2 \operatorname{Re} \left\{ \sum_{l=1}^L |\gamma_l|^2 \tilde{\mathbf{d}}_i^H(l) \tilde{\mathbf{d}}_j(l) \right\} \end{aligned} \quad (\text{A.11})$$

where we have used [23]

$$\operatorname{Re}(a) \operatorname{Re}(b) = \frac{1}{2} \operatorname{Re}(ab^* + ab) \quad (\text{A.12})$$

and the properties of Chapter 4

$$E[\mathbf{w}_i \mathbf{w}_j^T] = 0 \quad (\text{A.13})$$

$$E[\mathbf{w}_i \mathbf{w}_j^H] = \mathbf{C}_j \delta(i - j) \quad (\text{A.14})$$

Using (A.11), the entire upper 3×3 block may be written as

$$\text{FIM}_{(1-3), (1-3)} = 2 \operatorname{Re} \left\{ \sum_{l=1}^L |\gamma_l|^2 \mathbf{D}^H(l) \mathbf{C}_l^{-1} \mathbf{D}(l) \right\} \quad (\text{A.15})$$

$$= 2 \sum_{l=1}^L |\gamma_l|^2 \tilde{\mathbf{D}}^H(l) \tilde{\mathbf{D}}(l) \quad (\text{A.16})$$

$$\triangleq \mathbf{F}_q \quad (\text{A.17})$$

where

$$\mathbf{D}(l) = [\mathbf{d}_1(l) \ \mathbf{d}_2(l) \ \mathbf{d}_3(l)] \quad (\text{A.18})$$

and

$$\tilde{\mathbf{D}}(l) = [\tilde{\mathbf{d}}_1(l) \ \tilde{\mathbf{d}}_2(l) \ \tilde{\mathbf{d}}_3(l)] \quad (\text{A.19})$$

In the “attitude-real gain” (and transpose of the “real gain-attitude”) block of the FIM, the component corresponding to attitude term i and gain j is

$$\text{FIM}_{i, j+3} = 2 \operatorname{Re} \left\{ \gamma_j \mathbf{a}^H(j) \mathbf{C}_i^{-1} \mathbf{d}_i(j) \right\} \quad (\text{A.20})$$

$$= 2 \operatorname{Re} \left\{ \gamma_j \tilde{\mathbf{a}}^H(j) \tilde{\mathbf{d}}_i(j) \right\} \quad (\text{A.21})$$

Using this, the entire row (column) corresponding to the i th attitude and the L real components of L γ 's is found as

$$\text{FIM}_{i, (4, 5, \dots, 3+L)} = 2 \operatorname{Re} \left\{ \operatorname{diag} \left\{ \Gamma \mathbf{A}^H \mathbf{C}_i^{-1} \Delta_i \right\} \right\} \quad (\text{A.22})$$

$$= 2 \operatorname{Re} \left\{ \operatorname{diag} \left\{ \Gamma \tilde{\mathbf{A}}^H \tilde{\Delta}_i \right\} \right\} \quad (\text{A.23})$$

where

$$\Gamma = \begin{bmatrix} \gamma_1 & 0 & \cdots & 0 \\ 0 & \gamma_2 & 0 & 0 \\ 0 & \cdots & \ddots & 0 \\ 0 & \cdots & 0 & \gamma_L \end{bmatrix} \quad (\text{A.24})$$

$$\mathbf{A} = [\mathbf{a}_1 \ \mathbf{a}_2 \ \cdots \ \mathbf{a}_L] \quad (\text{A.25})$$

$$\tilde{\mathbf{A}} = [\tilde{\mathbf{a}}_1 \ \tilde{\mathbf{a}}_2 \ \cdots \ \tilde{\mathbf{a}}_L] \quad (\text{A.26})$$

and the $M \times L$ matrices Δ_i and $\tilde{\Delta}_i$ are

$$\Delta_i = [\mathbf{d}_i(1) \ \mathbf{d}_i(2) \ \cdots \ \mathbf{d}_i(L)] \quad (\text{A.27})$$

$$\tilde{\Delta}_i = [\tilde{\mathbf{d}}_i(1) \ \tilde{\mathbf{d}}_i(2) \ \cdots \ \tilde{\mathbf{d}}_i(L)] \quad (\text{A.28})$$

Here $\text{diag}(x)$ forms a row or column of the diagonal elements of the square matrix \mathbf{x} as appropriate. Mathematically, this operation is implemented as

$$\text{diag}(\mathbf{x}) = [1 \ 1 \ \cdots \ 1] (\mathbf{d} \odot \mathbf{I}) \quad (\text{A.29})$$

where \mathbf{I} is an identity matrix. The entire “attitude-real gain” (and transpose of the “real gain-attitude”) block of the FIM is found from the rows defined in (A.22) and (A.23).

$$\text{FIM}_{(1-3), (4, 5, \dots, 3+L)} = 2 \text{Re} \begin{bmatrix} \text{diag} \{ \Gamma \mathbf{A}^H \mathbf{C}_i^{-1} \Delta_1 \} \\ \text{diag} \{ \Gamma \mathbf{A}^H \mathbf{C}_i^{-1} \Delta_2 \} \\ \text{diag} \{ \Gamma \mathbf{A}^H \mathbf{C}_i^{-1} \Delta_3 \} \end{bmatrix} \quad (\text{A.30})$$

$$= 2 \text{Re} \begin{bmatrix} \text{diag} \{ \Gamma \tilde{\mathbf{A}}^H \tilde{\Delta}_1 \} \\ \text{diag} \{ \Gamma \tilde{\mathbf{A}}^H \tilde{\Delta}_2 \} \\ \text{diag} \{ \Gamma \tilde{\mathbf{A}}^H \tilde{\Delta}_3 \} \end{bmatrix} \quad (\text{A.31})$$

$$\triangleq \text{Re}[\mathbf{F}_{q,\gamma}] \quad (\text{A.32})$$

In the “attitude-imaginary gain” (and transpose of the “imaginary gain-attitude”) block of the FIM, the component corresponding to attitude term i and gain k is

$$\text{FIM}_{i, L+k+3} = 2 \operatorname{Re} \{ j \gamma_k^* \mathbf{d}_i^H(k) \mathbf{C}_l^{-1} \mathbf{a}_k \} \quad (\text{A.33})$$

$$= 2 \operatorname{Im} \{ \gamma_k \mathbf{a}_k^H \mathbf{d}_i(k) \} \quad (\text{A.34})$$

$$= 2 \operatorname{Im} \{ \gamma_k \tilde{\mathbf{a}}_k^H \tilde{\mathbf{d}}_i(k) \} \quad (\text{A.35})$$

using $\operatorname{Re}(jx^*) = \operatorname{Im}(x)$.

Using the approach above, the entire $3 \times L$ “attitude-imaginary gain” block is

$$\text{FIM}_{(1-3), (4+L, 5+L, \dots, 3+2 \times L)} = 2 \operatorname{Im} \begin{bmatrix} \operatorname{diag} \{ \Gamma \mathbf{A}^H \mathbf{C}_l^{-1} \Delta_1 \} \\ \operatorname{diag} \{ \Gamma \mathbf{A}^H \mathbf{C}_l^{-1} \Delta_2 \} \\ \operatorname{diag} \{ \Gamma \mathbf{A}^H \mathbf{C}_l^{-1} \Delta_3 \} \end{bmatrix} \quad (\text{A.36})$$

$$= 2 \operatorname{Im} \begin{bmatrix} \operatorname{diag} \{ \Gamma \tilde{\mathbf{A}}^H \tilde{\Delta}_1 \} \\ \operatorname{diag} \{ \Gamma \tilde{\mathbf{A}}^H \tilde{\Delta}_2 \} \\ \operatorname{diag} \{ \Gamma \tilde{\mathbf{A}}^H \tilde{\Delta}_3 \} \end{bmatrix} \quad (\text{A.37})$$

$$\triangleq \operatorname{Im} [\mathbf{F}_{q, \gamma}] \quad (\text{A.38})$$

Using (A.14), the only non-zero terms of the “real gain-real gain” block of the FIM are along the diagonal. The k th term along the diagonal (corresponding to the real part of γ_k) is

$$\text{FIM}_{3+k, 3+k} = 2 \operatorname{Re} \{ \mathbf{a}_k^H \mathbf{C}_l^{-1} \mathbf{a}_k \} \quad (\text{A.39})$$

$$= 2 \operatorname{Re} \{ \tilde{\mathbf{a}}_k^H \tilde{\mathbf{a}}_k \} \quad (\text{A.40})$$

$$= 2 \tilde{\mathbf{a}}_k^H \tilde{\mathbf{a}}_k \quad (\text{A.41})$$

and the entire “real gain-real gain” block of the FIM is

$$\text{FIM}_{(4, 5, \dots, 3+L), (4, 5, \dots, 3+L)} = \mathbf{A}^H \mathbf{C}_l^{-1} \mathbf{A} \odot \mathbf{I} \quad (\text{A.42})$$

$$= \tilde{\mathbf{A}}^H \tilde{\mathbf{A}} \odot \mathbf{I} \quad (\text{A.43})$$

$$\triangleq \mathbf{F}_\gamma \quad (\text{A.44})$$

Similarly, the “imaginary gain-imaginary gain” block of the FIM is also diagonal. The k th term along the diagonal (corresponding to the imaginary part of γ_k) is

$$\text{FIM}_{3+L+k, 3+L+k} = 2 \operatorname{Re} \{ j^* j \mathbf{a}_k^H \mathbf{C}_l^{-1} \mathbf{a}_k \} \quad (\text{A.45})$$

$$= 2 \operatorname{Re} \{ \tilde{\mathbf{a}}_k^H \tilde{\mathbf{a}}_k \} \quad (\text{A.46})$$

$$= 2 \tilde{\mathbf{a}}_k^H \tilde{\mathbf{a}}_k \quad (\text{A.47})$$

and the entire “imaginary gain-imaginary gain” block of the FIM is

$$\text{FIM}_{(4+L, 5+L, \dots, 3+2 \times L), (4+L, 5+L, \dots, 3+2 \times L)} = \mathbf{A}^H \mathbf{C}_l^{-1} \mathbf{A} \odot \mathbf{I} \quad (\text{A.48})$$

$$= \tilde{\mathbf{A}}^H \tilde{\mathbf{A}} \odot \mathbf{I} \quad (\text{A.49})$$

$$\triangleq \mathbf{F}_\gamma \quad (\text{A.50})$$

The remaining block is the “real gain-imaginary gain” block. From (A.4) and (A.5), the FIM component corresponding to real gain i and imaginary gain k is

$$\text{FIM}_{3+i, 3+L+k} = \operatorname{E} [4 \operatorname{Re} \{ \mathbf{a}_i^H \mathbf{C}_l^{-1} \mathbf{w}_i \} \operatorname{Im} \{ \mathbf{a}_k^H \mathbf{C}_l^{-1} \mathbf{w}_k \}] \quad (\text{A.51})$$

$$= \operatorname{E} [\mathbf{a}_i^H \mathbf{C}_l^{-1} \mathbf{w}_i \mathbf{w}_k^T \mathbf{C}_l^{-T} \mathbf{a}_k^T + (\mathbf{a}_i^H \mathbf{C}_l^{-1} \mathbf{w}_i \mathbf{w}_k^T \mathbf{C}_l^{-T} \mathbf{a}_k^T)^*] \quad (\text{A.52})$$

$$= 0 \quad \forall i, k = 1, 2, \dots, L \quad (\text{A.53})$$

Using (A.17), (A.32), (A.38), (A.44), (A.53), and (A.50), the FIM may be written as

$$\text{FIM} = \begin{bmatrix} \mathbf{F}_q & \operatorname{Re} [\mathbf{F}_{q,\gamma}] & \operatorname{Im} [\mathbf{F}_{q,\gamma}] \\ \operatorname{Re} [\mathbf{F}_{q,\gamma}]^T & \mathbf{F}_\gamma & \mathbf{0} \\ \operatorname{Im} [\mathbf{F}_{q,\gamma}]^T & \mathbf{0} & \mathbf{F}_\gamma \end{bmatrix} \quad (\text{A.54})$$

Of interest in this problem is the CRB for the attitude; the complex gain terms are essentially nuisance parameters. The CRB for the desired attitude parameters, $\mathbf{P}_{\text{cr}}(q)$, is found from the upper 3×3 block of the inverse of the FIM. Using the inverse identity of Li et al. [23],

$$\mathbf{P}_{\text{cr}}(q)^{-1} = \operatorname{Re} \{ \mathbf{F}_q - \mathbf{F}_{q,\gamma} \mathbf{F}_\gamma^{-1} \mathbf{F}_{q,\gamma}^H \} \quad (\text{A.55})$$

Now examine the terms of $\mathbf{P}_{\sigma}^{-1}(q)$. Since \mathbf{F}_{γ} is a diagonal matrix, $(\mathbf{F}_{\gamma})^{-1}$ is also diagonal.

Using this, the i, j element of $\mathbf{F}_{q,\gamma}\mathbf{F}_{\gamma}^{-1}\mathbf{F}_{q,\gamma}^H$ is found to be

$$\mathbf{F}_{q,\gamma}\mathbf{F}_{\gamma}^{-1}\mathbf{F}_{q,\gamma}^H(i, j) = 2 \sum_{l=1}^L |\gamma_l|^2 \mathbf{d}_i^H(l) \mathbf{C}_l^{-1} \mathbf{a}(l) \left(\frac{1}{\mathbf{a}^H(l) \mathbf{C}_l^{-1} \mathbf{a}(l)} \right)^* \mathbf{a}^H(l) \mathbf{C}_l^{-1} \mathbf{d}_j(l) \quad (\text{A.56})$$

$$= 2 \sum_{l=1}^L |\gamma_l|^2 \tilde{\mathbf{d}}_i^H(l) \frac{\tilde{\mathbf{a}}^H(l) \tilde{\mathbf{a}}(l)}{\tilde{\mathbf{a}}^H(l) \tilde{\mathbf{a}}(l)} \tilde{\mathbf{d}}_j(l) \quad (\text{A.57})$$

$$= 2 \sum_{l=1}^L |\gamma_l|^2 \tilde{\mathbf{d}}_i^H(l) \mathbf{P}_{\tilde{\mathbf{a}}(l)} \tilde{\mathbf{d}}_j(l) \quad (\text{A.58})$$

The entire 3×3 matrix of $\mathbf{F}_{q,\gamma}\mathbf{F}_{\gamma}^{-1}\mathbf{F}_{q,\gamma}^H$ is

$$\mathbf{F}_{q,\gamma}\mathbf{F}_{\gamma}^{-1}\mathbf{F}_{q,\gamma}^H = 2 \sum_{l=1}^L |\gamma_l|^2 \tilde{\mathbf{D}}_i^H(l) \mathbf{P}_{\tilde{\mathbf{a}}(l)} \tilde{\mathbf{D}}(l) \quad (\text{A.59})$$

Finally, recall that $\mathbf{F}_q = 2 \operatorname{Re} \left\{ \sum_{l=1}^L |\gamma_l|^2 \tilde{\mathbf{D}}^H(l) \tilde{\mathbf{D}}(l) \right\}$, so that

$$\mathbf{P}_{\sigma}^{-1}(q) = 2 \operatorname{Re} \left\{ \sum_{l=1}^L |\gamma_l|^2 \left\{ \tilde{\mathbf{D}}^H(l) \tilde{\mathbf{D}}(l) - \tilde{\mathbf{D}}^H(l) \mathbf{P}_{\tilde{\mathbf{a}}(l)} \tilde{\mathbf{D}}(l) \right\} \right\} \quad (\text{A.60})$$

$$= 2 \operatorname{Re} \left\{ \sum_{l=1}^L |\gamma_l|^2 \tilde{\mathbf{D}}^H(l) \mathbf{P}_{\tilde{\mathbf{a}}(l)}^{\perp} \tilde{\mathbf{D}}(l) \right\} \quad (\text{A.61})$$

APPENDIX B THE INTERFERENCE COVARIANCE MATRIX

B.1 Introduction

One of the fundamental requirements in the development of the maximum likelihood methods of this work is the knowledge of the statistics of the underlying interference. In this chapter two important topics are presented, the theoretical *calculation* of the interference and the *estimation* of the interference for a practical system. A two sensor system and a simplified receiver chain are used for the analytical calculation, as they provides a clear illustration of the underlying phenomena. This two sensor system is used to calculate the space-satellite covariance matrix defined in Chapter 4. Once the model for the interference has been developed, methods of estimating the interference are discussed. In particular, a method specific to this application is developed, which may prove useful from a computational standpoint.

In this chapter we remove the constraint of Chapter 4 that the interference is temporally uncorrelated and instead calculate the various interference statistics for a jammer with a band-limited power spectral density. The band-limited spectra, the derivations of the interference statistics, and the methods of estimating the interference developed in this chapter are implemented in the simulation used to produce the results of Chapter 8.

In the derivations that follow, accurate representations of the spatial covariance matrices are developed from the jammer temporal correlation functions. This is to ensure accuracy in the equations as the spacing between sensors increases. As the array spacing increases, the jammer signals experience decorrelation between the various sensors. For small spacing, the sensor to sensor correlation is adequately approximated by a phase difference between sensors (i.e. no amplitude decorrelation). In this case an adequate model for the jammer is simply the array response vector, which is composed of these phase differences. However, as the distance between sensors increases or the jammer

bandwidth increases, the *amplitude* of the sensor to sensor cross correlation is attenuated in addition to the phase shift. This amplitude decrease in fact degrades performance over the phase-only case.¹ Since Chapter 7 focuses on wider baseline lengths than typical (for array processing) half wavelength spacing, accurately representing the performance of the attitude determination algorithms of this work required a more detailed jammer decorrelation approach than the phase-only method.

Nomenclature

This chapter uses a considerable amount of nomenclature. To remove confusion, the important terms and their definitions are listed below.

At the sampler, the interference terms from Chapter 4 are composed of contributions from thermal noise and jammers.

$n[k]$ = k th sample of interference

$n_t[k]$ = Thermal Noise Contribution to k th sample of interference

$n_j[k]$ = Jammer Contribution to k th sample of interference

The spatial interference covariance is formed from samples taken at the A/D, i.e. before despreading. This is composed of contributions from the jammer and thermal noise.

\mathbf{R}_s = Spatial Covariance

\mathbf{R}_{sj} = Jammer Contribution to Spatial Covariance

\mathbf{R}_{st} = Thermal Noise Contribution to Spatial Covariance

(B.1)

¹ In the limiting case of no sensor to sensor correlation, the jammer power appears spatially white, like thermal noise. Here performance may be significantly reduced, as the situation may be viewed as an unjammed case with the thermal noise power equal to the sum of the actual thermal noise power and the (possibly very large) jammer power.

After demodulation, the interference is composed of contributions from the jammer, thermal noise, and multiple access interference (MAI) from other satellites.

$w_1 = M \times 1$ Interference Vector in the l th Satellite Channel

$w_{1j} =$ Jammer Contribution to the l th Interference Vector

$w_{1t} =$ Thermal Noise Contribution to the l th Interference Vector

$w_{1m} =$ MAI Contribution to the l th Interference Vector

The spatial -satellite interference covariance is formed from samples taken after despreading. This is composed of contributions from the jammer, thermal noise, and multiple access interference (MAI) from other satellites.

$R_{ss} =$ Spatial - Satellite Covariance

$R_{ssj} =$ Jammer Contribution to Spatial - Satellite Covariance

$R_{sst} =$ Thermal Noise Contribution to Spatial - Satellite Covariance

$R_{ssm} =$ MAI Contribution to Spatial - Satellite Covariance

$R_{ss}[lm] =$ The l, m $M \times M$ Block of Spatial - Satellite Covariance

(B.2)

Receiver and Assumptions

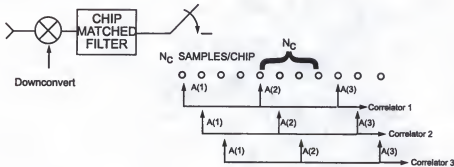


Figure B.1: The receiver model used in this dissertation. The output of the chip matched filter is oversampled by a factor of N_c , (N_c is 4 in this figure) and these samples are decimated into sequences composed of 1 sample per chip. The decimated sequences are then despread using the sequency $A(i)$ $i = 1, 2, \dots, N$ to form early, punctual, late, and other temporal gates.

The general receiver design of Figure B.2 is similar to the DS-SS receiver described in [45]. This system employs an anti-aliasing filter matched to the chip waveform, and then oversamples the output of this filter. The samples are then decimated and each decimated sequence is individually de-spread to provide a punctual output and possibly several other outputs delayed and advanced in time as required for acquisition and tracking. With this method, only one sample per chip is used in any correlation (despreading) function, and up to N_c correlators could be implemented in the time span of one chip.

The spatial interference covariance matrix is composed of contributions from all jammers and thermal noise. A few reasonable assumptions allow straightforward calculation of this covariance. First, we assume that all jamming sources are zero mean, circularly symmetric, wide-sense stationary complex Gaussian random processes, and that each jammer's waveform is independent from those of all other jammers. Second, we assume that the physical nature of the thermal noise causes it to be uncorrelated from channel to channel (spatially white), and that its power spectral density is uniform over the frequencies of interest (temporally white). Finally, we assume that all jammer waveforms are uncorrelated from all satellite waveforms.

B.2 Derivation of Interference Statistics

Space-Satellite Interference

The required statistics of all interference sources are captured in the space-satellite covariance matrix \mathbf{R}_{ss} . To review from Chapter 4, this is composed of the expected value of the outer product of the space-satellite interference vector, \mathbf{W} , a $ML \times 1$ vector containing the interference in each satellite channel.

$$\mathbf{R}_{ss} = \mathbf{E} [\mathbf{W}\mathbf{W}^H] \quad (\text{B.3})$$

$$\mathbf{W} = \begin{bmatrix} \mathbf{w}_1 \\ \mathbf{w}_2 \\ \vdots \\ \mathbf{w}_L \end{bmatrix} \quad (\text{B.4})$$

For this work, the interference is comprised of contributions from three types of source: jammers, interfering satellites (i.e. multiple access interference), and thermal noise.

$$\mathbf{w}_1 = \mathbf{w}_{1j} + \mathbf{w}_{1t} + \mathbf{w}_{1m} \quad (\text{B.5})$$

This can be seen from equation (4.37), the interference in each satellite channel is composed of the thermal noise and jammers, and the multiple access interference (MAI).

$$\mathbf{w}_1 = \frac{1}{\varepsilon_l} \left[[\mathbf{n}[t_1], \mathbf{n}[t_2], \dots, \mathbf{n}[t_N]] + \sum_{p=1, p \neq l}^L \gamma_p \mathbf{a}_p(\hat{q}) \mathbf{y}_p \right] \hat{\mathbf{y}}_l^H \quad (\text{B.6})$$

since the $\mathbf{n}[k]$ terms were defined in Chapter 4 to contain contributions from thermal noise and jammers, i.e.

$$\mathbf{n}[k] = \mathbf{n}_j[k] + \mathbf{n}_t[k] \quad (\text{B.7})$$

As is the assumption throughout this work, each of these are independent from one another, and therefore the total interference realization and its covariance are simply the sum of each of the individual realizations and covariances, respectively.

$$\mathbf{R}_{ss} = \mathbf{R}_{ssj} + \mathbf{R}_{sst} + \mathbf{R}_{ssm} \quad (\text{B.8})$$

Since the jammer and thermal noise components of the space-satellite covariance matrix are found from the spatial covariance \mathbf{R}_s , we begin by examining the components of spatial covariance.

Jammer Contribution to \mathbf{R}_s

This section calculates the interference covariance for one jammer. Since each jammer (if more than one exist) is independent from all others, their contributions would all be calculated independently using the method described in this section, and simply summed.

The receiver model described earlier in this chapter consists of a mixer, which downconverts the random process to baseband, a matched filter, and a sampler (A/D converter). Following the sampler, the direct sequence spread spectrum (DS-SS) modulation is removed, and the de-modulated samples are summed, resulting in an output data vector w_{lj} , $l = 1, \dots, L$ which is used for the attitude determination. Repeating this process with various time-shifted replicas of the spreading sequence generates the appropriate data for code tracking (e.g. late gate, early gate, etc.).

We define the random process corresponding to the jammer signal that we will evaluate as $x(t)$. The shape of power spectral density (PSD) is assumed to be flat across the frequency band $f_c - B < f < f_c + B$, where f_c is the GPS center (carrier) frequency. The autocorrelation function corresponding to this flat spectrum has the familiar sinc shape in amplitude, and a phase related to the carrier frequency and time delay. P_x is the power (variance) of the process.

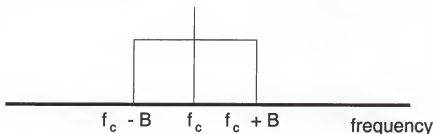


Figure B.2: One sided jammer PSD

$$\begin{aligned} R_{xx}(\tau) &= E[x^*(t)x(t+\tau)] \\ &= P_x e^{j\omega_c \tau} \frac{\sin(\pi 2B\tau)}{\pi 2B\tau} \end{aligned} \quad (\text{B.9})$$

$$= P_x e^{j\omega_c \tau} \text{sinc}(2B\tau) \quad (\text{B.10})$$

where

$$\text{sinc}(\alpha) = \frac{\sin(\pi\alpha)}{\pi\alpha} \quad (\text{B.11})$$

The two sensors receive this random process, with the second sensor receiving the process delayed by an amount of time Δ , which is related to the direction of arrival of the

source and the physical arrangement of the two sensors. Denote the two signals received in the two sensors as $s_1(t)$ and $s_2(t)$.

$$s_1(t) = x(t) \quad (\text{B.12})$$

$$s_2(t) = x(t - \Delta) \quad (\text{B.13})$$

The receiver will downconvert these bandpass processes to baseband random processes. We denote the baseband processes in each channel corresponding to the downconverted waveform $x(t)$ as $S_1(t)$ and $S_2(t)$.

$$S_1(t) = s_1(t)e^{-j\omega_c t} \quad (\text{B.14})$$

$$= x(t)e^{-j\omega_c t} \quad (\text{B.15})$$

$$S_2(t) = s_2(t)e^{-j\omega_c t} \quad (\text{B.16})$$

$$= x(t - \Delta)e^{-j\omega_c t} \quad (\text{B.17})$$

The process $S_1(t)$ is a zero mean normal wide sense stationary random process with autocorrelation function $R_{S_1, S_1}(\tau)$.

$$\begin{aligned} R_{S_1, S_1}(\tau) &= E[S_1^*(t)S_1(t + \tau)] \\ &= E[x^*(t)e^{+j\omega_c t}x(t + \tau)e^{-j\omega_c(t + \tau)}] \\ &= E[x^*(t)x(t + \tau)]e^{-j\omega_c \tau} \\ &= P_x e^{j\omega_c \tau} \text{sinc}(2B\tau) e^{-j\omega_c \tau} \\ &= P_x \text{sinc}(2B\tau) \end{aligned} \quad (\text{B.18})$$

Since $x(t)$ is wide sense stationary, then $S_2(t)$ is wide sense stationary as well. In addition, $R_{S_1, S_1}(\tau)$ and $R_{S_2, S_2}(\tau)$ are identical, which can be easily seen by letting $y(t) = x(t - \Delta)$ and observing that the statistics of y and x are identical.

$$R_{S_1, S_1}(\tau) = R_{S_2, S_2}(\tau) \quad (\text{B.19})$$

The cross correlation function is found in a similar manner.

$$\begin{aligned}
 r_{S_1, S_2}(\tau) &= E[S_1^*(t)S_2(t+\tau)] \\
 &= E[x^*(t)e^{+j\omega_c t}x(t+\tau-\Delta)e^{-j\omega_c(t+\tau)}] \\
 &= E[x^*(t)x(t+\tau-\Delta)]e^{-j\omega_c\tau} \\
 &= R_{xx}(\tau-\Delta)e^{-j\omega_c\tau} \\
 &= P_x \text{sinc}(2B(\tau-\Delta))e^{j\omega_c(\tau-\Delta)}e^{-j\omega_c\tau} \\
 &= P_x \text{sinc}(2B(\tau-\Delta))e^{-j\omega_c\Delta}
 \end{aligned} \tag{B.20}$$

Two observations may be made in comparing the cross correlation term R_{S_1, S_2} to the autocorrelation term (either R_{S_1, S_1} or R_{S_2, S_2}). First, the amplitude of the cross correlation term at $\tau = 0$ is reduced by an amount corresponding to the time delay between reception at the sensors and the process bandwidth. Second, a carrier frequency phase shift is imposed.

Following the downconverter, the signal in each channel is matched filtered, sampled, and decimated by a factor of N_c , producing two discrete time sequences, one per channel. The matched filter for the BPSK type GPS signals is simply an ideal integrator. In practice, however, a small SNR penalty could be paid for deviating from the matched filter to one with a sharper transition region, greater stop band rejection, or easier implementation (see, for example, Chapter 10 of [46]). We denote these sequences as $S_1[k]$ and $S_2[k]$, where k is the time (sample) index. The integration time the chip period T_c .

$$S_1[k] = \int_{(k-1)T_c}^{kT_c} S_1(t)dt \tag{B.21}$$

$$S_2[k] = \int_{(k-1)T_c}^{kT_c} S_2(t)dt \tag{B.22}$$

Notice that $S_1[k]$ and $S_2[k]$ are zero mean normal wide sense stationary random sequences, as shown below for by its mean,

$$\begin{aligned}
 E[S_1[k]] &= \int_{(k-1)T_c}^{kT_c} E[S_1(t)]dt \\
 &= 0
 \end{aligned} \tag{B.23}$$

and its autocorrelation:

$$\begin{aligned}
 r_{S_1, S_1}[l] &= E[S_1^*[k]S_1[k+l]] \\
 &= \int_{(k-1)T_c}^{kT_c} \int_{(k+l-1)T_c}^{(k+l)T_c} E[S_1^*(\tau)S_1(\lambda)] d\tau d\lambda \\
 &= \int_{(k-1)T_c}^{kT_c} \int_{(k+l-1)T_c}^{(k+l)T_c} R_{S_1, S_1}(\lambda - \tau) d\tau d\lambda \\
 &= \int_0^{T_c} \int_{lT_c}^{(l+1)T_c} P_x \text{sinc}(2B(\lambda - \tau)) d\tau d\lambda \quad (B.24)
 \end{aligned}$$

The cross correlation function between the discrete sequences is similarly found by direct evaluation.

$$\begin{aligned}
 r_{S_1, S_2}[l] &= E[S_1^*[k]S_2[k+l]] \\
 &= \int_{(k-1)T_c}^{kT_c} \int_{(k+l-1)T_c}^{(k+l)T_c} E[S_1^*(\tau)S_2(\lambda)] d\tau d\lambda \\
 &= \int_{(k-1)T_c}^{kT_c} \int_{(k+l-1)T_c}^{(k+l)T_c} R_{S_1, S_2}(\lambda - \tau) d\tau d\lambda \\
 &= \int_0^{T_c} \int_{lT_c}^{(l+1)T_c} P_x \text{sinc}(2B(\lambda - \tau - \Delta)) e^{-j\omega_c \Delta} d\tau d\lambda \quad (B.25)
 \end{aligned}$$

The sequences $S_1[k]$ and $S_2[k]$ form the vector of jammer contributions to interference at the A/D, $\mathbf{n}_j[k]$.

$$\mathbf{n}_j[k] = \begin{bmatrix} S_1[k] \\ S_2[k] \end{bmatrix} \quad (B.26)$$

The jammer covariance at the A/D, \mathbf{R}_{s_j} is obtained from $\mathbf{n}_j[k]$ as

$$\mathbf{R}_{s_j} = E[\mathbf{n}_j[k]\mathbf{n}_j^H[k]] \quad (B.27)$$

$$= \begin{bmatrix} r_{S_1, S_1}[0] & r_{S_1, S_2}[0] \\ r_{S_1, S_2}^*[0] & r_{S_2, S_2}[0] \end{bmatrix} \quad (B.28)$$

This can be written concisely to show the two cross correlation properties of phase change and amplitude reduction.

$$\mathbf{R}_{s_j} = P_x P_{\text{auto}} \begin{bmatrix} 1 & (1 - \alpha) e^{-j\omega_c \Delta} \\ (1 - \alpha) e^{j\omega_c \Delta} & 1 \end{bmatrix} \quad (B.29)$$

where

$$P_{auto} = \int_{(k-1)T_c}^{kT_c} \int_{(k-1)T_c}^{kT_c} P_x \text{sinc}(2B(\lambda - \tau)) d\tau d\lambda \quad (\text{B.30})$$

$$P_{cross} = \int_{(k-1)T_c}^{kT_c} \int_{(k-1)T_c}^{kT_c} P_x \text{sinc}(2B(\lambda - \tau - \Delta)) d\tau d\lambda \quad (\text{B.31})$$

$$\alpha = 1 - P_{cross}/P_{auto} \quad (\text{B.32})$$

Approximation for Narrow-Band Jammers

Consider the diagonal terms of (B.29) for narrow-band processes. If the time bandwidth product BT_c is small, then the $\text{sinc}(BT_c)$ function is essentially constant and equal to 1. In this case, nearly all of the power in $x(t)$ passes through the matched filter.

$$\begin{aligned} r_{S_1, S_1}(0) &= \int_{(k-1)T_c}^{kT_c} \int_{(k-1)T_c}^{kT_c} P_x \text{sinc}(2B(\lambda - \tau)) d\tau d\lambda \\ &\approx \int_0^{T_c} \int_0^{T_c} P_x d\tau d\lambda \\ &\approx P_x T_c^2 \end{aligned} \quad (\text{B.33})$$

A similar narrow-band analysis may be performed for the off-diagonal terms of (B.29) by using the cross-correlation term. However, in this case the additional delay corresponding due to the difference in signal arrival times between the two sensors must be considered. If the time bandwidth product $B(T_c + \Delta)$ is small, then the sinc function is essentially constant and the cross correlation value is equal to the autocorrelation value multiplied by a complex exponential phase shift.

$$\begin{aligned} r_{S_1, S_2}(0) &= \int_{(k-1)T_c}^{kT_c} \int_{(k-1)T_c}^{kT_c} P_x \text{sinc}(2B(\lambda - \tau - \Delta)) e^{-j\omega_c \Delta} d\tau d\lambda \\ &\approx \int_0^{T_c} \int_0^{T_c} P_x e^{-j\omega_c \Delta} d\tau d\lambda \\ &\approx P_x T_c^2 e^{-j\omega_c \Delta} \\ &= e^{-j\omega_c \Delta} r_{S_1, S_1}(0) \end{aligned} \quad (\text{B.34})$$

For the small time bandwidth cases described above, P_{auto} and P_{cross} are essentially equal to T_c^2 , and $\mathbf{R}_{s_j}[0]$ is now the rank 1 matrix.

$$\mathbf{R}_{s_j} \approx P_x T_c^2 \begin{bmatrix} 1 & e^{-j\omega_c \Delta} \\ e^{j\omega_c \Delta} & 1 \end{bmatrix} \quad (\text{B.35})$$

The eigenvector of this matrix corresponding to the non-zero eigenvalue is the array response vector (i.e. spatial steering vector) associated with the direction of arrival of this interference source. In many array processing applications this steering vector model is adequate. However, since this dissertation explores large array spacing, it uses the more accurate amplitude decorrelation version.

Thermal Noise Contribution to \mathbf{R}_s

The non-zero temperature of physical devices causes motion of electrons (i.e. current) inside the material, resulting in a random voltage at the terminals of the device [47]. This thermal noise is an important factor in system performance. The common “Additive White Gaussian Noise” (AWGN) model for thermal noise considers the noise to be spectrally white, normally distributed, and independent of all other signals in the receiver. Because of the physical differences between receiver channels, the noise one receiver channel is assumed independent from that in all the other channels.

Define $n_{t_i}(t)$ as the thermal noise waveform appearing in the i th hardware channel. After matched filtering and sampling, the resulting random sequence $n_{t_i}[k]$, $i = 1, 2$ forms the thermal noise contribution to the interference vector $\mathbf{n}_t[k]$.

$$n_{t_i}[k] = \int_{(k-1)T_c}^{kT_c} n_{t_i}(t) dt \quad i = 1, 2 \quad (\text{B.36})$$

$$\mathbf{n}_t[k] = \begin{bmatrix} n_{t_1}[k] \\ n_{t_2}[k] \end{bmatrix} \quad (\text{B.37})$$

Using the assumptions imposed on $\mathbf{n}_t[k]$ the thermal noise covariance at the A/D, \mathbf{R}_{st} is the diagonal matrix \mathbf{R}_{st}

$$\mathbf{R}_{st} = \mathbb{E} [\mathbf{n}_t[k] \mathbf{n}_t^H[k]] \quad (\text{B.38})$$

$$= \begin{bmatrix} P_{t_1} T_c & 0 \\ 0 & P_{t_2} T_c \end{bmatrix} \quad (\text{B.39})$$

where P_{t_1} and P_{t_2} are the power spectral density level of the thermal noise in channels 1 and 2, respectively.

Spreading Sequence Model

The demodulation waveform \mathbf{y}_l is the complex sequence composed of the spreading sequence and estimated Doppler to the l th satellite. Although this sequence is deterministic (it is, of course, known to the receiver) it is useful to model it as a random process when the spreading gain is large (i.e. the number of chips integrated is large). The model for the random process uses the common approach of considering each of the terms in the sequence to be independent, identically distributed variables, giving rise to the following properties:

$$\mathbb{E}[y_i[n] y_i^*[n - k]] = \delta[k] \quad (\text{B.40})$$

$$\mathbb{E}[y_i[n] y_l^*[k]] = 0 \quad l \neq i, \quad \forall n, k \quad (\text{B.41})$$

where

$$\delta[k] = \begin{cases} 1 & k = 0 \\ 0 & k \neq 0 \end{cases} \quad (\text{B.42})$$

These above relationships flow from the asymptotic properties of the GPS P(Y) code spreading sequences:

$$\lim_{N \rightarrow \infty} \frac{1}{\varepsilon_i} \sum_{n=1}^N y_i[n] y_i^*[n - k] = 0 \quad k \neq 0 \quad (\text{B.43})$$

$$\lim_{N \rightarrow \infty} \frac{1}{\varepsilon_i} \sum_{n=1}^N y_i[n] y_l^*[n - k] = 0 \quad \forall k \quad (\text{B.44})$$

Where ε_i the energy in the i th sequence, is defined as

$$\varepsilon_i \triangleq \sum_{n=1}^N y_i[n] y_i^*[n] \quad (\text{B.45})$$

Jammer Contribution to \mathbf{R}_{ss}

To calculate the jammer contribution to the space-satellite interference covariance matrix, we partition \mathbf{R}_{ssj} into $M \times M$ blocks, and consider blocks on the diagonal and blocks off the diagonal separately. First consider the i th diagonal block, which is calculated from \mathbf{w}_{ji} , the jammer waveforms despread using the i th despreading sequence:

$$\mathbf{w}_{ji} = \frac{1}{\varepsilon_i} \sum_{n=1}^N \mathbf{n}_j[n] y_i^*[n] \quad (\text{B.46})$$

Using this, the i th diagonal block of the jammer contribution to \mathbf{R}_{ss} is found from

$$\mathbf{R}_{ssj}[ii] = \mathbb{E} [\mathbf{w}_{ji} \mathbf{w}_{ji}^H] \quad (\text{B.47})$$

$$= \frac{1}{\varepsilon_i^2} \sum_{\alpha=1}^N \sum_{\beta=1}^N \mathbb{E} [\mathbf{n}_j[\alpha] \mathbf{n}_j^H[\beta]] y_i^*[\alpha] y_i[\beta] \quad (\text{B.48})$$

Using the statistical properties of the spreading sequence defined in equation (B.40) (i.e. treating y_i as sequence of independent random variables), this evaluates to

$$\mathbf{R}_{ssj}[ii] \simeq \frac{1}{\varepsilon_i^2} \sum_{\alpha=1}^N \sum_{\beta=1}^N \mathbb{E} [\mathbf{n}_j[\alpha] \mathbf{n}_j^H[\beta]] \mathbb{E} [y_i^*[\alpha] y_i[\beta]] \quad (\text{B.49})$$

$$= \frac{1}{\varepsilon_i^2} \sum_{\alpha=1}^N \mathbf{R}_{sj} |y_i[\alpha]|^2 \quad (\text{B.50})$$

$$= \frac{1}{\varepsilon_i} \mathbf{R}_{sj} \quad (\text{B.51})$$

This is an important result: the diagonal blocks of the space-satellite covariance matrix are all equal to the jammer spatial covariance matrix.

In a similar fashion, the off diagonal blocks may be calculated as well. Consider the $i - j$ block

$$\mathbf{R}_{ssj}[ij] = \frac{1}{\varepsilon_i} \frac{1}{\varepsilon_j} \sum_{\alpha=1}^N \sum_{\beta=1}^N \mathbb{E} [\mathbf{n}_j[\alpha] \mathbf{n}_j^H[\beta]] \mathbb{E} [y_i^*[\alpha] y_j[\beta]] \quad (\text{B.52})$$

Again using the properties of the spreading sequence (specifically equation (B.41)), the off-diagonal terms evaluate to zero.

$$\mathbf{R}_{ssj}[il] = 0 \quad (\text{B.53})$$

Combining the diagonal and off-diagonal terms produces the total contribution of the jammer to the space satellite interference covariance matrix. Since the energies in each of the spreading sequences is the same, we may drop the satellite subscript on the energy, and write the jammer contribution as

$$\mathbf{R}_{ssj} = \frac{1}{\varepsilon} \begin{bmatrix} \mathbf{R}_{sj} & 0 & \cdots & 0 \\ 0 & \mathbf{R}_{sj} & 0 & 0 \\ 0 & \cdots & \ddots & 0 \\ 0 & \cdots & 0 & \mathbf{R}_{sj} \end{bmatrix} \quad (\text{B.54})$$

Thermal Noise Contribution to \mathbf{R}_{ss}

Using the same methodology as for the jammer, the contribution from the thermal noise is found to be

$$\mathbf{R}_{sst} = \frac{1}{\varepsilon} \begin{bmatrix} \mathbf{R}_{st} & 0 & \cdots & 0 \\ 0 & \mathbf{R}_{st} & 0 & 0 \\ 0 & \cdots & \ddots & 0 \\ 0 & \cdots & 0 & \mathbf{R}_{st} \end{bmatrix} \quad (\text{B.55})$$

and since \mathbf{R}_{st} is a diagonal matrix, \mathbf{R}_{sst} is as well.

MAI Contribution to \mathbf{R}_{ss}

The third type of interference considered is that from satellites other than the desired satellite in each satellite channel, i.e. the multiple access interference (MAI). Conceptually, if there are L satellites being tracked and used for attitude estimation, then in the first satellite channel satellites $2 - L$ are interferers. Similarly, in the second channel, satellites 1 and $3 - L$ are interferers, and so on. The MAI in the l th satellite channel, \mathbf{w}_{lm} , is composed of contributions from all satellites but the l th:

$$\mathbf{w}_{lm} = \frac{1}{\varepsilon_l} \left[\sum_{p=1, p \neq l}^L \gamma_p \mathbf{a}_p(q) y_p \right] \hat{\mathbf{y}}_l^H \quad (\text{B.56})$$

To calculate the contribution of MAI to the space-satellite interference covariance matrix, we partition \mathbf{R}_{ss} into $M \times M$ blocks, and consider blocks on the diagonal and blocks off the diagonal separately.

$$\mathbf{W}_m = \begin{bmatrix} \mathbf{w}_{1m} \\ \mathbf{w}_{2m} \\ \vdots \\ \mathbf{w}_{Lm} \end{bmatrix} \quad (\text{B.57})$$

$$\mathbf{R}_{ssm} = \mathbf{E} [\mathbf{W}_m \mathbf{W}_m^H] \quad (\text{B.58})$$

The i th diagonal block of \mathbf{R}_{ssm} is found to be:

$$\mathbf{R}_{ssm}[ll] = \mathbf{E} [\mathbf{w}_{lm} \mathbf{w}_{lm}^H] \quad (\text{B.59})$$

$$= \frac{1}{\varepsilon_l^2} \mathbf{E} \left[\sum_{i=1}^L \sum_{j=1, j \neq l}^L \gamma_i \gamma_j^* \mathbf{a}_i(\hat{q}) \mathbf{a}_j^H(\hat{q}) \mathbf{y}_i \mathbf{y}_l^* \mathbf{y}_l \mathbf{y}_j^* \right] \quad (\text{B.60})$$

$$= \frac{1}{\varepsilon_l} \sum_{i=1, i \neq l}^L |\gamma_i|^2 \mathbf{a}_i(\hat{q}) \mathbf{a}_i^H(\hat{q}) \quad (\text{B.61})$$

The $l - p$ off-diagonal block is calculated to be:

$$\mathbf{R}_{ssm}[lp] = \mathbf{E} [\mathbf{w}_{lm} \mathbf{w}_{pm}^H] \quad (\text{B.62})$$

$$= \frac{1}{\varepsilon_l \varepsilon_p} \mathbf{E} \left[\sum_{i=1}^L \sum_{j=1, j \neq p}^L \gamma_i \gamma_j^* \mathbf{a}_i(\hat{q}) \mathbf{a}_j^H(\hat{q}) \mathbf{y}_i \mathbf{y}_l^* \mathbf{y}_p \mathbf{y}_j^* \right] \quad (\text{B.63})$$

$$= 0 \quad (\text{B.64})$$

Combining these diagonal and (zero) off-diagonal terms, the total MAI contribution to the space-satellite interference covariance matrix is a block diagonal matrix:

$$\mathbf{R}_{ssm} = \begin{bmatrix} \mathbf{R}_{ssm}[11] & 0 & \cdots & 0 \\ 0 & \mathbf{R}_{ssm}[22] & 0 & 0 \\ 0 & \cdots & \ddots & 0 \\ 0 & \cdots & 0 & \mathbf{R}_{ssm}[LL] \end{bmatrix} \quad (\text{B.65})$$

An important observation is that since the satellites that compose the MAI in each satellite channel are different, each of the blocks that make up \mathbf{R}_{ssm} are different as well. It is for this reason that in the derivations of Chapter 4, the covariances are indexed by the satellite channel subscript.

B.3 Estimation of Interference Statistics

It is very important in estimation of the statistics of the interference to ensure that the training data for the estimation are free of the desired signal. If the desired signals exist in the training data, the estimate of the desired parameter (attitude or direction in this work) will be degraded. For a pulsed radar, estimation of the interference may be performed during the portion of the pulse repetition interval corresponding to where the desired target is not expected to be (i.e. ranges away from the target). However, for a communication system where the communication waveforms are present at all times, other methods must be employed. In this section we briefly discuss methods to estimate the space-satellite interference covariance matrix \mathbf{R}_{ss} .

Estimation of $\mathbf{R}_{ss}[ii]$

Knowledge of the time waveforms of the signals provides an advantage in estimating the interference covariance. Since for any satellite channel the desired (matched) satellite waveform lies in 1 dimension of an N dimensional space containing all possible length- N BPSK signals, the desired signal may be removed for interference estimation by projecting the received data onto a subspace of this N dimensional space that is orthogonal to the satellite time signals. Examples of this method of time-series projection may be found in Vaidyanathan et al. [48] for CDMA communication system with an antenna array that does not make use of the LOS to the source, in Jones and Wikert [49] for a robust system that incorporates both LOS information (in a generalized side-lobe canceller architecture) and knowledge of the desired waveform, and in Li et al. [22, 23] for a direction finding application.

Recall that the $M \times N$ data matrix \mathbf{X} of equation (4.25) contains the data samples from each sensor for N time snapshots. Using this, an estimate of the i th diagonal block

of the space-satellite covariance matrix can be found by “projecting out” (i.e. projecting onto a space orthogonal to) the i th satellite waveform:

$$\begin{aligned}
 \hat{\mathbf{R}}_{ss}[ii] &= \frac{1}{N\varepsilon} \left[\mathbf{X}\mathbf{X}^H - \frac{1}{\mathbf{y}_i\mathbf{y}_i^H} (\mathbf{X}\mathbf{y}_i^H) (\mathbf{y}_i\mathbf{X}^H) \right] \\
 &= \frac{1}{N\varepsilon} \left[\mathbf{X}\mathbf{I}_N\mathbf{X}^H - \sum_{l=1}^L \mathbf{X}\mathbf{P}_{y_l}\mathbf{X}^H \right] \\
 &= \frac{1}{N\varepsilon} [\mathbf{X}(\mathbf{I}_N - \mathbf{P}_i)\mathbf{X}^H] \\
 &= \frac{1}{N\varepsilon} [\mathbf{X}\mathbf{P}_{y_i}^\perp\mathbf{X}^H]
 \end{aligned} \tag{B.66}$$

where

$$\mathbf{P}_{y_i} = \frac{\mathbf{y}_i^H\mathbf{y}_i}{\mathbf{y}_i\mathbf{y}_i^H} \tag{B.67}$$

$$\mathbf{P}_{y_i}^\perp = \mathbf{I}_N - \sum_{l=1}^L \mathbf{P}_{y_l} \tag{B.68}$$

GPS Receiver Considerations

Recall from Section 2.2 that the signal level of the satellite waveforms at the sampler is much less than that of even the thermal noise. This requires that many chips be de-spread and integrated to provide appreciable SNR, and as discussed earlier this function is typically implemented in hardware. Therefore, to calculate covariance snapshots using the entire data matrix, as described in (B.66), would likely be computationally prohibitive and unnecessary. In addition, it would be desirable to explore the potential to simplify calculations by using a single $M \times M$ interference covariance matrix, instead of L matrices.

To explore these two desires, consider augmenting the receiver by an additional satellite (vector) demodulation channel, and denoting this as channel 0. As in (4.35), the output of this channel, \mathbf{u}_0 , is composed of the sum of satellite and interference projections onto the demodulation waveform, \mathbf{y}_0 .

$$\mathbf{u}_0 = \mathbf{z}_0 + \mathbf{w}_0 \tag{B.69}$$

Now if the receiver is designed to collect the output of channel 0 at a rate much faster than the other channels (i.e. much faster than the attitude update rate), yet much slower

than the system sample rate², and if we choose the channel 0 waveform properly, then we may estimate the interference covariance matrix from the samples of \mathbf{u}_0 . This will produce the same covariance matrix for each satellite channel. If N_i is the number of snapshots of channel 0 available, the the covariance estimate is found as

$$\hat{\mathbf{R}}_{\text{as}}[ii] = \sum_{n=1}^{N_i} \mathbf{u}_0[n] \quad i = 1, 2, \dots, L \quad (\text{B.70})$$

In order to employ this method, an appropriate demodulation waveform for channel 0 must be chosen. Assume that a waveform \mathbf{y}_\perp exists that satisfies the two properties of the spreading sequence model described in equations (B.40) and (B.41). That is,

$$\mathbb{E}[\mathbf{y}_\perp[n] \mathbf{y}_\perp^*[n-k]] = \delta[k] \quad (\text{B.71})$$

and

$$\mathbb{E}[\mathbf{y}_\perp[n] \mathbf{y}_l^*[k]] = 0 \quad l \neq i, \quad \forall n, k \quad (\text{B.72})$$

then by using \mathbf{y}_\perp is the demodulation sequence, $\hat{\mathbf{R}}_{\text{as}}[ii]$ is an approximation to *each* of the diagonal blocks of $\mathbf{R}_{\text{as}}[ii]$. The difference is that since all satellites are present in this data, the desired satellite is present in the estimated interference covariance matrix in each channel, where in the true covariance matrix the desired signal is absent. However, the desired satellite's contribution is attenuated significantly, since its projection onto \mathbf{y}_\perp is small. In fact, its amplitude is attenuated to the level of the MAI, which is very small for the GPS P(Y) waveform in general.

To summarize, employing the above covariance estimation approach, two important gains are made in computational efficiency. First, the number of outer products is reduced by using multiple snapshots of despread data to estimate the covariance, as opposed to

² For example, if the attitude update rate is 100Hz, and the GPS waveforms are sampled at 10MHz, then the output of channel 0 could be at 10kHz. This would provide 100 samples from which to estimate covariance, and the spreading gain would be 1000, sufficient to satisfy the asymptotic assumptions made earlier. In general, the number of snapshots from which to estimate covariance must be several times greater than the number of sensors.

the spread data at the sampler. Second, by paying a small price in accuracy, a single covariance matrix may be used for all satellite channels, reducing by a factor of L the computational requirements for estimating the covariance.

APPENDIX C RESOLUTION OF THE ATTITUDE AMBIGUITY BY TWO SATELLITES

In this appendix we review the attitude ambiguity and show that only two sources are required to eliminate the ambiguity in the array response vector. We begin by defining the terms used in this chapter. Let \mathbf{v}_1 and \mathbf{v}_2 be the LOS vectors to two sources such that $\mathbf{v}_1 \neq \mathbf{v}_2$. Also let $\mathbf{q}_1(\omega_1)$ represent the locus of possible attitudes that produce the same array response vector from source \mathbf{v}_1 , and let $\mathbf{q}_2(\omega_2)$ represent the locus of possible attitudes that produce the same array response vector from source \mathbf{v}_2 . Finally, define the true attitude as $\mathring{\mathbf{q}}$, and partition its components into the 3×1 vector \mathbf{z} and the scalar s .

$$\mathring{\mathbf{q}} = \begin{bmatrix} \mathbf{z} \\ s \end{bmatrix} \quad (\text{C.1})$$

As presented in Chapter 4, the locus of possible attitudes from either of the two sources may be written as the quaternion multiplication

$$\mathbf{q}_i(\omega_i) = \check{\mathbf{q}}_i(\omega_i) * \mathring{\mathbf{q}} \quad i = 1, 2 \quad (\text{C.2})$$

where

$$\check{\mathbf{q}}_i(\omega_i) = \begin{bmatrix} \sin(\frac{\omega_i}{2})\mathbf{v}_i \\ \cos(\frac{\omega_i}{2}) \end{bmatrix} \quad i = 1, 2 \quad (\text{C.3})$$

Using these definitions, we present the following theorem.

Theorem 4 *The attitude ambiguity in the array response vector for one satellite intersects the ambiguity in the array response vector for a satellite at a different direction in a single attitude, the true attitude of the antenna array. That is,*

$$\mathbf{q}_1(\omega_1) \cap \mathbf{q}_2(\omega_2) = \mathring{\mathbf{q}} \quad (\text{C.4})$$

Proof: Begin by noting that when the two attitude quaternions, $\mathbf{q}_1(\omega_1)$ and $\mathbf{q}_2(\omega_2)$, are equal (i.e. the attitudes intersect), their difference is the 4×1 zero vector.

$$\mathbf{q}_1(\omega_1) - \mathbf{q}_2(\omega_2) = \begin{bmatrix} 0 & 0 & 0 & 0 \end{bmatrix}^T \quad (\text{C.5})$$

Basic quaternion multiplication rules can be used to express $\mathbf{q}_1(\omega_1)$ and $\mathbf{q}_2(\omega_2)$ in terms of the components of the vector and scalar parts of the true attitude quaternion.

It is useful to consider the first three elements of the attitude ambiguity quaternions $\mathbf{q}_1(\omega_1)$ and $\mathbf{q}_2(\omega_2)$ separately from the fourth element, in a similar manner to the partitioning of $\hat{\mathbf{q}}$. These first three elements are found from evaluation of equation (C.2).

$$\mathbf{q}_i(\omega_i)_{1-3} = \cos\left(\frac{\omega_i}{2}\right)\mathbf{z} + s \sin\left(\frac{\omega_i}{2}\right)\mathbf{v}_i + \sin\left(\frac{\omega_i}{2}\right)\mathbf{v}_i \times \mathbf{z} \quad i = 1, 2 \quad (\text{C.6})$$

where \times represents the vector cross product. The fourth elements of the attitude ambiguity quaternions are also found from equation (C.2).

$$\mathbf{q}_i(\omega_i)_4 = s \cos\left(\frac{\omega_i}{2}\right) - \sin\left(\frac{\omega_i}{2}\right)\mathbf{v}_i \cdot \mathbf{z} \quad i = 1, 2 \quad (\text{C.7})$$

where \cdot represents the vector dot product.

In order to determine the intersection of these two attitude ambiguities, we take the difference between the two quaternions to find which ω_1 and ω_2 cause the difference to be zero. The difference of the first three elements is found from equation (C.6).

$$\begin{aligned} \mathbf{q}_1(\omega_1)_{1-3} - \mathbf{q}_2(\omega_2)_{1-3} = & \left(\cos\left(\frac{\omega_1}{2}\right)\mathbf{z} + s \sin\left(\frac{\omega_1}{2}\right)\mathbf{v}_1 + \sin\left(\frac{\omega_1}{2}\right)\mathbf{v}_1 \times \mathbf{z} \right) - \\ & \left(\cos\left(\frac{\omega_2}{2}\right)\mathbf{z} + s \sin\left(\frac{\omega_2}{2}\right)\mathbf{v}_2 + \sin\left(\frac{\omega_2}{2}\right)\mathbf{v}_2 \times \mathbf{z} \right) \end{aligned} \quad (\text{C.8})$$

By collecting terms, equation (C.8) can be written as

$$\mathbf{q}_1(\omega_1)_{1-3} - \mathbf{q}_2(\omega_2)_{1-3} = \alpha\mathbf{z} + s\mathbf{v}_d + \mathbf{v}_d \times \mathbf{z} \quad (\text{C.9})$$

where we have defined α and \mathbf{v}_d as

$$\alpha = \cos\left(\frac{\omega_1}{2}\right) - \cos\left(\frac{\omega_2}{2}\right) \quad (\text{C.10})$$

$$\mathbf{v}_d = \sin\left(\frac{\omega_1}{2}\right)\mathbf{v}_1 - \sin\left(\frac{\omega_2}{2}\right)\mathbf{v}_2 \quad (\text{C.11})$$

Similarly, the difference of the fourth components of $\mathbf{q}_1(\omega_1)$ and $\mathbf{q}_2(\omega_2)$ may be expressed in terms of the new parameters α and \mathbf{v}_d .

$$\begin{aligned} \mathbf{q}_1(\omega_1)_4 - \mathbf{q}_2(\omega_2)_4 &= w \cos\left(\frac{\omega_1}{2}\right) - \sin\left(\frac{\omega_1}{2}\right)\mathbf{v}_1 \cdot \mathbf{v} \\ &\quad - \left[s \cos\left(\frac{\omega_2}{2}\right)\mathbf{z} - \sin\left(\frac{\omega_2}{2}\right)\mathbf{v}_2 \cdot \mathbf{v} \right] \\ &= - \left[\sin\left(\frac{\omega_1}{2}\right)\mathbf{v}_1 - \sin\left(\frac{\omega_2}{2}\right)\mathbf{v}_2 \right] \cdot \mathbf{z} \\ &\quad + s \left[\cos\left(\frac{\omega_1}{2}\right) - \cos\left(\frac{\omega_2}{2}\right) \right] \end{aligned} \quad (\text{C.12})$$

$$= -\mathbf{v}_d \cdot \mathbf{v} + \alpha s \quad (\text{C.13})$$

The attitude ambiguity intersections are found where (C.9) and (C.13) are equal to zero. The free parameters in these two equations are α and \mathbf{v}_d , which are in turn set by ω_1 and ω_2 . We first consider the situation where equation (C.9) is set to the 3×1 zero vector. Notice that of the three vectors in equation (C.9), two of them, namely \mathbf{z} and \mathbf{v}_d are (by definition, always) co-planar, regardless of the constants that scale them. The third vector, $\mathbf{v} \times \mathbf{v}_d$ is always orthogonal to the plane that contains the first two vectors. So for equation (C.9) to equal zero, the sum of two vectors lying in a plane and a vector orthogonal to this plane must equal zero. This can only occur if the two coplanar vectors are equal in magnitude and anti-parallel, and the length of the orthogonal vector is zero. For this particular case, the length of the orthogonal vector will go to zero when the two co-planar vectors are parallel or antiparallel, since it is defined as the cross product of the coplanar vectors. So for a solution to exist, the two co-planar vectors must be equal in magnitude and of opposite sign, or of zero length. That is, either

$$\alpha \mathbf{v} = -w \mathbf{v}_d \quad (\text{C.14})$$

or both α and \mathbf{v}_d have a magnitude of zero. The consequences of the condition where α and \mathbf{v}_d are zero is discussed later, so consider the case where equation (C.14) holds. This may be written as

$$\mathbf{v}_d = \frac{-\alpha}{s} \mathbf{z} \quad (\text{C.15})$$

At an intersection of the two attitude ambiguities the scalar equation (C.13) will equal zero as well. Inserting the above expression for \mathbf{v}_d into equation (C.13) yields

$$0 = -\frac{-\alpha}{s} \mathbf{z} \cdot \mathbf{z} + \alpha s \quad (\text{C.16})$$

$$= \alpha \left[\frac{1}{s} + s \right] \quad (\text{C.17})$$

which has a solution only at $\alpha = 0$. Since $\alpha = 0$, equation (C.14) implies that \mathbf{v}_d must be zero length as well, since s is arbitrary.¹ From the definition of α and \mathbf{v}_d , and the fact that $\mathbf{v}_1 \neq \mathbf{v}_2$, this implies that at an intersection of the two attitude ambiguities:

$$\omega_1, \omega_2 = n(2\pi) \quad (\text{C.18})$$

and therefore $\mathbf{q}_1(\omega_1)$ and $\mathbf{q}_2(\omega_2)$ are equal to the true attitude quaternion $\mathring{\mathbf{q}}$. That is,

$$\mathbf{q}_1(\omega_1) \cap \mathbf{q}_2(\omega_2) = \mathring{\mathbf{q}} \quad (\text{C.19})$$

■

An extension of this to multiple satellites is straightforward. Since the attitude ambiguities from any two satellites intersect only at the *true* attitude, the intersection of *all* ambiguities is at the true attitude as well.

¹ Even if $s = 0$, equation (C.9) can only equal zero when $\alpha = 0$, since in this case $|\mathbf{z}| \neq 0$.

REFERENCES

- [1] Christopher Comp, *GPS Carrier Phase Multipath Characterization and a Mitigation Technique Using the Signal-to-Noise Ratio*, Ph.D. dissertation, Department of Aerospace Engineering Sciences, University of Colorado, Boulder, 1996.
- [2] Alison Brown, Dale Reynolds, Capt. Darren Roberts, and Major Steve Serie, "Jammer and interference location system - Design and initial test results," *Proceedings of the ION GPS '99*, pp. 137-142, September 1999.
- [3] Ken Falcone, George Dimos, Chun Yang, Faye Nim, Stan Wolf, David Yarq, John Weinfeldt, and Paul Olson, "Small affordable anti-jam gps antenna (saaga) development," *ION GPS '99*, pp. 1149-1156, September 1999.
- [4] Matthew Markel, Eric Sutton, and Henry Zmuda, "An antenna array-based approach to attitude determination in a jammed environment," in *Proceedings of the ION GPS '01*, Salt Lake City, Utah, September 2001.
- [5] John B. Schleppe, "Development of a real-time attitude system using a quaternion parameterization and non-dedicated GPS receivers," Department of Geomatics Engineering, University of Calgary, 1996.
- [6] Frank Van Graas and Michael Braasch, "GPS interferometric attitude and heading determination: Initial flight test results," *Navigation: Journal of the Institute of Navigation*, vol. 38, no. 4, pp. 297-316, 1991-1992.
- [7] Clark E. Cohen, "Attitude determination," in *Global Positioning System: Theory and Applications*, Bradford W. Parkinson and James J. Spilker JR., Eds., vol. 2, pp. 519-538. American Institute of Aeronautics and Astronautics, Washington, DC, 1996.
- [8] Eric Sutton, "Optimal search space identification for instantaneous integer cycle ambiguity resolution," *Proceedings of the ION GPS '97*, September 1997.
- [9] Petre Stoica and Randolph Moses, *Introduction to Spectral Analysis*, Prentice Hall, Upper Saddle River, NJ, 1997.
- [10] R.C. Davis, L.E. Brennan, and I.S. Reed, "Angle estimation with adaptive arrays in external noise fields," *IEEE Transactions on Aerospace and Electronic Systems*, vol. AES-12, no. 2, pp. 179-186, March 1976.
- [11] Feng Ling C. Lin and Frank F. Kretschmer Jr., "Angle measurement in the presence of mainbeam interference," *IEEE AES Magazine*, vol. 26, no. 6, pp. 19-25, November 1990.
- [12] U. Nickel, "Monopulse estimation with adaptive arrays," *IEE Proceedings-F*, vol. 140, no. 5, pp. 303-307, October 1993.

- [13] JR. J. Liberti and T. S. Rappaport, *Smart Antennas for Wireless Communications: IS-95 and Third Generation CDMA Applications*, Prentice Hall, Upper Saddle River, NJ, 1999.
- [14] Ilan Ziskind and Mati Wax, "Maximum likelihood localization of multiple sources by alternating projection," *IEEE Transactions on Acoustics, Speech, and Signal Processing*, vol. 36, no. 10, pp. 1553–1560, October 1988.
- [15] Mats Viberg and Björn Ottersten, "Sensor array processing based on subspace fitting," *IEEE Transactions on Signal Processing*, vol. 39, no. 5, pp. 1110–1121, May 1991.
- [16] Petre Stoica and Ayre Nehorai, "MUSIC, Maximum Likelihood, and Cramer-Rao Bound," *IEEE Transactions on Acoustics, Speech, and Signal Processing*, vol. 37, no. 5, pp. 720–741, May 1989.
- [17] Petre Stoica and Ayre Nehorai, "Performance study of conditional and unconditional direction-of-arrival estimation," *IEEE Transactions on Acoustics, Speech, and Signal Processing*, vol. 10, no. 38, pp. 1783–1795, October 1990.
- [18] A. Swindlehurst, "An alternative algorithm for maximum likelihood DOA estimation and detection," *IEE Proceedings – Radar, Sonar, and Navigation*, vol. 141, no. 6, pp. 293–299, December 1994.
- [19] Björn Ottersten, Mats Viberg, and Thomas Kailath, "Analysis of subspace fitting and ML techniques for parameter estimation from sensor array data," *IEEE Transactions on Signal Processing*, vol. 40, no. 3, pp. 590–600, March 1992.
- [20] Jian Li, *Array Signal Processing for Polarized Signals and Signals with Known Waveforms*, Ph.D. dissertation, Ohio State University, Columbus Ohio, 1991.
- [21] Jian Li and R. T. Compton, "Maximum likelihood angle estimation for signals with known waveforms," *IEEE Transactions on Signal Processing*, vol. 41, no. 9, pp. 2850–2862, September 1993.
- [22] Jian Li, Bijit Halder, Petre Stoica, and Mats Viberg, "Computationally efficient angle estimation for signals with known waveforms," *IEEE Transactions on Signal Processing*, vol. 43, no. 9, pp. 2154–2163, September 1995.
- [23] Jian Li, Bijit Halder, Petre Stoica, Mats Viberg, and Thomas Kailath, "Decoupled maximum likelihood angle estimation for signals with known waveforms," Tech. Rep. No. CTH-TE-8, Chalmers University of Technology, Gothenburg, Sweden, February 1994.
- [24] Ralph O. Schmidt, "Multiple emitter location and signal parameter estimation," *IEEE Transactions on Antennas and Propagation*, vol. AP-34, no. 3, pp. 276–280, March 1986.
- [25] Gary F. Hatke and Keith W. Forsythe, "A class of polynomial rooting algorithms for joint azimuth/elevation estimation using multidimensional arrays," *Conference Record of the Twenty-Eighth Asilomar Conference on Signals, Systems and Computers*, vol. 1, pp. 694–699, 1994.

- [26] Richard Roy and Thomas Kailath, "ESPRIT – Estimation of signal parameters via rotational invariance techniques," *IEEE Transactions on Acoustics, Speech, and Signal Processing*, vol. 37, no. 7, pp. 984–995, July 1989.
- [27] A. Swindlehurst and T. Kailath, "Azimuth/elevation direction finding using regular array geometries," *IEEE Transactions on Aerospace and Electronic Systems*, vol. 29, no. 1, pp. 145–156, 1993.
- [28] Lal C. Godara, "Application of antenna arrays to mobile communications, part II: Beam-forming and direction-of-arrival considerations," *Proceedings of the IEEE*, vol. 85, no. 8, pp. 1195–1245, August 1997.
- [29] Hamid Krim and Mats Viberg, "Two decades of array signal processing research," *IEEE Signal Processing Magazine*, July 1996.
- [30] Gary F. Hatke, "Adaptive array processing for wideband nulling in gps systems," *Conference Record of the Thirty-Second Asilomar Conference on Signals, Systems, & Computers*, vol. 2, pp. 1332–1336, 1998.
- [31] Ronald L. Fante and John J. Vacarro, "Cancellation of jammers and jammer multipath in a GPS receiver," *IEEE AES Systems Magazine*, vol. 13, no. 11, pp. 25–28, November 1998.
- [32] Ronald L. Fante and John J. Vacarro, "Wideband cancellation of interference in a gps receive array," *IEEE Transactions on aerospace and electronic systems*, vol. 36, no. 2, pp. 549–564, April 2000.
- [33] James Ward, "Space-Time Adaptive Processing for Airborne Radar," *Acoustics, Speech, and Signal Processing, 1995 International Conference on*, vol. 5, pp. 2809–2812, 1995.
- [34] Petre Stoica and Kenneth C. Sharman, "Maximum likelihood methods for direction-of-arrival estimation," *IEEE Transactions on Acoustics, Speech, and Signal Processing*, vol. 38, no. 7, pp. 1132–1143, July 1990.
- [35] Harry L. Van Trees, *Detection, Estimation, and Modulation Theory, Part I*, chapter 2, pp. 63–66, John Wiley & Sons, New York, 1968.
- [36] Richard Klemm, *Space-Time Adaptive Processing, Principles and Applications*, chapter 3, pp. 71–72, Institution of Electrical Engineers, London, 1998.
- [37] Elliot D. Kaplan, *Understanding GPS Principles and Applications*, Artech House, 1996.
- [38] William H. Press, Saul A. Teukolsky, William T. Vetterling, and Brian P. Flannery, *Numerical Recipes in Fortran*, chapter 10, pp. 406–407, Press Syndicate of the University of Cambridge, New York, 1986.
- [39] K.C. Sharman and G.D. McClurkin, "Genetic algorithms for maximum likelihood parameter estimation," in *Proceedings of the 1989 Conference on Acoustics, Speech, and Signal Processing*, Glasgow, Scotland, 1989, vol. 4, pp. 2716–2719.

- [40] G.D. McClurkin, K.C. Sharman, and T.S. Durrani, "Genetic algorithms for spatial spectral estimation," in *Fourth Annual ASSP Workshop on Spectrum Estimation and Modeling*, Minneapolis, Minnesota, 1988, pp. 318–322.
- [41] Mats Viberg, Petre Stoica, and Björn Ottersten, "Maximum likelihood array processing in spatially correlated noise fields using parameterized signals," *IEEE Transactions on Signal Processing*, vol. 45, no. 4, pp. 996–1004, April 1997.
- [42] Sidney P. Applebaum, "Adaptive arrays," *IEEE Transactions on Antennas and Propagation*, vol. AP-24, no. 5, pp. 585–597, September 1976.
- [43] Richard C. Johnson, *Antenna Engineering Handbook*, chapter 20, McGraw-Hill, New York, 1993.
- [44] Alan V. Oppenheim and Ronald W. Shafer, *Discrete-time Signal Processing*, chapter 3, pp. 86–88, Prentice Hall, Englewood Cliffs, NJ, 1989.
- [45] Tan F. Wong, Tat M. Lok, James S. Lehnert, and Michael D. Zoltowski, "A linear receiver for direct-sequence spread-spectrum multiple-access systems with antenna arrays and blind adaptation," *IEEE Transactions on Information Theory*, vol. 44, no. 2, pp. 659–676, March 1998.
- [46] Merrill I. Skolnik, *Introduction to Radar Systems*, McGraw-Hill, New York, 1980.
- [47] Peyton Z. Peebles Jr., *Radar Principles*, chapter 4, p. 165, John Wiley & Sons, New York, 1998.
- [48] Chandra Vaidyanathan, Kevin M. Buckley, and Srinath Hosur, "A blind adaptive antenna array for CDMA systems," in *ASILOMAR Conference on Signals, Systems, and Computers*, Pacific Grove, California, 1995, pp. 1373–1377.
- [49] Mark A. Jones and Mark A. Wickert, "Direct-sequence spread-spectrum using directionally constrained adaptive beam forming to null interference," *IEEE Journal on Selected Areas in Communications*, vol. 13, no. 1, pp. 71–79, January 1995.

BIOGRAPHICAL SKETCH

Matthew David Markel was born March 24, 1968, in Kansas City, Missouri, to David Frank and Linda Darlene Markel. His family moved between Kansas City, Missouri, and Chicago, Illinois, and in 1976 settled in Saint Louis, Missouri, where he attended elementary school, middle school, and high school. In 1986 he graduated from Lindbergh High School with a 4. GPA, and began attending the University of Missouri - Rolla (UMR) as a Missouri Curators and National Merit Scholar.

As an undergraduate, Mr. Markel was a member of the Lambda Chi Alpha social fraternity, and the Phi Eta Sigma (freshman), Tau Beta Pi (engineering), and Eta Kappa Nu (electrical engineering) honor societies. In addition, he performed with several university musical groups and was the featured soloist with the Jazz, Marching, and Symphonic Bands during his four years at UMR. In 1990 Mr. Markel graduated *magna cum laude* from the University of Missouri - Rolla.

After receiving his undergraduate degree, Mr. Markel joined the technical staff at Dynetics, Inc., in Fort Walton Beach, Florida. At Dynetics he specialized in analysis and simulation of military radar systems and radar signal processing. As the manager of the Air to Air Section he led the Dynetics effort that provided technical support to the System Performance group of the Advanced Medium Range Air to Air Missile (AMRAAM) Systems Program Office. Mr. Markel earned his master's degree in electrical engineering (M.S.) from the University of Florida satellite campus at Eglin Air Force Base in 1992, while working at Dynetics.

In 1996 Mr. Markel joined Sverdrup Technology at Eglin AFB. As a senior member of the technical staff on the Technical Engineering and Acquisition Support (TEAS) contract, he supports a wide range of organizations at Eglin with his signal processing, radar, Global Positioning System, and weapons experience. In 1999 he began work on his Ph.D. in electrical engineering at the University of Florida when he was awarded the first

Sverdrup Edwin "Bud" George Ph.D. Fellowship. His research on anti-jam GPS attitude determination has been beneficial to both the academic and military communities.

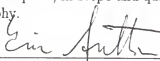
Mr. Markel married Colleen McGuire of Shalimar Florida on March 13, 1993. They currently reside in Fort Walton Beach, Florida, where Mr. Markel is an active musician and member of his church.

I certify that I have read this study and that in my opinion it conforms to acceptable standards of scholarly presentation and is fully adequate, in scope and quality, as a dissertation for the degree of Doctor of Philosophy.



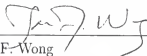
Henry Zmuda, Chair
Associate Professor of Electrical and
Computer Engineering

I certify that I have read this study and that in my opinion it conforms to acceptable standards of scholarly presentation and is fully adequate, in scope and quality, as a dissertation for the degree of Doctor of Philosophy.



Eric Sutton, Cochair
Assistant Professor of Electrical and
Computer Engineering

I certify that I have read this study and that in my opinion it conforms to acceptable standards of scholarly presentation and is fully adequate, in scope and quality, as a dissertation for the degree of Doctor of Philosophy.



Tan F-Wong
Assistant Professor of Electrical and
Computer Engineering

I certify that I have read this study and that in my opinion it conforms to acceptable standards of scholarly presentation and is fully adequate, in scope and quality, as a dissertation for the degree of Doctor of Philosophy.



Pasquale M. Sforza
Professor of Aerospace Engineering,
Mechanics, and Engineering Science

This dissertation was submitted to the Graduate Faculty of the College of Engineering and to the Graduate School and was accepted as partial fulfillment of the requirements for the degree of Doctor of Philosophy.

May 2002



Pramod P. Khargonekar
Dean, College of Engineering

Winfred M. Phillips
Dean, Graduate School